A LIGHT-SCATTERING STUDY OF THE KINETIC SIZE DISTRIBUTION CHANGES OF AEROSOLS

A thesis submitted for the degree of
Doctor of Philosophy in the Faculty of Engineering
of the University of London

by

Alan Peter Moore

Department of Chemical Engineering and Chemical Technology
Imperial College of Science and Technology
London S. W. 7.

February 1974

IN MEMORY OF

MY

FATHER

ABSTRACT

This thesis describes the design and development of a scanning laser light scattering instrument to provide size distribution data on dispersions of particles as a function of time. A computer analysis was developed simultaneously to predict the two parameters of the zeroth-order logarithmic distribution (ZOLD) which best fit, on a least squares basis, the angular scattering intensities. This inversion technique was extensively tested using theoretical values of these intensities for a range of modal diameters (up to 2 μm) and spread parameters (up to 0.6). For this range of distribution parameters it was found that vertically polarised light was in general more suited to the inversion analysis than horizontally polarised light and furthermore as the width of distribution increased the degree of uncertainty in the assignment of these parameters also increased. Following the successful sizing of four different latex samples having modal diameters in the same range, the instrument was used in a preliminary study on the aerosol produced by the chemical reaction of ammonia and sulphur dioxide, two of the more common air pollutants. It was observed that particles in detectable numbers were produced within approximately fifteen seconds of the gases mixing, even in the absence of daylight, but little substantiable information on particle size was gained from inverting the scattering data. Several reasons for this have been put forward and discussed, together with suggestions for improvements to the prototype instrument to increase its potential in the field of in situ particle size determination.

ACKNOWLEDGEMENTS

I should like to thank Professor A. R. Ubbelohde, C. B. E., F. R. S., for allowing me to carry out this work in his department and for providing financial support in conjunction with the Courtauld's Education Trust Fund.

Grateful appreciation is expressed to all the technical staff in the department for their invaluable assistance and advice. In particular, I should like to mention John Locke, Bert Lucas and Ted Barnes for their work in constructing the scattering instrument; Len Tyley and Trevor Hunt who designed and built the electronic equipment and provided the information for Fig. 4.8; Ken Grose of the glassblowers for building the gas rig and for his patience in making the scattering cell window; Linda Ward and Jacob Dipchan, the former for all her computer card punching and the latter for providing a courier service to and from the computing centre.

I should also like to thank Dr. Michael Carabine for accepting me as one of his first postgraduate students and together with my colleague John Maddock, for being a source of inspiration and constructive criticism throughout my research.

My final thanks must go to Diana Bishop and Jean Craig for their accurate typing of this thesis.

CONTENTS

GLOSSARY OF PRINCIPAL SYMBOLS

C_{sca}, C_{ext}	cross sections for scattering, extinction,
C_{abs}, C_{pr}	absorption, radiation pressure
F	sum of squares in least squares analysis
I	intensity
L	length
N	number of particles per unit volume
P	form factor
Q_{sca}, Q_{ext}	efficiencies for scattering, extinction,
Q_{abs}, Q_{pr}	absorption, radiation pressure
R	experimentally determined scattering intensity
S_1, S_2	scattering amplitudes for sphere
T	transmission
V	volume
a	radius
$\bar{a}$	mean of a
a_M	mode of a
a_m	median of a
a_n, b_n	scattering coefficients
d	diameter
i	$(-1)^{\frac{1}{2}}$
i_1, i_2	intensity functions
k	propagation constant $2\pi/\lambda$
m	relative refractive index m_1/m_2
m_1, m_2	refractive index of particle, medium
n	real part of refractive index

$p(a)$	size distribution function
r	radial distance
α	dimensionless size parameter ($\pi d/\lambda$)
β	$m\alpha$
$\zeta_n(z)$, $\chi_n(z)$, $\psi_n(z)$	Ricatti-Bessel functions
Θ	scattering angle
λ	wavelength
$\pi_n(\cos\Theta)$, $\tau_n(\cos\Theta)$	angular functions
σ	standard deviation
σ_g	geometric mean standard deviation
σ_o	breadth parameter of ZOLD
τ	turbidity

CHAPTER 1

Introduction

Dispersed systems composed of particles suspended in gases are frequently observed in nature and in urban surroundings. The term aerosol has, through common usage, come to refer to any suspension of particulate matter of microscopic or sub-microscopic size but larger than molecular dimensions. Among the processes that affect the size distribution of an aerosol are coagulation, sedimentation, and the rate of generation of particles. These are themselves influenced by the particle characteristics e.g. size and shape, and the dynamics of the fluid in which the particles are suspended.

Generation of aerosols can be achieved through one of two fundamental mechanisms, either by the agglomeration of molecules or by the break up of material to form particles of colloidal size.

Most common amongst the agglomeration processes is the nucleation of a saturated vapour. Nuclei may consist of either groups of molecules of condensed vapour or 'foreign' material such as ions or dust particles. Supersaturation can be brought about for example by physical processes e.g. adiabatic expansion or mixing a warm gas with a cool gas, or by means of chemical reaction. In the latter case a mixture of chemically reactive gases yield a product which when first formed is in a molecularly dispersed condition since the reaction is intermolecular. The newly formed molecules then aggregate and condense to form very fine solid primary particles at a rate determined by the supersaturation of the product.

When considering the role of particulates in air pollution the dependence of the number concentration and size distribution on the physical and chemical processes occurring in the urban atmosphere is of particular interest. The work of Junge (1954) and more recently Heard and Whiffen (1969) and Eggleton and Atkins (1969) has shown

ammonium sulphate to be an important constituent of atmospheric aerosols in the submicron size range.

Various mechanisms have been put forward for the formation of atmospheric sulphate particles (Carabine, 1972; Cadle, 1972; Urone and Schroeder, 1969).

Considering first the gas-phase reactions; in humid air ammonia and sulphur dioxide react to produce solid $(NH_4)_2SO_3$ or $(NH_4)_2S_2O_3$ according to the conditions and these compounds are readily oxidised to ammonium sulphate (Healy et al., 1970). In the absence of water the reaction occurs at temperatures below $10^{\circ}C$ yielding solid products with the stoichiometry of $NH_3.SO_2$ in the presence of excess SO_2 and $2NH_3.SO_2$ with excess NH_3(Scott et al., 1969). Infra-red spectra of the products at room temperature (Hata and Kinumaki, 1964), indicated gas-phase HNSO and particles of $(NH_4)_2S_2O_5$.

The photochemical oxidation of SO_2 can be accelerated by the presence of nitrogen oxides and hydrocarbons (Urone and Schroeder, 1969) but only at relatively high concentrations. Significant amounts of ammonium sulphate could possibly be formed therefore in urban areas where there are large numbers of motor vehicle exhausts, providing sufficient sunlight is forthcoming.

Aerosol particles of ammonium sulphate may also be the result of the reaction of ammonia and sulphur dioxide in water droplets which later evaporate. Van den Heuvel and Mason (1963) showed this to be possible in their study of this reaction in macroscopic droplets of pure water. A considerable increase in the rate of reaction is possible if the droplets contain dissolved catalysts e.g. manganese salts (Johnstone and Coughanowr, 1958). Further laboratory experiments by Cadle and Robbins (1960) showed how rapidly ammonia reacted with sulphuric acid aerosol droplets of 0.2 - 1μm diameter.

Kiang et al. (1973) have recently shown how their heteromolecular nucleation theory could be applied to atmosphere gas-to-particle conversions. For the reaction of ammonia and sulphur dioxide they suggest an initial gas phase reaction to form $NH_3.SO_2$ followed by heteromolecular nucleation in the presence of water to produce the aerosol. The laboratory observations of Friend et al. (1972) on the formation of particles in systems of air containing traces of H_2O, SO_2, NH_3 and O_3 in varying proportions and under varying conditions of radiation with ultra-violet light indicated that addition compounds of NH_3 and SO_2 if they form, are not precursors to the formation of ammonium sulphate in the atmosphere. Instead they proposed a three stage mechanism involving the initial formation of sulphuric acid nuclei which are neutralised by NH_3 producing embryonic salt solution droplets and providing the catalyst (NH_4^+) for the rapid oxidation of SO_2.

All these studies have been almost entirely directed towards either the chemical or physical mechanisms involved in the formation of ammonium sulphate in the atmosphere, little attention being paid to the actual size of the resultant aerosol. A kinetic study of the size development of the aerosol resulting from the reaction of gaseous ammonia and sulphur dioxide was therefore embarked upon. Since in practice all aerosols are, to a greater or lesser degree, polydisperse and bearing in mind the size range of particles normally encountered in the atmosphere i.e. from 1 μm diameter downwards, it was essential to first establish both a reliable and accurate method of particle size distribution analysis in the sub-micron range.

Probably the most reliable method of analysis is the direct size determination of a large number of individual particles, for example, by means of an optical or electron microscope, ultramicroscope, with a subsequent statistical treatment of the results. However, these methods are often not applicable. This is particularly true for particles of a

volatile or hygroscopic nature where evaporation or absorption of water may be appreciable during sampling and measurement. Liquid droplets also tend to spread over the sampling substrate, while delicately structured particles can often be severely distorted by electron microscope preparation procedures. The ultramicroscope measurement of the sedimentation rate of particles, or of their motion in an electric field is a practical possibility, according to Gladkova and Natanson (1958), only at a particle radius above 0.15 μm, errors arising in the sizing of individual particles due to Brownian motion.

Among other methods of estimating the size of aerosol particles, the most widely used are ones based on the extinction and/or scattering of a beam of light passing through a suspension of the particles. Of all the methods of size measurement these involve the least disturbance of the particles being measured and, since they can be made almost instantaneous and recorded continuously, they are particularly suited to studying rate processes.

Light scattering methods are absolute in the sense that theory permits the reduction of data directly to the final desired results without the need of secondary schemes for calibration. The number of particles under observation at any one time is usually sufficiently large to provide a representative sample, of particular importance when a distribution of sizes is present.

From the previous discussion it can be seen that a size analysis method based on light scattering provides the best practical means by which the temporal changes in size distribution of an aerosol can be monitored. However, since the exact solution of the scattering by particles of arbitrary size and refractive index having edges and/or corners is extremely difficult, it is advisable where solid particles of unknown shape are concerned to supplement this technique by a preliminary electron microscopic examination.

CHAPTER 2

Theory of Light Scattering by a Sphere

2.1 Introduction

Of the multitude of scattering phenomena only single particle scattering in which the scattered radiation has the same frequency as the incident radiation will be considered here. This excludes effects such as fluorescence and the Raman effect which involve quantum transitions, and Brillouin scattering which arises from the Doppler shifts associated with the motion of the scattering particles. The restriction to single scattering implies that the scattering by a particular particle is unaffected by the presence of neighbouring particles. Thus, after the incident beam has encountered a particle the scattered radiation should proceed directly to the observer without further interference from any other particle.

Three main theories, attributed to Rayleigh, Rayleigh, Gans and Debye, and Mie respectively, have been developed to predict the scattering behaviour of spheres which are isotropic in composition and have either a constant refractive index (m) or one which varies in a radially symmetric manner only. Before discussing these in any detail a general survey will be conducted of the light scattering features in the refractive index - particle size domain, assuming that the particles are non-absorbing spheres (i.e. have a real refractive index). For the purpose of characterising the size of a particle its diameter (d) is combined with the radiation wavelength (λ) in the size parameter ratio $\alpha = \pi d/\lambda$.

Reference to Fig. 2.1 shows that there are six outer regions (1 to 6) in which one of the three parameters, α , (m-1), and the phase shift $\alpha(m-1)$, may have an arbitrary value ranging from near zero to infinity.

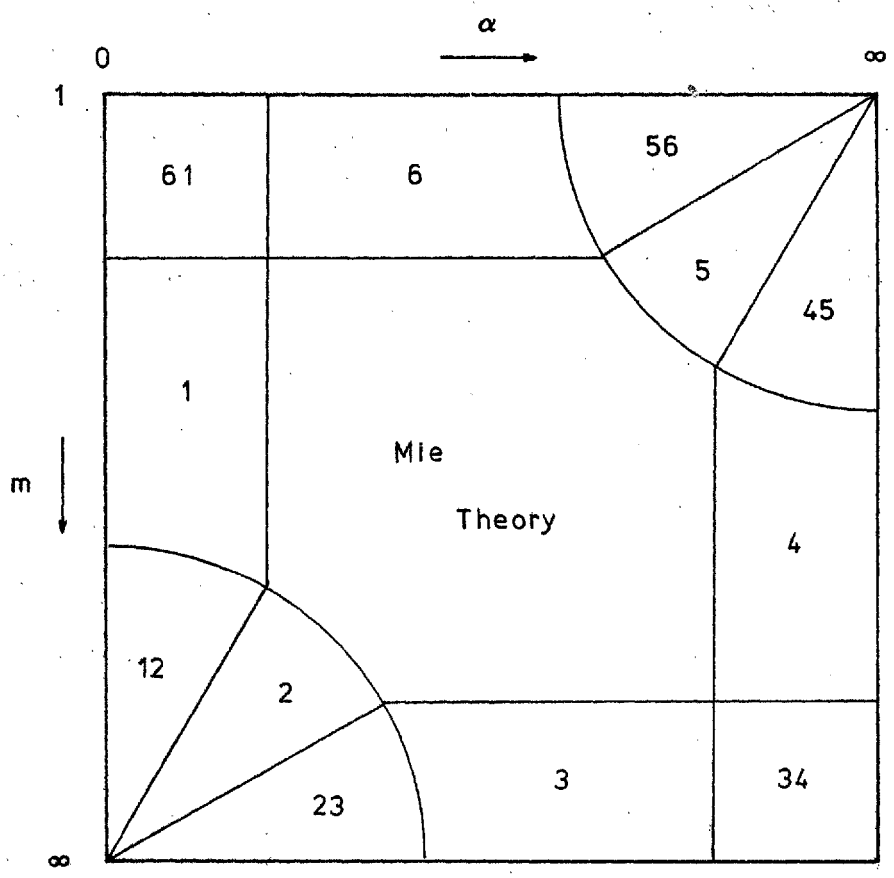

FIG. 2.1 Survey of limiting cases in the m-α domain

Region	α	(m-1)	α(m-1)	Name
1	s	arb	s	Rayleigh
12	s	lge	s	
2	s	lge	arb	optical resonance
23	s	lge	lge	
3	arb	lge	lge	total reflection
34	lge	lge	lge	
4	lge	arb	lge	geometrical optics
45	lge	s	lge	
5	lge	s	arb	anomalous diffraction
56	lge	s	s	
6	arb	s	s	Rayleigh-Gans-Debye
61	s	s	s	

s - small lge - large arb - arbitrary

Pairs of these regions overlap in areas numbered 12, 23 etc. and here identical results are obtained from the somewhat different approaches that hold for the two adjoining regions. Relevant features of the scattering phenomena in each boundary region are briefly described in the following summary.

The simplest patterns are produced in region 1 where both α and the phase shift are small resulting in the predominance of one term in the Mie formulae. This corresponds to dipole or Rayleigh scattering outlined in Section 2.2. In the lower left-hand corner (2), higher order terms become important but there are defined values of α for which one of these terms predominates, giving rise to a resonance phenomenon. As m tends to infinity the particles become perfect reflectors and there is no internal field to consider. Thus for region 3 the scattering coefficients are particularly simple (Kerker, 1969 p. 90). The next region (4) is that of geometrical optics. Here the scattering diagram is a combination of a diffraction pattern (dependent on α but not on m) and a reflection plus refraction pattern (dependent on m but not on α). For large m reflection prevails but as m decreases the radiation is refracted by the sphere until finally most of it is transmitted after two refractions without an inner reflection. If m decreases still further (region 5), the transmitted light becomes less divergent and its intensity increases until it is of the same order as the diffracted light. Here optical interference appears and the light is scattered in diffraction rings of varying size and distribution of intensity.

The limiting case of small phase shift characterises Rayleigh - Gans - Debye scattering in region 6 (see Section 2.3). Here purely geometrical interference effects cause a scattering diagram with successive bright and dark rings, most of the light being strongly forward directed for large α . As α decreases, the angular distance between rings widens and

one by one they disappear, so that for α much less than one the scattering pattern takes on the symmetrical appearance of the Rayleigh scatterer. Only the central area of the m - α plane now remains, and it is here that the rigorous scattering theory of Mie, as outlined in Section 2.4, must be used.

2.2 Rayleigh Theory

As a result of his research into the colour and polarisation of skylight, Lord Rayleigh (1881) produced a theory of light scattering for small dielectric spheres.

When illuminated by a parallel beam of linearly polarised radiation the dielectric composing the particle becomes polarised in the same direction as the field. If the sphere has a radius a, small compared to the radiation wavelength, λ , ($a/\lambda \leq 0.05$) then the instantaneous electromagnetic field over its extent is uniform. The particle thus acts as an oscillating electric dipole which radiates secondary or scattered waves in all directions.

For incident light of unit intensity linearly polarised with azimuthal angle χ , the light scattered a distance r from the particle at angle Θ (see Fig. 2.2) will consist of two linearly polarised components:

$$I_v(\chi) = \frac{16\pi^4 a^6}{r^2 \lambda^4} \left(\frac{n^2 - 1}{n^2 + 2} \right)^2 \sin^2 \chi \qquad 2.1$$

and

$$I_h(\chi) = \frac{16\pi^4 a^6}{r^2 \lambda^4} \left(\frac{n^2 - 1}{n^2 + 2} \right)^2 \cos^2 \chi \cos^2 \Theta \qquad 2.2$$

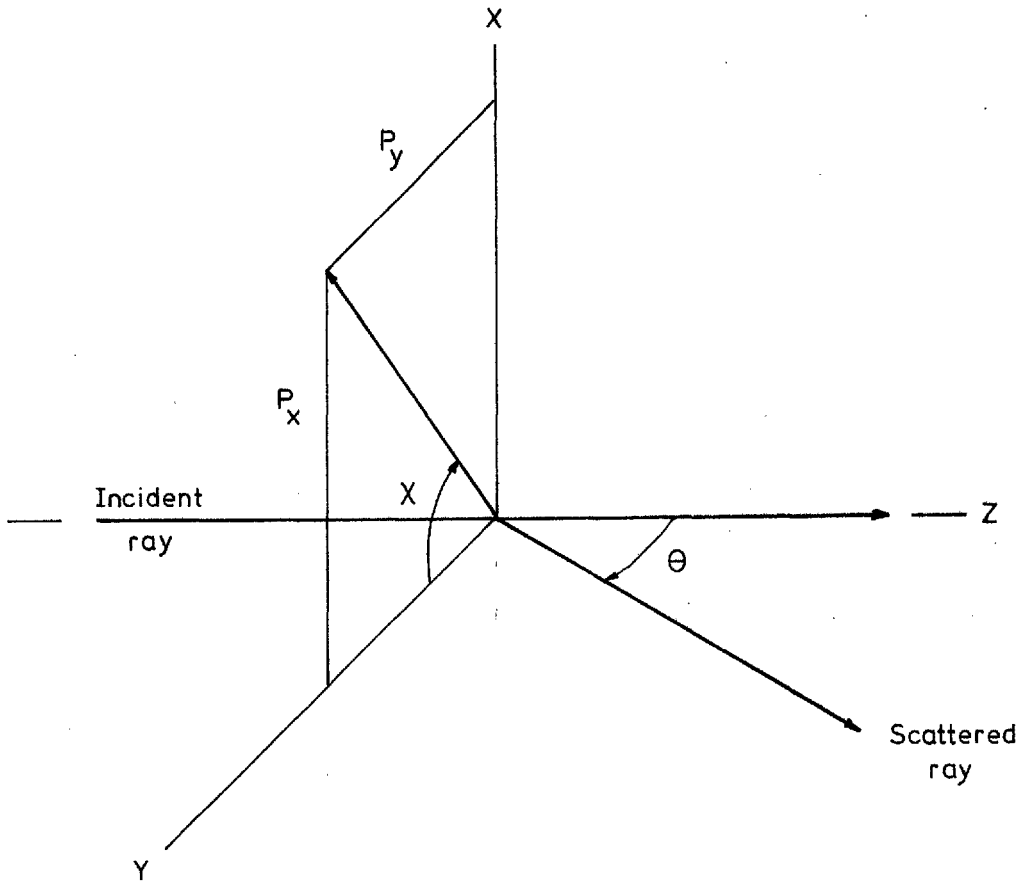

FIG. 2.2 Geometry for Scattering

YZ is the horizontal plane, and the electric vector of the incident wave is in the XY-plane. P_x and P_y are the vertical and horizontal or alternatively the perpendicular and parallel components of the radiation. θ is the scattering angle and χ the azimuthal angle of polarisation.

where $I_v(\chi)$ and $I_h(\chi)$ are respectively the intensities of the vertical and horizontal components of the scattered light.

An unpolarised incident wave can be resolved into two incoherent linearly polarised components which are perpendicular and parallel to the scattering plane. In this case:-

$$I_u = \frac{8\pi^4 a^6}{r^2 \lambda^4} \left(\frac{n^2 - 1}{n^2 + 2} \right)^2 (\cos^2\theta + 1) \qquad 2.3$$

The resultant scattered intensities for the three main cases of interest i.e. when the incident light is vertically polarised ($\chi = 90^\circ$), horizontally polarised ($\chi = 0^\circ$), or unpolarised are I_1, I_2 and I_u respectively and are illustrated in Fig. 2.3 below.

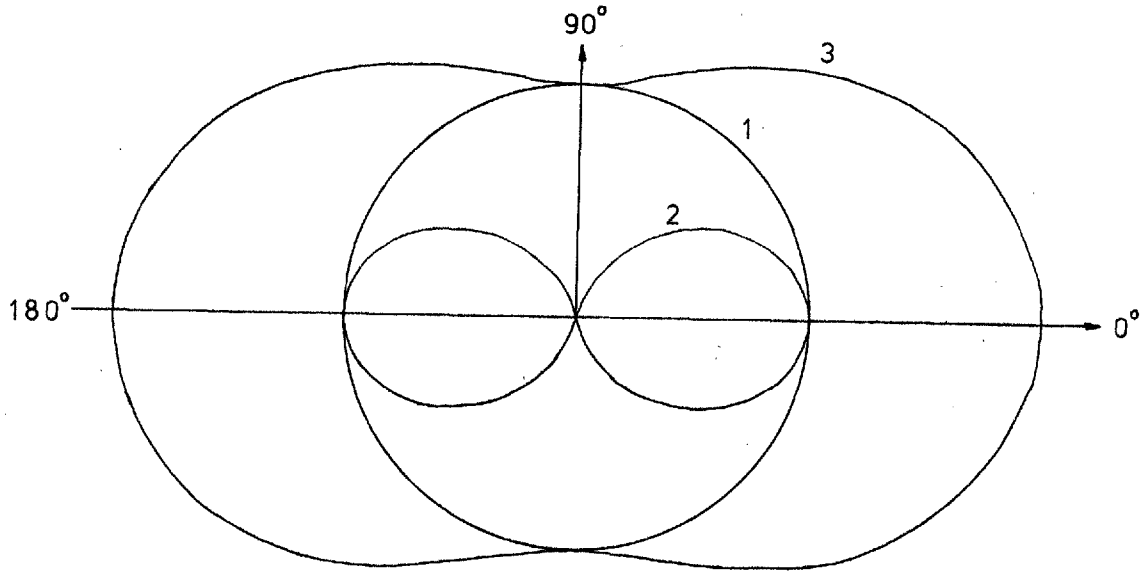

FIG. 2.3 Polar Diagram for Rayleigh Scattering

The radius vector to each curve is proportional to the scattered intensity at the corresponding angle.

1 = polarised perpendicular to plane of paper (I_1)
2 = polarised parallel to plane of paper (I_2)
3 = superposition of 1 and 2, unpolarised radiation

2.3 Rayleigh - Gans - Debye Scattering

In conjunction with his theory of scattering by small particles, Rayleigh (1881) also produced an approximate theory for particles of arbitrary shape and size having a refractive index close to that of the medium. Further contributions were made by Debye (1915) and by Gans (1925) who rederived the scattering formula for a homogenous sphere.

In order to distinguish this approach from that restricted to particles small compared with the wavelength it has been termed Rayleigh-Gans-Debye (R.G.D.) scattering. The fundamental assumption behind this theory is that the phase shift corresponding to any point in the particle is negligible i.e. that $2ka(m-1) \ll 1$, where k is the propagation constant $(2\pi/\lambda)$. It follows therefore that neither a the longest dimension through the particle, nor m the relative refractive index can become very large.

The particle is divided into a number of volume elements each of which is treated as a Rayleigh scatterer receiving incident light which is assumed to be unperturbed by the presence of the remainder of the particle. This is illustrated in Fig. 2.4 for two such elements A and B. If m is real and tending to unity the resultant scattered intensity for incident radiation polarised perpendicular to the scattering plane is given by:

$$I_1 = \frac{k^4 V^2}{4\pi^2 r^2} (m-1)^2 P(\theta) \qquad 2.4$$

and similarly for that parallel by:

$$I_2 = \frac{k^4 V^2}{4\pi^2 r^2} (m-1)^2 \cos^2\theta P(\theta) \qquad 2.5$$

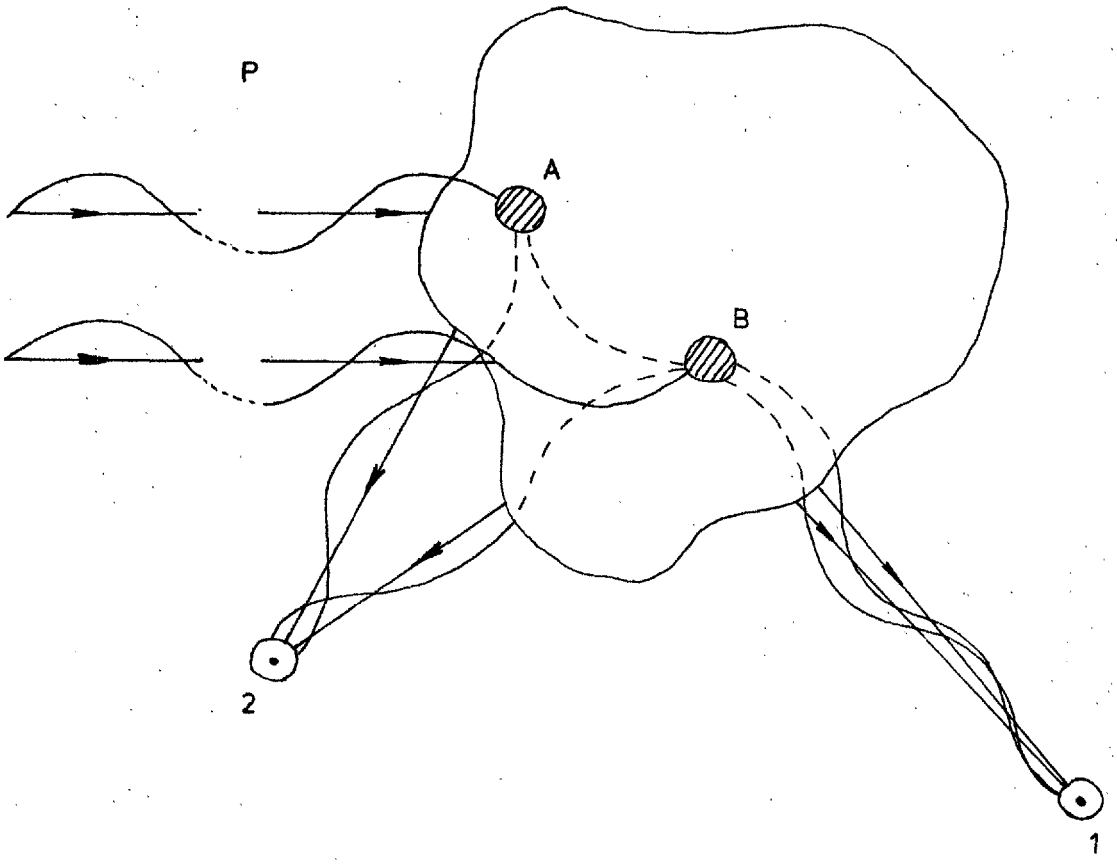

FIG. 2.4 Rayleigh-Gans-Debye Scattering

Mutual interference of wavelets emanating from A and B observed at points 1 and 2 far removed from the particle. P is a common reference plane. (Kerker, 1969)

V is the particle volume and the term $P(\theta)$ represents the modification of the intensity due to the finite size of the particle and its deviation from sphericity. This form factor has been evaluated for a number of configurations including homogeneous spheres (Rayleigh, 1881) radially inhomogeneous spheres (Rayleigh, 1918) coated spheres (Kerker et al, 1962), macromolecules (Debye, 1915, 1930, 1947), cylinders (Rayleigh 1881; Neugebauer, 1943) and thin disks (Kratky and Perod, 1949; Picot et al., 1968).

2.4 General or Mie Theory

A scattered wave is generated whenever a plane wave is incident upon any interface between two media of different refractive index. The field vectors describing the electromagnetic properties of space may be resolved into three parts; the incident wave, the wave inside the particle and the scattered wave. For regions where the physical properties of the medium are continuous, these quantities satisfy Maxwell's equations and the nonhomogeneous equations for damped wave motion. A solution of these equations is then sought for which the field inside the object and the external field (sum of incident and scattered fields) satisfy the condition that the tangential components of the electric and magnetic field intensities are each continuous across the boundary.

The treatment of the scattering of a plane electromagnetic wave by an isotropic homogeneous sphere of arbitrary size given by Kerker (1969) follows that of Debye (1909). Mie, after whom this theory is generally named, first produced his scattering formulae, using a different approach in 1908 . Other treatments of the basic theory may be found in Stratton (1941), van de Hulst (1957) and Born and Wolf (1964).

The same notation as that adopted by Kerker (1969) is used here in the following summary which gives the essential equations required in computational work to utilise the Mie theory.

From a consideration of the wave equation and the relevant boundary conditions, two scattering coefficients, a_n and b_n, can be formulated in terms of the relative refractive index (m) and the size parameter (α).

$$a_n = \frac{\psi_n(\alpha)\,\psi_n'(\beta) - m\,\psi_n(\beta)\,\psi_n'(\alpha)}{\zeta_n(\alpha)\,\psi_n'(\beta) - m\,\psi_n(\beta)\,\zeta_n'(\alpha)} \qquad 2.6$$

$$b_n = \frac{m\,\psi_n(\alpha)\,\psi_n'(\beta) - \psi_n(\beta)\,\psi_n'(\alpha)}{m\,\zeta_n(\alpha)\,\psi_n'(\beta) - \psi_n(\beta)\,\zeta_n'(\alpha)} \qquad 2.7$$

where $\beta = m\alpha$.

$\psi_n(z)$ and $\zeta_n(z)$ are Ricatti - Bessel functions and the addition of a prime to these functions denotes differentiation with respect to their arguments.

The amplitude functions S_1 and S_2 resulting from the solution for the scattered wave in the far-field zone, the region where in practice light scattering observations are normally carried out, are given by:

$$S_1 = \sum_{n=1}^{\infty} \frac{2n+1}{n(n+1)} \left\{ a_n \pi_n(\cos\Theta) + b_n \tau_n(\cos\Theta) \right\} \qquad 2.8$$

$$S_2 = \sum_{n=1}^{\infty} \frac{2n+1}{n(n+1)} \left\{ a_n \tau_n(\cos\Theta) + b_n \pi_n(\cos\Theta) \right\} \qquad 2.9$$

Here $\pi_n(\cos\theta)$ and $\tau_n(\cos\theta)$ are Legendre functions depending only upon the scattering angle θ .

The squares of the moduli of these amplitude functions are respectively the intensity functions perpendicular and parallel to the scattering plane

$$i_1 = \left| S_1 \right|^2 \quad \text{and} \quad i_2 = \left| S_2 \right|^2 \qquad 2.10$$

The angular variation of i_1 and i_2 for a series of particle diameters (D in μm) is shown in Fig. 2.5 for m = 1.19 and in Fig. 2.6 for m = 1.52. In both cases the incident wavelength is 632.8 nm. and hence the size parameter $\alpha \simeq 5D$. Several characteristic features are apparent especially the increasing preponderence of forward scattering and the oscillation with scattering angle as the particle size increases from that near the Rayleigh regime.

These intensity functions, i_1 and i_2, when multiplied by $\lambda^2/4\pi$ give the intensity of light scattered by a single spherical particle per unit solid angle at a particular angle of observation θ , for a plane polarised incident beam of unit intensity whose electric vectors vibrate respectively perpendicular and parallel to the scattering plane.

2.5 Cross Sections and Efficiencies

Let the total energy scattered in all directions be equal to the energy of the incident beam falling on the area C_{sca}. Likewise the energy removed from the original beam may, by definition, be put equal to the energy incident on the areas C_{abs} and C_{ext} respectively. It follows therefore from the law of conservation energy that:

$$C_{ext} = C_{abs} + C_{sca} \qquad 2.11$$

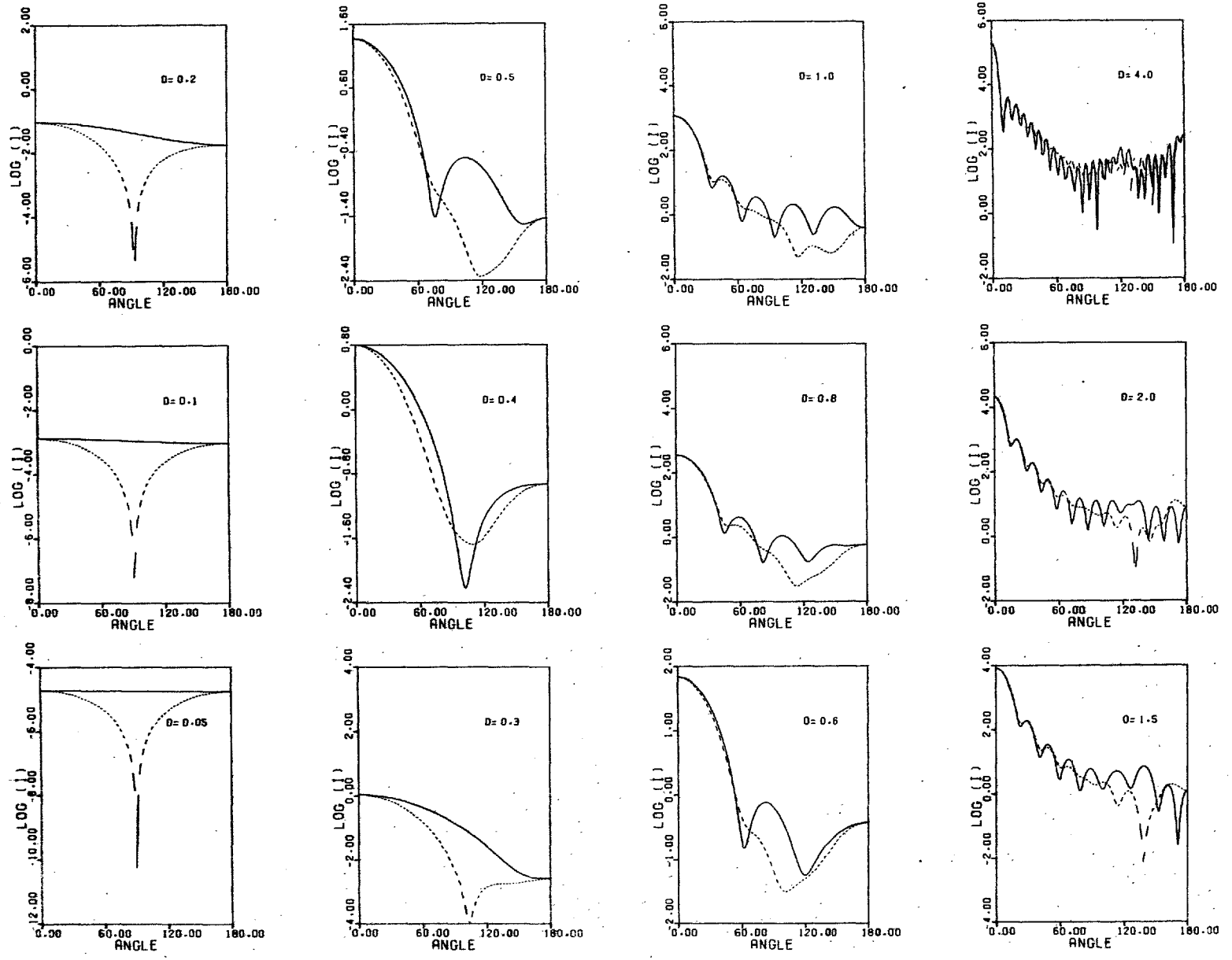

FIG. 2.5 Single Particle Scattering Diagrams for m = 1.19; Vertical Polarisation (solid line), Horizontal (dashed)

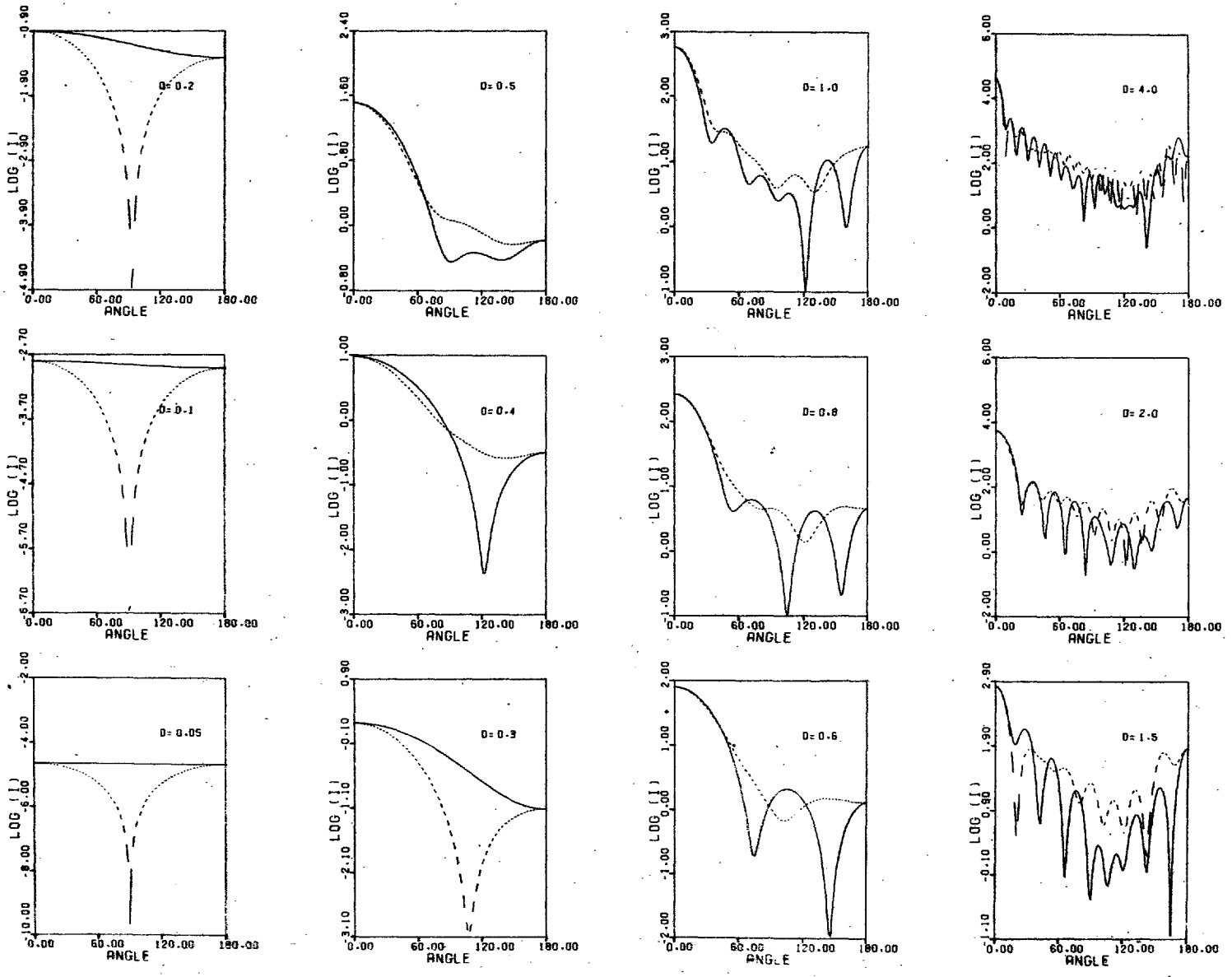

FIG. 2.6 Single Particle Scattering Diagrams for m = 1.52; Vertical Polarisation (solid line), Horizontal (dashed)

where the quantities C_{ext}, C_{abs}, C_{sca} are the particle cross sections for extinction, absorption and scattering respectively. Mie (1908) evaluated these cross sections for spheres from a consideration of the radial flow of energy over the entire surface of the particle:

$$C_{sca} = \frac{\lambda^2}{2\pi} \sum_{n=1}^{\infty} (2n+1) \left\{ |a_n|^2 + |b_n|^2 \right\} \qquad 2.12$$

$$C_{ext} = \frac{\lambda^2}{2\pi} \sum_{n=1}^{\infty} (2n+1) \left\{ \mathrm{Re}\,(a_n + b_n) \right\} \qquad 2.13$$

Whenever the electromagnetic momentum of an incident field is changed by absorption or deflection there is a resultant radiation pressure or force. Now the momentum removed from the original beam is proportional to C_{ext} and of this the part C_{abs} is not replaced but the part C_{sca} is partially replaced by the forward component of the momentum of the scattered light. The part of the forward momentum that is removed from the incident beam and not replaced by the forward scattered component is therefore proportional to:

$$C_{pr} = C_{ext} - \overline{\cos\theta}\; C_{sca} \qquad 2.14$$

where $\overline{\cos\theta}$, the asymmetry factor, is the mean of $\cos\theta$ with the angular intensity as the weighting function. Debye (1909) has shown that the asymmetry function may be expressed in terms of the scattering coefficients by:

$$\overline{\cos\theta} \qquad C_{sca} = \frac{\lambda^2}{\pi} \sum_{n=1}^{\infty} \left\{ \left[n(n+2)/(n+1) \right] \mathrm{Re}\, (a_n^{*} a_{n+1} + b_n^{*} b_{n+1}) + \left[(2n+1)/n(n+1) \right] \mathrm{Re}\, a_n^{*} b_n \right\} \qquad 2.15$$

where * indicates that the complex conjugate is to be taken.

The extinction cross section can be related to the transmission of a beam of monochromatic radiation through a suspension of uniform spherical particles. For a parallel beam of light traversing a dispersion of length L and having a concentration of N particles per unit volume the intensity is reduced according to the transmission equation which is similar in form to the Lambert-Beer Law,

$$T = I_L / I_o = \exp(-N C_{ext} L) = \exp(-\tau L) \qquad 2.16$$

where I_o is the incident intensity, I_L the intensity of the emerging beam at the distance L and τ the turbidity.

Dimensionless efficiency factors for scattering Q_{sca}, extinction Q_{ext}, absorption Q_{abs} and radiation pressure Q_{pr} are obtained by dividing the corresponding cross-sections by the actual geometric particle cross section, πa^2 in the case of a sphere. In general these factors depend on the orientation of the particle and on the state of polarisation of the incident light, but for spheres they are independent of both.

The extinction efficiency, and of course the scattering efficiency of dielectric spheres, exhibit the characteristic patterns shown in Fig.

2.7 where Q_{ext} is plotted against α for different refractive indices. It can be seen that Q_{ext} first increases to a maximum and then undergoes a damped oscillation about the limiting value $Q_{ext} = 2$. Superimposed on these oscillations is a further ripple structure which is more apparent at the higher refractive index.

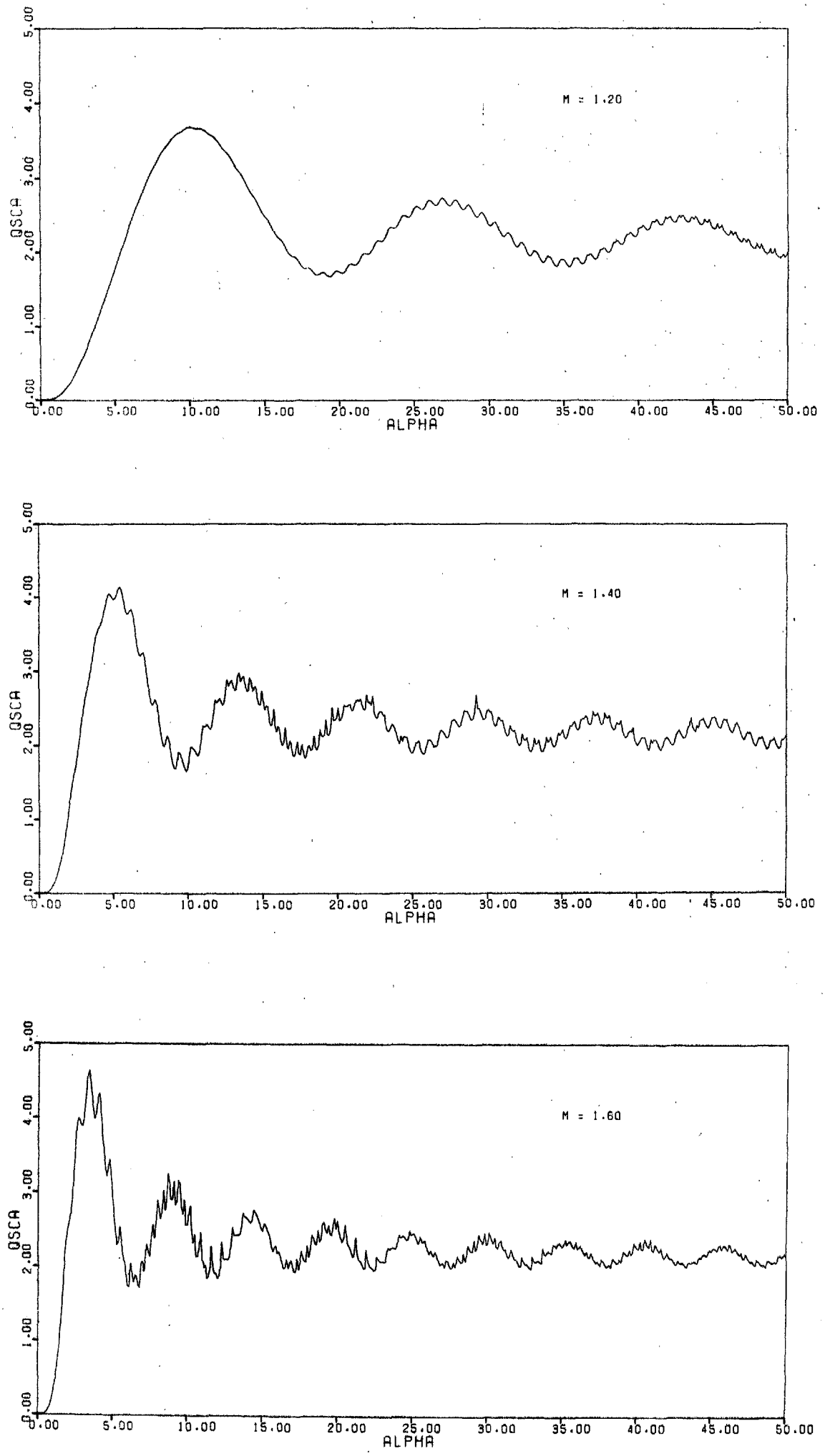

FIG. 2.7 Scattering Efficiency as a Function of Size Parameter for m = 1.2, 1.4 and 1.6

CHAPTER 3

Light Scattering Techniques for Particle Size Analysis

3.1 Introduction

In previous sections it has been shown how the scattering of electromagnetic radiation by spheres is dependent upon particle size, refractive index and wavelength of the incident light. It is now required to solve the inverse problem, that of determining particle size from scattering data.

The two major difficulties in applying light scattering techniques to particle size analysis are the complexity of the numerical computation of the scattering functions and the possible multivaluedness of the resulting scattering data with respect to particle size. The first of these deterrents has now been removed with the increasing availability of high-speed digital computers with large memory banks. This allows the rapid calculation of the scattering functions over the range of parameters required without the need to resort to interpolating the values from amongst the extensively published sets of tables.

With regard to the multivaluedness of the scattering data it becomes essential to consider the uniqueness of a particular solution. This applies especially when considering particle size distributions where there may be several sets of distribution parameters that satisfy the same scattering data within the experimental uncertainty.

In size analysis where a number of particles are present within the light scattering volume, the total scattered intensity is usually assumed to be the sum of the intensities of the waves scattered by each particle as if it were present alone. However, three additional effects

may be present which could result in the intensities not being directly additive; (i) interaction of the multipole fields of the particles if the interparticle spacing is less than several particle diameters (ii) long-range interference of the waves scattered by different particles (i. e. dependent scattering) if the particles are not randomly positioned (iii) multiple scattering, i. e. radiation scattered by one particle is incident upon a second particle which then rescatters it. It is usually possible to avoid these effects by diluting the system sufficiently so that the scattering results can be interpreted in terms of single particle scattering. Van de Hulst (1957) suggests that a transmission of more than 90% reduces concentration effects to negligible proportions. For a relative refractive index (m) of 1.5 this corresponds to a number concentration of approximately 4×10^{15} per m^3 for 0.1 μm diameter particles and 10^{11} per m^3 for 1.0 μm diameter.

Much of the early practical work involving light scattering by particles was performed with a view to verifying the Mie theory. Model systems of monosize particles (or more correctly dispersions with a very narrow size distribution) were prepared; for example using the aerosol generator developed by Sinclair and La Mer (1949), in order to show that the scattering by the particles could be accurately represented by theory.

The discussion which follows is concerned firstly with the techniques and their range of applicability for determining the average size of near monosize dispersions. After a brief digression to introduce the size distribution functions most commonly used in light scattering those techniques which have been used to measure distribution parameters are more fully outlined. Finally a brief summary is made of the use of light scattering for sizing non-spherical particles and particles undergoing coagulation.

3.2 Average Size Determination

The extinction or attenuation of a beam of light by a cloud of particles can provide a simple method of estimating a mean particle size, or the number concentration should the size already be known. For diameters up to approximately 2 μm, depending on the refractive index, the multivaluedness of the specific turbidity is reduced to the possibility of two values. By comparing measurements at a minimum of three wavelengths with the theoretical curve the size parameter can be obtained. The feasibility of using such methods for determining a mean size for near monodisperse colloids has been tested by Dezelic and Kratohvil (1961), Maron et al, (1963c) and Bateman et al. (1959).

Before discussing techniques involving the angular distribution of scattered light it is perhaps appropriate to define two of the more commonly used terms, namely the polarisation ratio and the scattering ratio. If the incident beam is unpolarised and an analyser used to determine the intensity of that component of the scattered beam which vibrates in the plane of observation, I_2, and perpendicular to it, I_1, respectively then the ratio of the two is the polarisation ratio ρ :

$$\rho = (I_2 / I_1)u \qquad 3.1$$

On the other hand if the total intensity of the scattered beam is determined for incident light which is polarised parallel and perpendicular respectively then the ratio of the two scattered intensities is the scattering ratio :

$$\sigma = (I_2 / I_1)p \qquad 3.2$$

Providing the scatterers are isotropic spheres $\rho = \sigma$ but should they for example be non-spherical $\rho \neq \sigma$.

The intensity of light scattered at a particular angle increases rapidly with particle size up to a maximum $\alpha = 2$ and then begins to oscillate as the size increases further. Tabibian and Heller (1958) have discussed the limitations of determining the particle size of polystyrene latexes from a single measurement of the scattered intensity at 90°.

Maddock (1970) has produced a series of graphs and polar diagrams which clearly show the complicated oscillatory nature with which the intensity function, for both horizontal and vertical orientation of the polarisation plane, varies with the angle of observation, a particular pattern being dependent on both the size parameter α and the relative refractive index. (See also Fig. 2.5 and 2.6).

The first and most successful application of light scattering, for sizing monodisperse spherical particles of known refractive index, has been for the diameter range 0.1 to 2 μm. As α increases from 0.3 to 2.0 the disymmetry ratio, namely $I(45^{\circ}) / I(135^{\circ})$, increases monotonically from 1 to 10. (Heller and Nakagaki, 1959; Kerker and Matijevic, 1960.) Similarly, the polarisation ratio increases from its value of $\cos^2\theta$ for small particles (Rayleigh regime) to a maximum at $\alpha \simeq 2.5$ (Kerker and La Mer, 1950; Kerker, 1950; Kerker and Hampton, 1953; Heller at al., 1961; Maron et al., 1963a). The location of the maxima and minima in the angular scattered intensity distribution has been successfully used for the analysis of dispersions of narrow size range (Maron and Elder, 1963a; Maron et al., 1963b; Pierce and Maron 1964; Nakagaki and Heller, 1960; Dezelic and Kratohvil, 1961). The measurements are all made at known wavelengths and the particle size determined by comparison with values from the Mie theory for spheres of the appropriate refractive index.

Incident white light when scattered by particles produces a series of spectral colours, known as higher-order Tyndall spectra (HOTS). The colours arise because the magnitude of the scattered intensity at any given angle and particle size is different for each wavelength. Since each particle of a particular size generates a characteristic band of colours the presence of a distribution of sizes leads to a washout of the colours. A similar washout also occurs if the particles exceed approximately 2 μ m. in diameter, the precise size being dependent on their refractive index.

Techniques using HOTS for size analysis, involving the location of the angular position of the red and green orders, have been developed by La Mer and co-workers; Sinclair and La Mer (1949), Johnson and La Mer (1947); and subsequently used by Kerker et al. (1963), Maron and Elder (1963b), Kitani (1960), Pierce and Maron (1964).

The variation in the angular distribution of the forward scattering lobe can provide a useful means of estimating the average particle size for $\alpha \geq 2$ (Hodkinson, 1966). The relative scattering at different angles within this lobe varies little with refractive index since the intensity is due primarily to the diffraction of the light passing near the particle rather than from rays undergoing reflection and refraction.

Full details of all these methods can be found in the references cited and in the many others listed in the reviews by Kratohvil, (1964, 1966) and by Kerker (1969).

3.3 Size Distribution Determination

3.31 Distribution Functions

A distribution or frequency function, p(a) will be defined such that

$$P(a) = \int_{a}^{a + \Delta a} p(a)\, da \qquad 3.3$$

gives the fraction of the population between a and a + Δ a. This function is normalised so that the integral over all possible values of a is unity.

To determine the entire shape of this distribution curve experimentally would require a great deal of experimental data of high precision. Therefore the values of a few parameters in an approximate presupposed equation are usually determined. This method is not unsatisfactory if the actual distribution has one maximum only.

The distribution functions most widely used in light scattering studies have been those defined by two parameters. Nakagaki and Shimoyama (1964) discussed the use of a three parameter distribution function for scattering at 45°, 90°, 135° but concluded the required experimental accuracy was excessively high and recommended the use of a two parameter function.

The normal distribution is probably the best known distribution function but it cannot truly represent a distribution of particle sizes because it admits negative values of size. This distribution is also symmetrical whereas naturally occurring populations are frequently skewed. These can usually be represented by a log-normal distribution as defined by:

$$p(a) = \frac{1}{(2\pi)^{\frac{1}{2}} \sigma_g a} \exp\left[- \frac{(\ln a - \ln a_m)^2}{2\sigma_g^2} \right] \qquad 3.4$$

In this distribution it is lna which is normally distributed; a_m being both the median and the geometric mean of a. The second parameter σ_g, the geometric mean standard deviation, is the standard deviation of lna.

A further distribution function has been used by Kerker and co-workers, although in their early work (Kerker et al., 1963; Espensheid et al., 1964 b) they still referred to it as the log-normal distribution. This function is characterised by a_M, the modal value of a, and σ_o which is a measure of the width and skewness of the distribution.

$$p(a) = \frac{\exp\left[-(\ln a - \ln a_M)^2 / 2\sigma_o^2\right]}{(2\pi)^{\frac{1}{2}} \sigma_o a_M \exp(\sigma_o^2 / 2)} \qquad 3.5$$

The relations between these two parameters and the mean ($\bar{a}$) and the standard deviation (σ) are given by:-

$$\ln \bar{a} = \ln a_M + 1.5 \sigma_o^2 \qquad 3.6$$

$$\sigma = a_M \left[\exp(4\sigma_o^2) - \exp(3\sigma_o^2)\right]^{\frac{1}{2}} \qquad 3.7$$

For a sufficiently narrow distribution ($\sigma_o << 1$) the latter equation reduces to

$$\sigma = a_M \sigma_o \qquad 3.7a$$

Espenscheid et al. (1964a) have described the properties of this function which they term the zeroth-order logarithmic distribution (ZOLD) function. Curves of ZOLD functions are plotted in Fig. 3.1 adjacent to a set of log-normal curves for the same range of the two characterising parameters. It can be seen that for a ZOLD function the maximum frequency of a remains invariant as the width of the distribution changes. Espenscheid et al.(1964a) also describe a generalised logarithmic function which allows selection of other moments of the distribution e.g. mean size, mean surface area, as the parameter appearing explicitly in the distribution function.

A less familiar type of distribution has been adopted by Heller and his co-workers (e.g. Stevenson et al., 1961) in their light scattering studies. This is defined by:-

$$p(a) = c(a-a_o) \exp - \left[(a-a_o) / s \right]^3, \quad a \geq a_o \qquad 3.8$$

$$= 0, \quad a < a_o$$

where c is the normalisation constant, a_o is the smallest particle present in significant numbers while s determines the modal radius a_M, the half-width w and the "half-spread" (a_M-a_o) through the relations:

$$w = 0.9015s \qquad 3.9$$

$$a_M-a_o = 3^{-1/3} s \qquad 3.10$$

The half-width is the distance between the two points of the distribution curve at which the frequency is half the value at the modal radius.

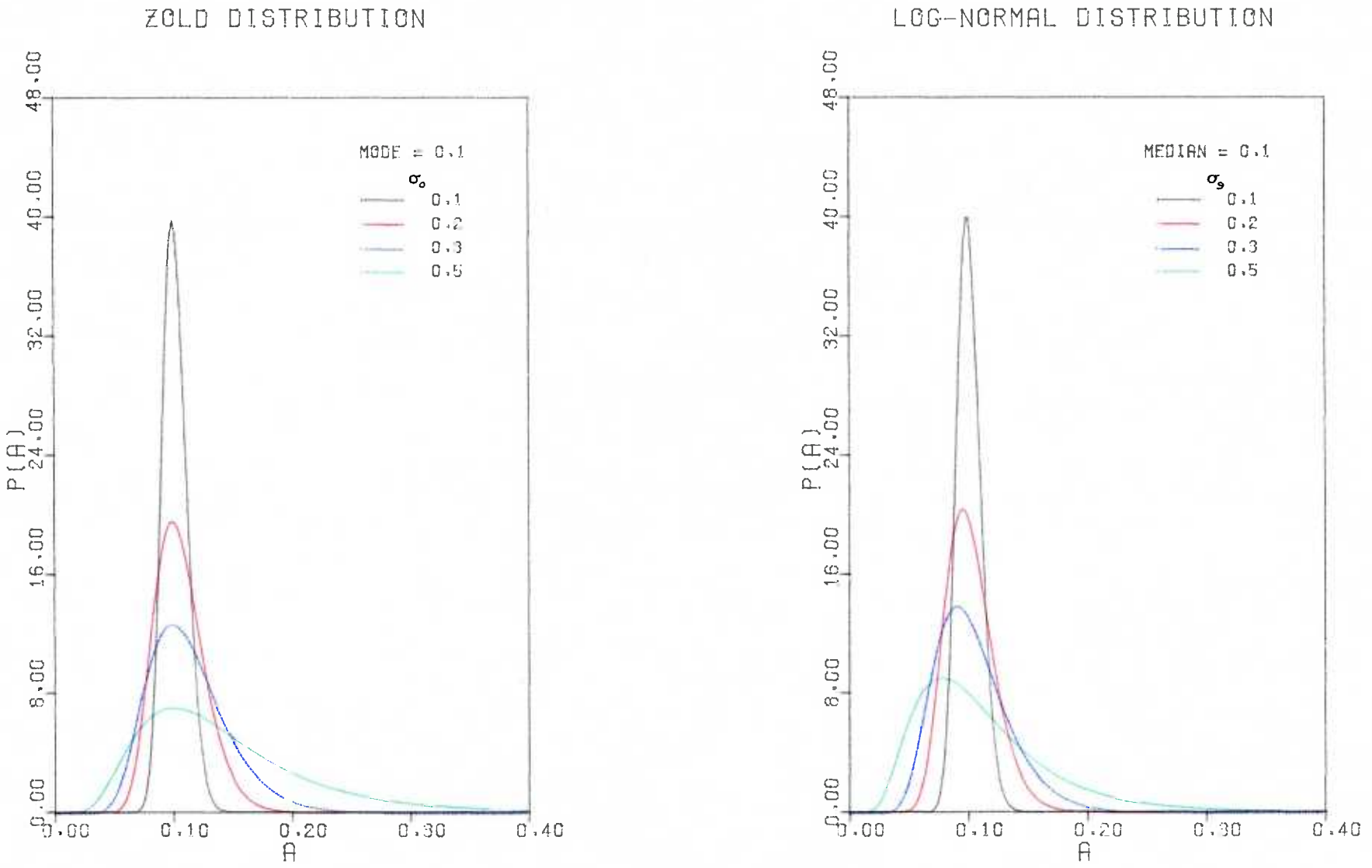

FIG. 3.1 Comparison of Distribution Functions

3.32 Techniques for Size Distribution Determination

The polarisation ratio measured at a number of different angles using monochromatic light has been used extensively by Kerker and co-workers to determine the size distribution of a number of different dispersions of spherical particles (Kerker et al., 1963, 1964; Matijevic et al., 1964; Espenscheid et al., 1964b; Kratohvil and Smart, 1965; Jacobsen et al., 1967; Coutarel et al., 1967; Rowell et al., 1968). The procedure was to compare experimental measurements for each observation angle with the corresponding theoretical values for an extensive array of over 6,000 combinations of α_M and σ_o in order to find a pair of these for which the mean square deviation between experiment and calculation was a minimum. In general, for the range searched α_M 1.9 (0.1)15.0; σ_o 0.005(0.005)0.155 and 0.16(0.01)0.3, a unique solution was always found. It would appear, however, that σ_o = 0.3 represents the upper limit of the polydispersion for which this method is applicable (Wallace and Krathovil, 1967).

Stevenson et al. (1961) based their method upon the variation with wavelength of the scattering ratio at a single angle. By comparing the normalised experimental results with the various theoretical values in a similar type of "grid-search" technique to that adopted by Kerker, an estimate of the distribution parameters was arrived at. Heller and Wallach (1963, 1964), who studied the size distribution of polystyrene latexes by this method, found polarisation spectra sensitive to changes in the smallest size a_o and provided the degree of polydispersity was moderate, there was no loss of sensitivity as the particles became large compared with the wavelength ($a_o \simeq 4\mu m$).

Turbidity spectra have been used, Wallach et al. (1961), in a procedure analogous to the polarisation spectra for the purpose of size analysis. This method has been further tested by Wallach and Heller

(1964) who found that provided the size of the smallest particles was less than 0.5μm. the sensitivity of turbidity spectra was retained even at relatively high degrees of dispersity (a half-width of 0.5μm.). The main draw backs were the approach of the scattering efficiency to its limiting value of two when the particles were large compared with the wavelength and the possibility of multivaluedness of the results, Maxim et al. (1966). Other turbidimetric methods using from two to four wavelengths only have been adopted with moderate success by Meehan and Beattie (1960) and by Gledhill (1962).

All the techniques previously described required an a priori assumption of an analytic expression for the distribution curve. One method put forward by Gumprecht and Sliepcevich (1953) does not suffer from this limitation but does require that the particles be sufficiently dense relative to the ambient medium and sufficiently large that differential settling measurements can be made. By recording the time rate of change of the optical transmission the frequency function of the distribution can be determined directly. A second method based upon the angular variation of the intensity of forward scattered light at very small angles and at a single wavelength has been proposed by Chin et al. (1955). They successfully evaluated the size distribution of a polydispersion consisting of glass spheres from 2 - 40 μm. in diameter which is considerably larger than can be successfully handled by the polarisation ratio and scattering spectra or turbidity spectra methods.

3.33 Non-Spherical Particles and Coagulating Systems

Provided that the phase shift corresponding to any point in the particle is negligible (i.e. $2ka(m-1)<1$) the Rayleigh -Gans-Debye theory can be applied to any shape of particle, including multiplets

of spheres. The only difficulty is to evaluate the appropriate form factor for the shape in question (see Section 2.3).

Napper and Ottewill (1963, 1964) have examined in detail the deviations obtained between experimental values of scattering by silver bromide hydrosols consisting of either cubes or octahedra and the results calculated on the assumption that these particles scatter as equivalent spheres. In calculating the various light scattering properties the radius of the equivalent sphere was taken to be half the face diagonal for the cube and the distance from the centre to a corner for the octahedra. There was reasonably good agreement between the experimental and calculated values of the turbidity for both shapes, and the angular intensities for the octahedral particles, but considerable discrepancy in the angular intensities for the cubes.

The specific turbidity at two wavelengths has also been found (Walton and Hlabse, 1963) to yield a good size estimate for irregularly shaped particles of barium sulphate.

Experimental studies, using optical methods, of the kinetics of coagulation of both hydrosols and aerosols have in general been restricted to following the time rate of change of the total number of particles in the system. A precise interpretation of the results requires a knowledge of both the variation of the number concentration of each size of aggregate with time and of their light scattering properties. The coagulation theories of Smoluchowski (1917) and Müller (1928) can be used to predict the growth of an aerosol as a result of Brownian motion.

If the model is restricted to spherical particles which coalesce upon impact to form larger spheres then the rigorous Mie theory can be applied to evaluate the light scattering properties of the aerosol. This approach has been used to evaluate the effect of Brownian coagulation on the light scattering of colloidal dispersions, Willis

et al. (1967) and Chao-Ming Huang et al. (1970), and subsequently to follow the changes in particle size distribution of a coagulating system of dibutyl phthalate, Nicoloan et al. (1972). Where the dispersion consists of solid particles this approach, although physically unrealistic, has proved useful in giving a relative measure of colloidal stability, Ottewill and Shaw (1966).

For particles with refractive index close to that of the dispersion medium the scattering properties of aggregates can be evaluated using the R-G-D theory (see Section 2.3). Primary particles within an aggregate are assumed to be independent scatterers and the light scattered by each interferes with that scattered by its neighbours. The intensity of the light scattered at an angle θ by an aggregate of k monodisperse spheres randomly oriented to the incident light beam can then be expressed as:

$$I_k(\theta) = k I_{sp}(\theta) \left[1 + P(k) / k\right] \qquad 3.11$$

where $I_{sp}(\theta)$ is the intensity of light scattered at an angle θ by a single primary sphere and P(k) is a configurational or form factor which is a function of the geometry of the aggregate and of the scattering angle θ. The form factor for two scattering centres, separated by a distance x is given by:

$$P(2) = \frac{2 \sin hx}{hx} \qquad 3.12$$

where

$$h = \frac{4\pi}{\lambda} \sin(\theta / 2) \qquad 3.13$$

For an aggregate of more than two spheres the form factor is the vector sum of all the vectors between pairs of scatterers.

Assuming the individual particles, whether they be singlet spheres or aggregates of spheres, scatter independently the intensity of light scattered by the system is:

$$I(\theta) = I_s(\theta)\left[1 + \sum_{k=2}^{\infty} (\upsilon_k / \upsilon)\, P(k)\right] \qquad 3.14$$

where $I_s(\theta)$ is the scattered intensity that would be obtained if all of the υ spheres were singlets. Each of the terms in the summation corrects for the effect of having υ_k particles of the k^{th} configuration.

Since this is an interference treatment Eqn. (3.11) and (3.14) are independent of the polarisation of the incident light. During coagulation therefore the polarisation ratio at all scattering angles should remain constant and independent of the amount of aggregation, in marked contrast to the changes predicted by the coalescing sphere models, Kerker (1972).

The form factors, and hence the scattering properties of the aggregate, depend upon the geometrical arrangement of the spheres within the aggregate. Now, since there will be an infinite number of possible arrangements for a coagulating sol the precise evaluation of Eqn. (3.14) is not feasible. However, using form factors evaluated for separation distances of two and four times the radius of the single sphere, Wippler et al. (1959) and Benoit et al. (1962) were able to determine the degree of aggregation, expressed as an average particle weight, of a coagulating P.V.C. latex. In their recent study of a rapidly coagulating polystyrene latex, Lips et al (1971) assumed the presence of linear, planar and three-dimensional close-packed aggregates in equal proportions when evaluating form factors for

aggregates of up to thirteen spheres. They further found that the polarisation ratios did not change even after extensive coagulation but remained in agreement with those calculated from the Mie theory for the single spheres.

CHAPTER 4

Development of the Light Scattering Instrument and the Associated Data Inversion Technique

4.1 Criteria for Choice of Method

In order to obtain a detectable level of scattered light from sub-micrometre particles present in low concentrations a high intensity light source was required. A He - Ne laser which produces a high intensity light beam that is also linearly polarised, coherent, monochromatic and parallel therefore has a considerable advantage over conventional light sources. Harris (1969) has shown that the best xenon source after collimation, polarisation and filtering for a 10 nm. band at the 632.8 nm. wavelength gave only the same intensity as obtained when a 1 mW He-Ne laser was operated at 1/30 mW. Experimental work (Harris et al. 1967; Sherman et al. 1968) has also indicated that there are no differences larger than the limits of data reproducibility in scattering behaviour between conventional incoherent light and coherent laser light sources.

A light scattering technique was needed in which a set of scattered intensity measurements at a number of angles could be completed in a relatively short period (a few seconds) and then repeated for a chosen number of scans. This requirement eliminates the polarisation ratio, scattering ratio or turbidity spectra methods, previously discussed in Section 3.3, which have been developed to study essentially stable dispersions with conventional light sources.

Using a laser light source the former method would require rotating the angle of polarisation through 90^{o} at each observation to record both the horizontal and vertical components of the scattered light while the other two techniques necessitate repeated retuning of the laser to one of its principal operating wavelengths.

The alternative is to record scattered intensity levels at a series of angles for a particular wavelength and orientation of the polarisation. This can be achieved by a light detector scanning round a range of angles, by positioning a detector at each angle or by altering the direction of the incident light relative to a single fixed detector.

The manual method of moving the photomultiplier tube adopted by Maddock (1970) was found to be too slow to follow aerosol formation by chemical reaction, and the moving parts were too cumbersome to be moved automatically with sufficient precision. The second alternative using multiple detectors requires either a number of matched photomultipliers or calibrated response curves for each tube, and a multi-channel data logging system which is unnecessarily complex and costly. It was therefore expedient to design and develop a new instrument incorporating a laser light source, a single stationary photomultiplier and a mirror system to direct the incident beam at varying angles into the aerosol under investigation.

4.2 Complications Arising in Angular Light Scattering Measurements

Before discussing the technical details of the light scattering instrument a brief review of the complications that have to be contended with in studies on the angular variation of scattered light will be made.

The optically effective scattering volume consists of all the volume elements which contribute to the observed scattering effect at a given angle of observation with respect to the incident beam. Considering a cylindrical cell uniformly full of aerosol and illuminated by a parallel beam of light, as indicated in Fig. 4.1, then the light scattered within the volume V_o makes the main contribution to the light received at the photodetector P, while the contributions from the remainder of the scattering volume V_1 decrease as one approaches the extremities of this volume at x_1 and x_2. Due to the widely differing statistical weight of these contributions it is almost impossible to define accurately the optical volume for the purpose of absolute measurement of the scattered intensity as a function of angle. Only in the idealised situation when a parallel beam is received at the detector does the scattering volume vary in direct proportion to $\sin\theta$ i.e.:

$$V_\theta = V_{90} / \sin\theta \qquad 4.1$$

This situation can be approached for example by the introduction of a double stop into the path of the scattered light and by increasing the optical path from detector to cell ($P\text{-}C_1C_2$).

If the particle concentration is not sufficiently small (how small depends, for a given wavelength and medium, very much on the refractive index and size of the scatterers) both turbidity and multiple scattering begin to cause complications. Using Fig. 4.1 as reference and considering firstly effects on the intensity of scattered light, there is a loss of intensity due to turbidity in the primary beam A to x_2 and in the scattered beam emerging from V_1 before reaching the

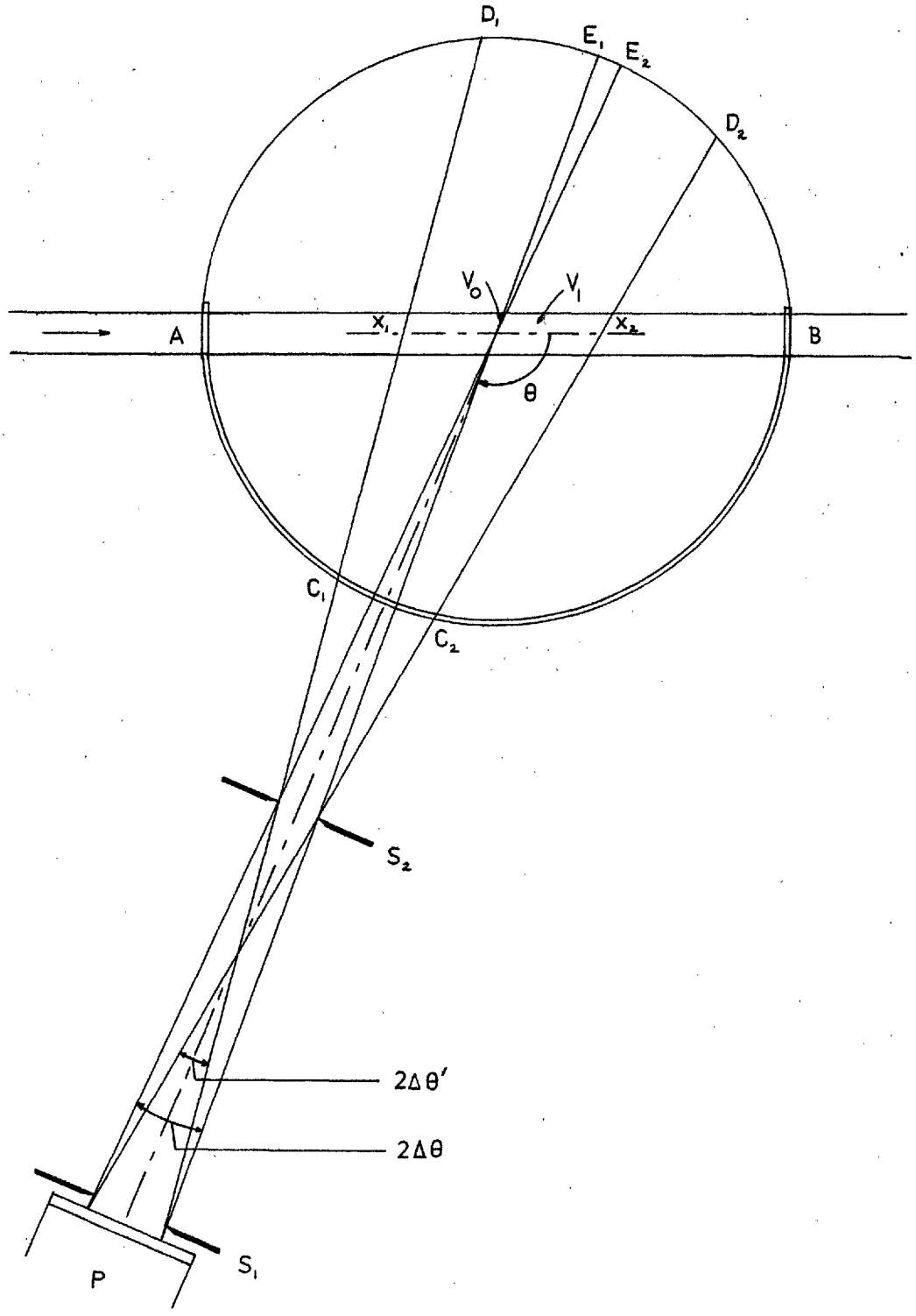

FIG. 4.1 Schematic Representation of Complications Arising in Angular Light Scattering Measurements

cell exit C_1C_2. This loss is partly compensated by small angle scattering within these two illuminated volumes, an effect which becomes more pronounced the larger the scatterers relative to the wavelength. The final complication is the secondary light for which the primary scattered light is the source, i.e. multiple scattering. Although this secondary light has a relatively very weak intensity per unit volume of the scattering system, this is partly offset by the considerably larger volume, as represented by the cross-section $C_1C_2D_2D_1$, from which the secondary light reaches the detector. To obtain significant results on the angular variation of scattered light the particle concentration should be made as low as is compatible with the collection of reasonably precise results or the data should be extrapolated to zero concentration, although some difficulties may be encountered in the latter case, Heller and Tabibian (1962).

Theoretical data on light scattering are computed for a specific angle Θ, whereas experimental data pertain to an angular range $\Theta \pm \Delta\Theta$. Consequently, even in the limiting case of a very small volume (V_1) or of a very large photometric distance (V_o-P) the light received at P includes radiation scattered within a finite solid angle ω_o, of which Fig. 4.1 shows the planar projection $2\Delta\Theta$. Should these limiting conditions not apply the solid angle varies from element to element within the scattering volume, the extreme solid angle being defined by the planar equivalent $2\Delta\Theta' > 2\Delta\Theta$. Operating with too large a solid angle results in a flattening out of the angular scattering maxima and minima. This gives the erroneous impression of a more polydisperse system in qualitatively the same way as operating with too high a concentration.

The scattering effect measure at P for the angle $\Theta \pm \Delta\Theta$ is primarily that produced by the incident beam illuminating the volume

V_1, but also includes an additional scattering increment due to light reflected back into it from the exit window B and scattered at the complementary angle $\left[180-(\theta \pm \Delta\theta)\right]$. If, as is assumed in Fig. 4.1, the cell is cylindrical then the scattered light received at P contains a further increment resulting from scattered light being reflected back from between D_1 and D_2. The magnitude of these two effects depends upon the refractive indices of the cell window and the media on either side and on the degree of dissymmetry of the angular intensity distribution. These reflection complications can be allowed for by the use of suitable correction equations (Kratohvil 1966) or, as will be described later, by using a specially moulded light trap.

4.3 Instrumentation

4.31 Mechanical and Optical Systems

The general arrangement of the instrument is shown schematically in Fig. 4.2. The plane mirror at position A is rotated by a stepper motor, having an incremental angular advance of 3.75°, about an axis perpendicular to the plane of the diagram. The beam from the laser, L, is reflected sequentially by this mirror on to a series of static plane mirrors, M, at the positions numbered. From each of the latter mirrors the beam is directed back to pass through the centre of the scattering system at C. A photomultiplier, at either of the positions PM, detects the light scattered by the aerosol within the illuminated volume. In order to keep the path length and hence the total beam divergence at the scattering volume constant the positions of the static mirrors lie on an ellipse with the principal foci at A and C. The scattering angles range from 8° to 172° and have a precision of $\pm$ 20 minutes, determined by the stepper motor currently in use. The laser beam and the line C-PM define the plane of observation, the horizontal plane of the instrument.

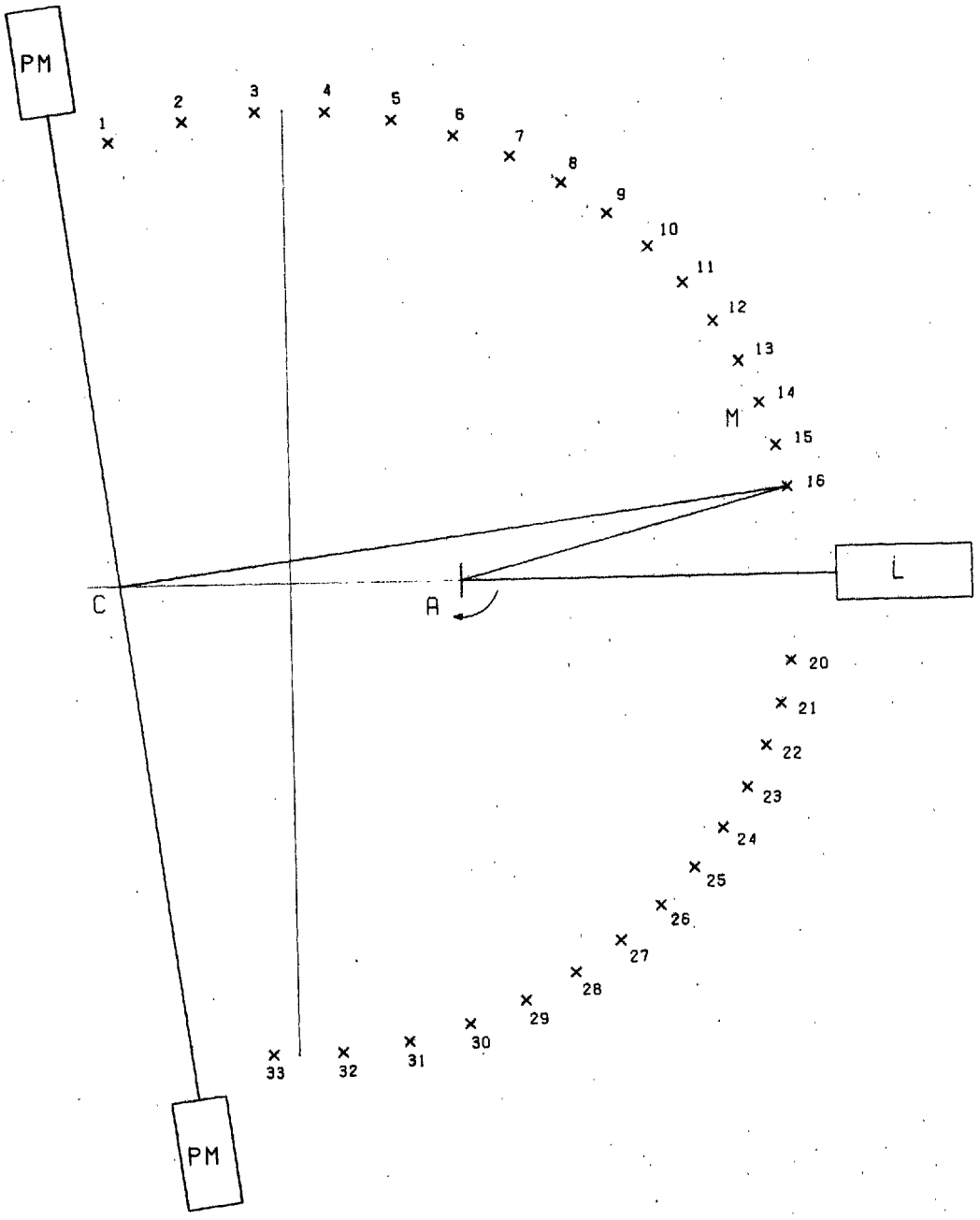

FIG. 4.2 Schematic Plan View of the Optical System

A Rotating Mirror; C Scattering Cell; L Laser

M Static Mirrors; PM Photomultiplier

This is perhaps better illustrated in the side view of Fig. 4.3 which also indicates how the mirrors and stepper motor are mounted on to the $\frac{1}{2}$ inch thick metal base plate. Also, beneath the base plate is the optical start position detector consisting of a small infra-red source and detector and a collar attached to the motor spindle with a small hole drilled through offset from the centre as shown in Fig. 4.4. This system is used to uniquely define a reference or start position for the stepper motor.

The light source is a Spectra Physics 15mW continuous helium-neon laser giving out a monochromatic beam at a wavelength of 632.8 nm linearly polarised to better than 1 part in a 1000. The plane of polarisation of the output can be rotated through a calibrated angle of 360° with an accuracy of $\pm 0.2^{\circ}$ by means of a polarisation rotator, incorporating a half-wave plate, attached to the laser.

Expansion of the beam from its initial diameter of 1.7 mm is achieved using two quality microscope objectives and a pinhole aperture arranged as shown in Fig. 4.5. The pinhole, with an aperture diameter in the region of 10μm. eliminates spatial noise thereby producing a smoth Gaussian intensity profile across the final collimated beam.

Plane front surface mirrors comprise the remainder of the optical system. These have an additional protective coating which although decreasing the reflectance by 1 or 2% facilitates cleaning without damage to the reflective surface. Precise alignment of the static mirrors is effected by three-point adjustable spring mountings. An exploded view of a mirror assembly is shown in Fig. 4.6.

An E.M.I. type 9658 modified S20 photomultiplier having a quantum efficiency in the region of 10% at the helium-neon wavelength (632.8) is employed to measure the scattered light intensity. It is operated by a regulated high voltage dc power supply, normally at -900V,

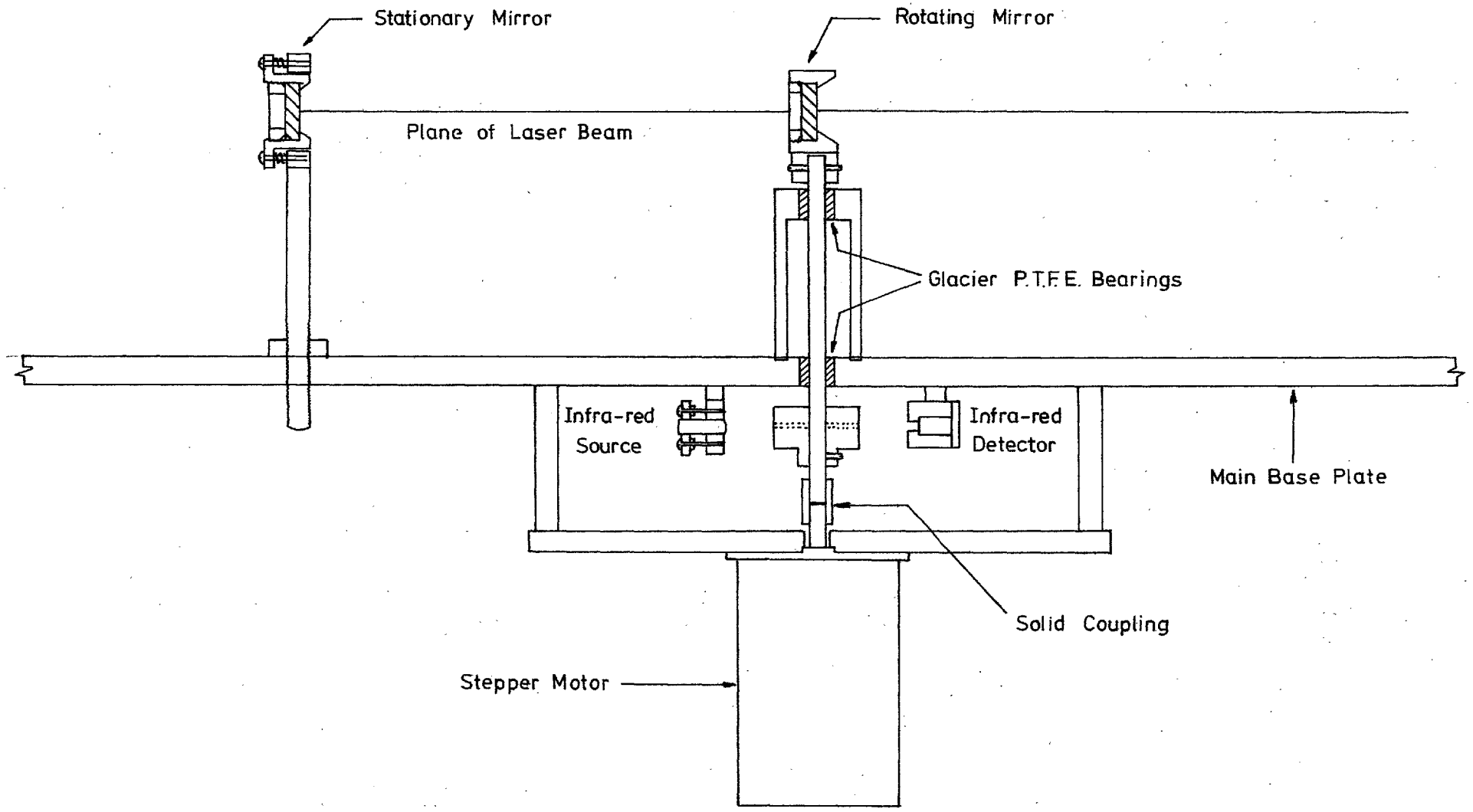

FIG. 4.3 Side Section through the Instrument

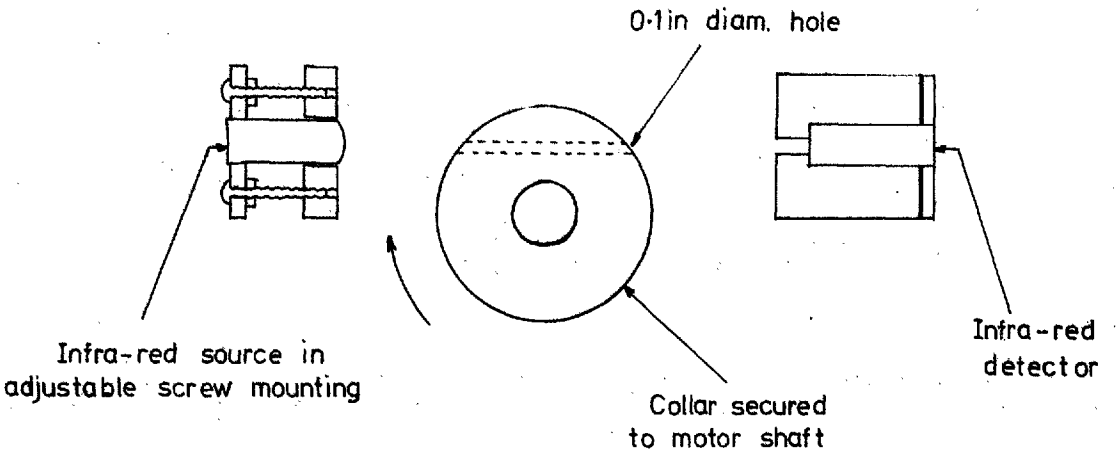

FIG. 4.4 Optical Start Position Detector System

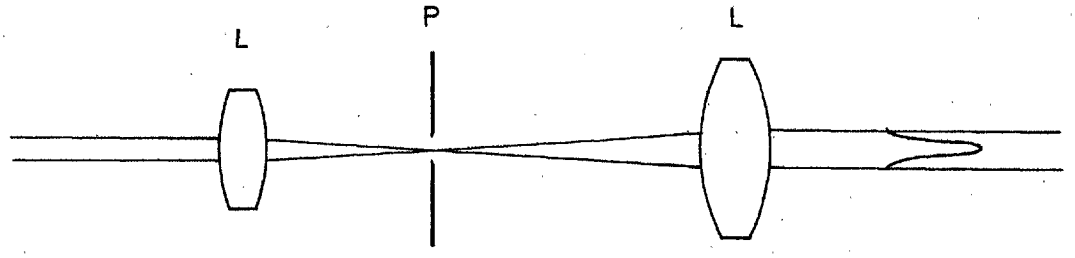

FIG. 4.5 Beam Expander and Spatial Filter

L microscope objective with screw adjustment for centring and vernier adjustment for focussing.

P pinhole aperture with vernier vertical and transverse adjustment.

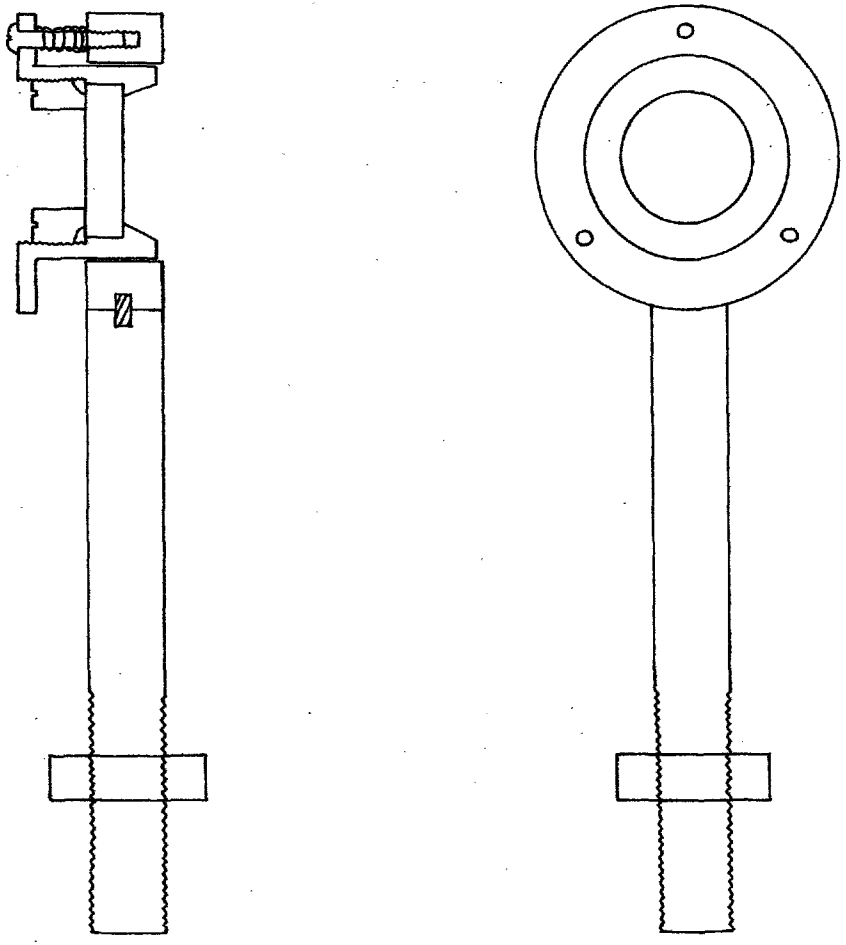

FIG. 4.6 Mirror Assembly

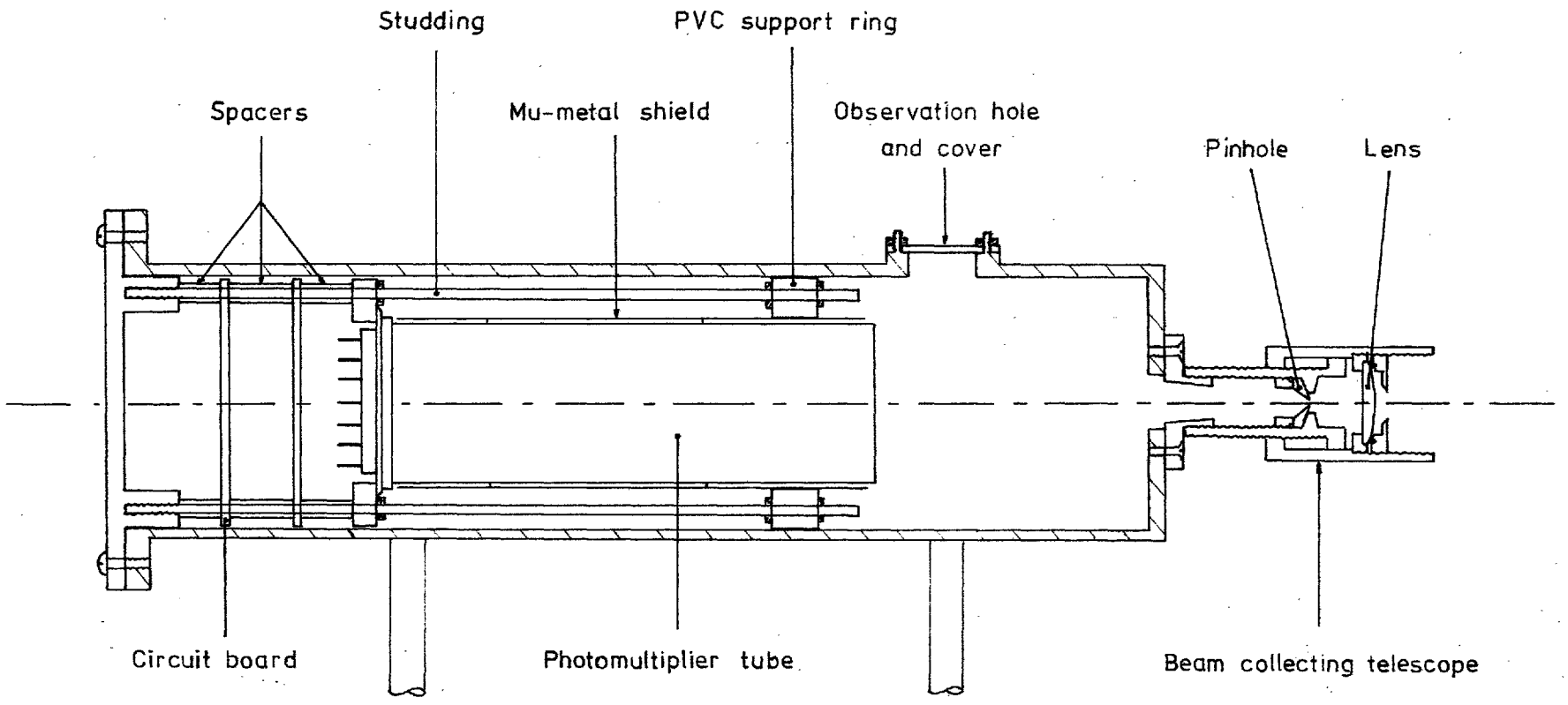

FIG. 4.7 Scattered Light Receiving System

and housed in a specially designed casing incorporating a mu-metal shield and the collecting telescope, the dimensions of which define the field of view of the detector (Fig. 4.7).

4.32 Scan Control and Data Acquisition

A block diagram of the control circuitry governing the stepper motor is shown in Fig. 4.8. The motor moves through 3.75^{o} at each step which corresponds to a movement through 7.5^{o} for the reflected beam. When a full scan is required to have eight angular stations, four steps are necessary between each station, and for sixteen stations, two steps. Provision is made for half scans and for the peripheral mirrors to be used in 'odd' as well as 'even' numbered positions.

The control logic is performed by standard integrated circuit techniques, the stepping rate and timings being derived throughout from the mains frequency with basic clock pulses at 100 Hz. The 'start' command releases the clock inhibiting gate to enable the motor to step continuously at the maximum rate (100 steps per sec.) until the infra-red start detector halts it at the start position. The rotating mirror then follows the stepping pattern according to the pre-set scan programme controls. A delay of 300 ms occurs before the first sample reading of the light intensity is taken at each new station, giving time for internal resets. The time interval between subsequent readings is 200 ms. The motor is stepped to a new station when the time interval for the set number of readings, which can be up to eight at each station, has elapsed.

A count of the number of steps taken determines the end of each scan, whereupon the mirror is rapidly stepped round to the start position and the scan programme repeated. Selection of 'end' inhibits the clock upon completion of the current scan, while 'stop' halts the motor immediately and no further readings are taken. The 'continuous sample' switch allows continual sampling of readings

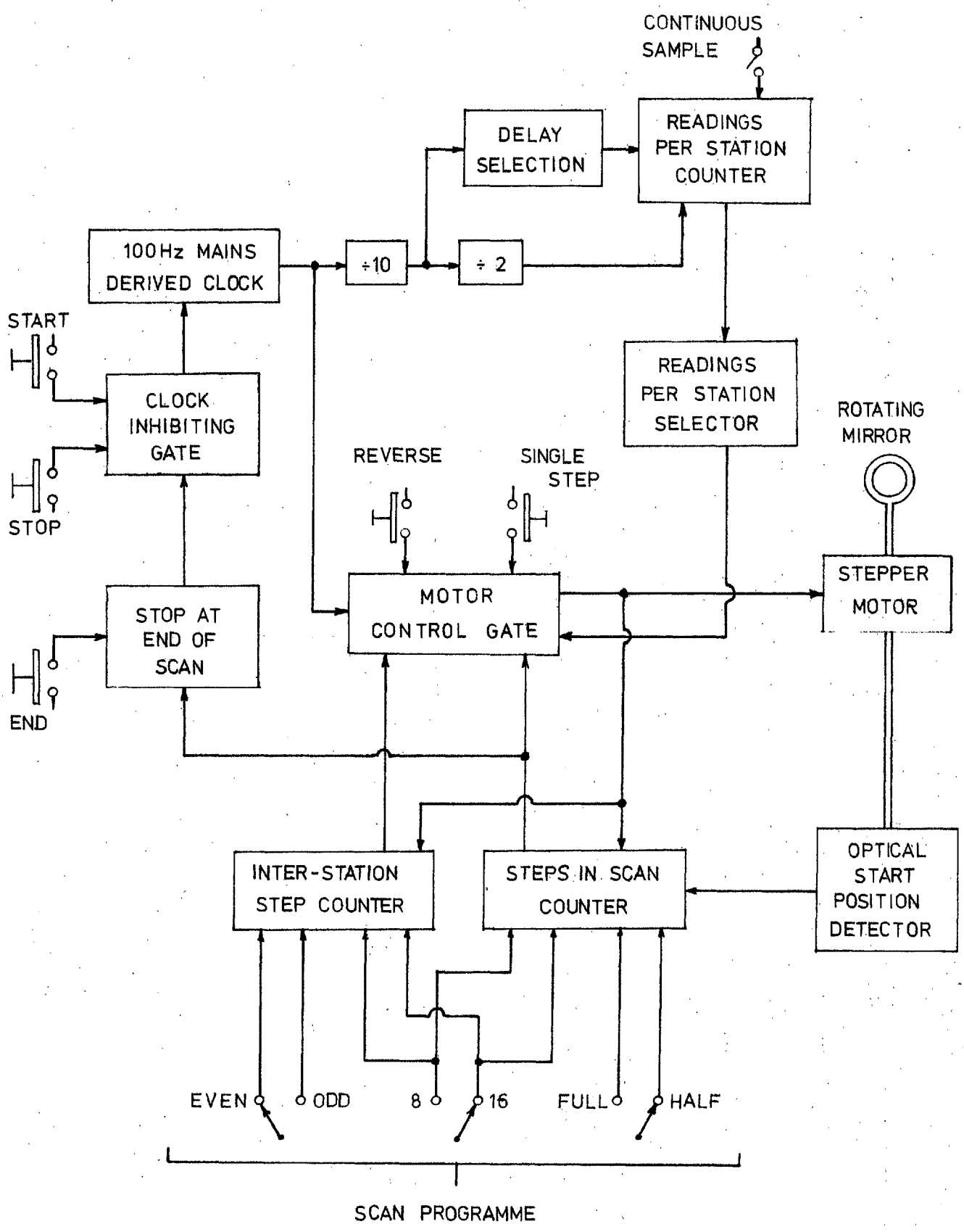

FIG. 4.8 Block Diagram of the Electronic System Controlling the Angular Scanning

at a single angle. Both the number of the current scan and the angular position are visually displayed on serial counters.

The scattered light intensity, proportional to the voltage output of the photomultiplier, is measured by a digital voltmeter and recorded on paper tape for subsequent analysis. The voltmeter is triggered externally to take sample readings at each station at 200 ms intervals by pulses from the control unit. Due to the possibility of orders of magnitude changes in the measured light intensity at consecutive angles it is always operated in the automatic range changing mode. Occasionally, when a double range change is required between readings, the time for that sample period extends beyond the normal 200 ms. The number of readings per station will thus be reduced by one each time this happens but readings remain accurate throughout since the trigger within the voltmeter becomes active only after the completion of a sample period so that a trigger pulse incurred during a sample period does not cause problems. The format of the paper tape output is controlled by pulses from the control unit; thus a line feed occurs before the first reading at each new station, a space between each reading and a double line feed indicates the end of a scan. This type of configuration greatly assists in decoding the data from the paper tape for an experimental run involving a considerable number of stations and scans.

4.33 Instrument Alignment and Operation

Optical alignment of the instrument is accomplished by first orientating the laser so that the beam is at the correct height and reflected from the approximate centre of the rotating mirror at right

angles to its axis of rotation. The static mirrors are positioned according to the desired scan programme and set approximately for height and direction using the screw thread adjustment. By releasing the securing screws and twisting the rotating mirror mount independently of the motor spindle the beam can be aligned so that the position number 16, for example, as indicated by the control unit corresponds to the 16th mirror position. This is a once only operation required to define the start position of the optical position detector relative to the static mirrors. Using a pointer of the correct height at C in Fig. 4.2 the reflected beams from each static mirror are in turn accurately aligned.

Once all the static mirrors are set up the pointer is moved to its peripheral position on the line C - PM being replaced with a mirror assembly mounted centrally on a small goniometer (Fig. 4.11). The laser beam is reflected off this mirror to align with the new pointer position and the image of the shadow thus formed positioned centrally on the face of the photomultiplier tube by transverse and vertical movement of the photomultiplier housing.

A second stop is then set up, as near to C (Fig. 4.2) as is practical when the scattering cell is in position, and aligned with the reflected beam. Having a slightly smaller diameter than the laser beam to reduce the effect of marginal vertical misalignment of the mirrors, it reduces the angular field of view of the photomultiplier to a half-angle of approximately 0.4°.

The goniometer pointer, having a rotary movement with a fine adjustment and a vernier reading to 0.1°, is successively aligned with the incident and reflected beams. The angular difference then gives an estimate of the scattering angle to within 0.4° as determined by the stopping accuracy of the stepper motor.

A further requirement is that each incident beam should have the same intensity as it enters the scattering cell. In order to check this a photodiode was set up at the scattering centre to measure the intensity of each beam. A second series of measurements was made with a Polaroid analyser placed in front of the diode and orientated to allow only the transmission of light polarised in the same direction as that emitted by the laser (i.e. perpendicular to the plane of the instrument). During both checks the intensity, as measured by the diode, varied by less than 2% over the complete angular range, the fluctuations being independent of the incident angle on the reflecting mirror.

Provision was also made for monitoring the intensity of the expanded laser beam by utilising a thin glass plate as a beam-splitter to provide light flux for a reference photodiode. The output from the diode could either be displayed on a chart recorder as a function of time or used as an input to the digital voltmeter to provide the denominator in ratio measurements where the numerator was the scattered intensity measured as described earlier. The latter method also has the effect, due to the increase in measuring time required by the voltmeter, of halving the pre-selected number of readings per station.

4.34 Light Scattering Cell

The light scattering instrument, described in the previous sections, was multi-purpose designed to allow variation of the manner in which the particles to be sized are contained within the intersecting light beam paths. This can include flow systems where the particles are contained by an outer sheath of inert carrier gas or specially constructed scattering cells of various geometries.

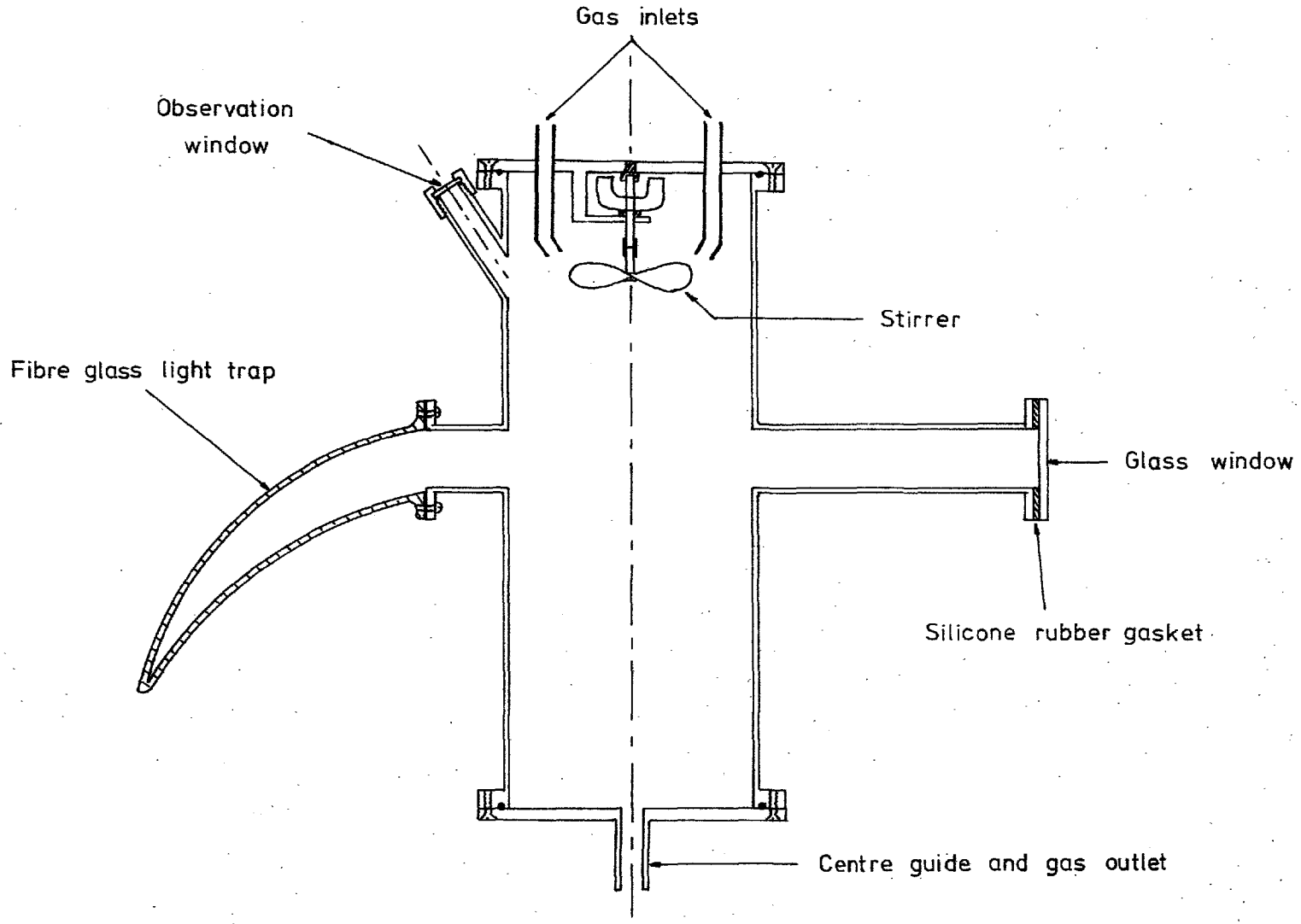

FIG. 4.9 Section through Scattering Cell

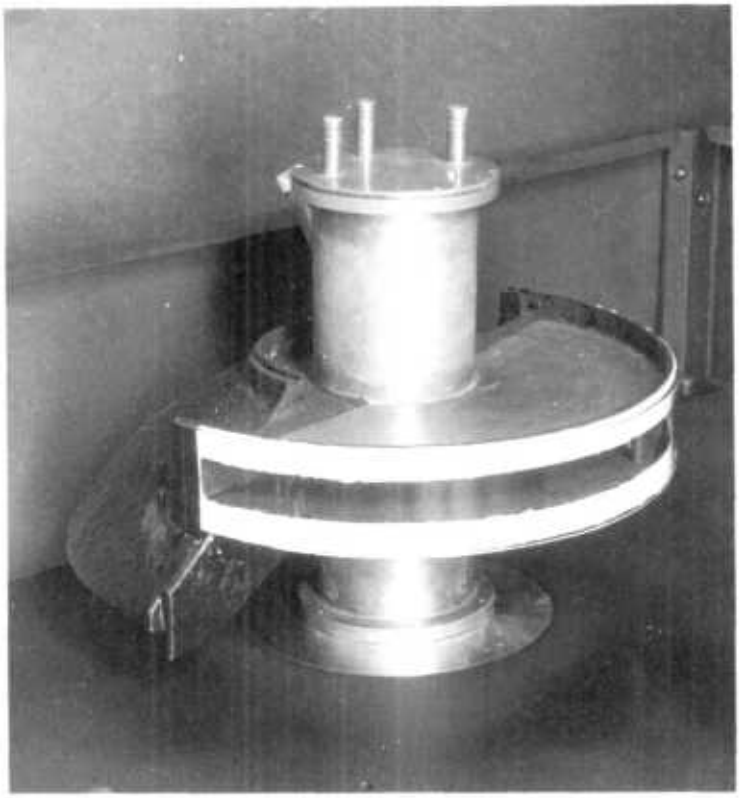

FIG. 4.10 Scattering Cell

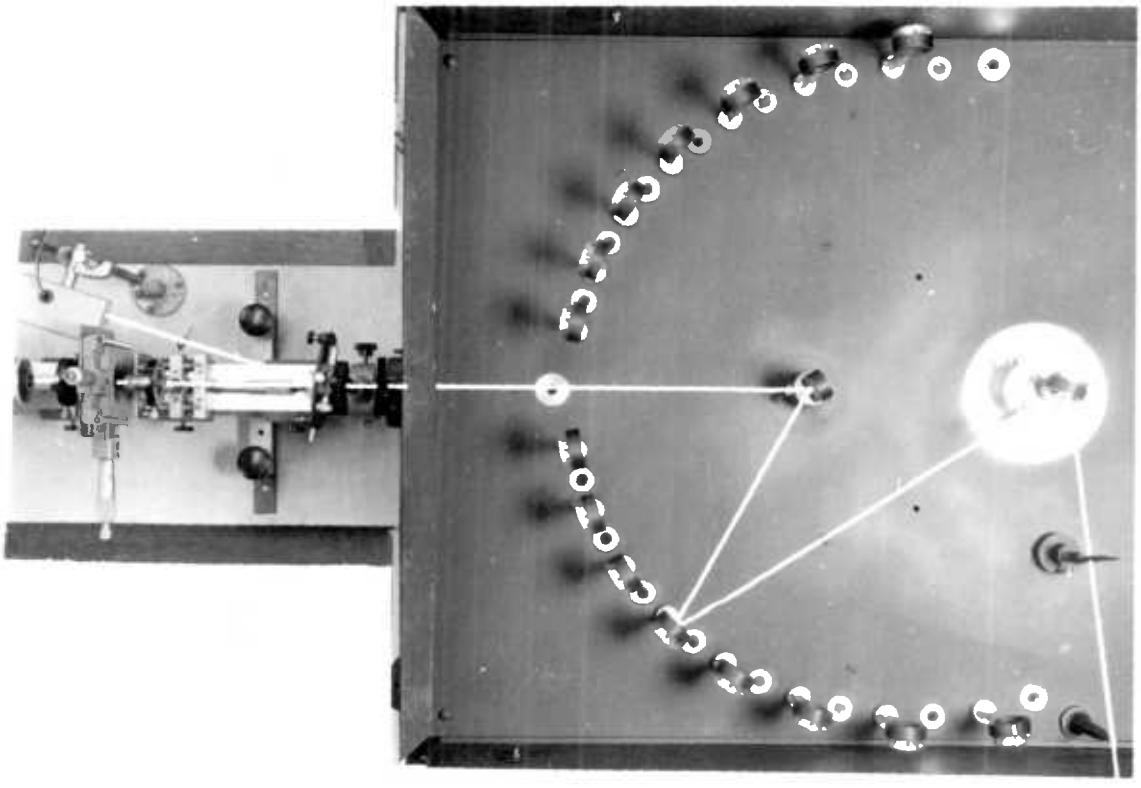

FIG. 4.11 Instrument from above; Aligned for Scattering Angle Determination

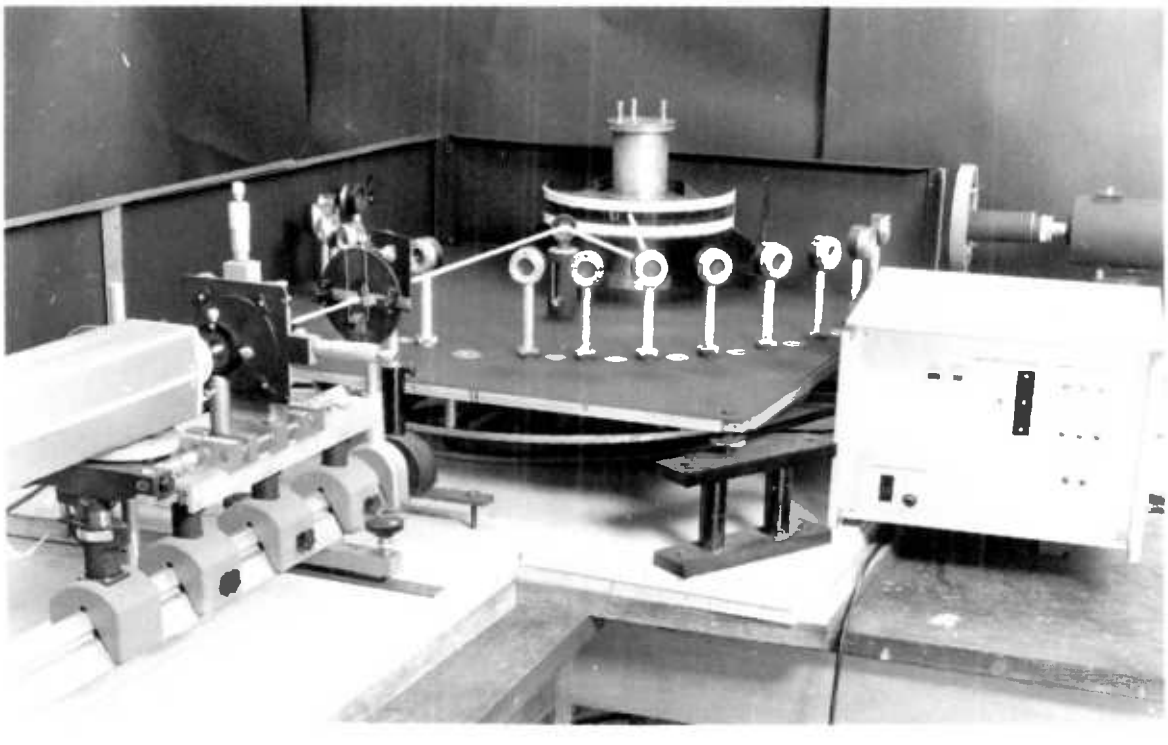

FIG. 4.12 Overall View of the Instrument

To exclude problems associated with reflections of the transmitted light beams a special light trap was constructed from black, glass fibre reinforced resin. Based on the conventional Rayleigh horn, but having a wide curving aperture, it traps any light entering within an angular range of 174°. In this instance it is attached directly to a gas tight scattering cell opposite to the curved entrance window. This window was originally made of 1.5 mm thick Perspex but this was found to be unsatisfactory as it caused considerable distortion of the laser beam. An alternative curved glass window was moulded from 2.5 mm thick plate glass, several attempts being necessary before one of the exact curvature and high optical quality was obtained.

A vertical cross section through the cell which also shows the gas inlets, outlet and magnetic stirrer is given in Fig. 4.9. It can be seen from this drawing and Fig. 4.10 that the light trap slopes downward in contrast to the upward slope of the conventional Rayleigh horn. This aids in filling the cell for hydrosol experiments by preventing the formation of a liquid-air interface within the horn. In view of the somewhat irregular appearance of the outside of the light trap, it is important to point out that the inside has the smooth geometrical contours of the aluminium mould used in its production. Apart from the light trap and window the cell was constructed of brass and sprayed matt black wherever this seemed advisable.

An overall view of the instrument with two sides and the top removed can be seen in Fig. 4.12. It shows the scattering cell in position, the control unit in the foreground and highlights one of the light paths from the laser source into the scattering cell.

4.4 Data Analysis

For a system of heterodisperse particles satisfying the number concentration conditions outlined in Section 3.1, the scattered intensity

at a particular angle Θ is given, for the perpendicular polarised case, by:

$$I_1(\Theta) = \int i_1(\alpha, \Theta)\, p(\alpha)\, d\alpha \qquad 4.2$$

where $p(\alpha)$ is the normalised size distribution function. A similar expression may also be written for parallel polarisation $I_2(\Theta)$. The experimentally determined scattering signals are related to $I(\Theta)$ as follows:

$$I(\Theta) = k\, R(\Theta) \qquad 4.3$$

where k is a constant proportional to the particle number concentration, and $R(\Theta)$ the corrected scattering signal:

$$\frac{R(\Theta)}{\sin\Theta} = \left(\frac{R_\Theta}{R_o}\right)_{\text{aerosol}} - \left(\frac{R_\Theta}{R_o}\right)_{\text{medium}} \qquad 4.4$$

Here $\sin\Theta$ is the factor which accounts for the change in observed volume at different angles. The correction term for the medium takes into account the background scattering and includes stray light, scattering from edges of stops etc. The subscript o refers to the incident beam intensity at the time of measuring the angular reading $R(\Theta)$.

The experimental light scattering data is analysed in terms of the unimodal zeroth-order logarithmic function (ZOLD). Typical curves of intensity against scattering angle, plotted at 5^o intervals, for both vertically and horizontally polarised light, are shown in Figs. 4.13-15.

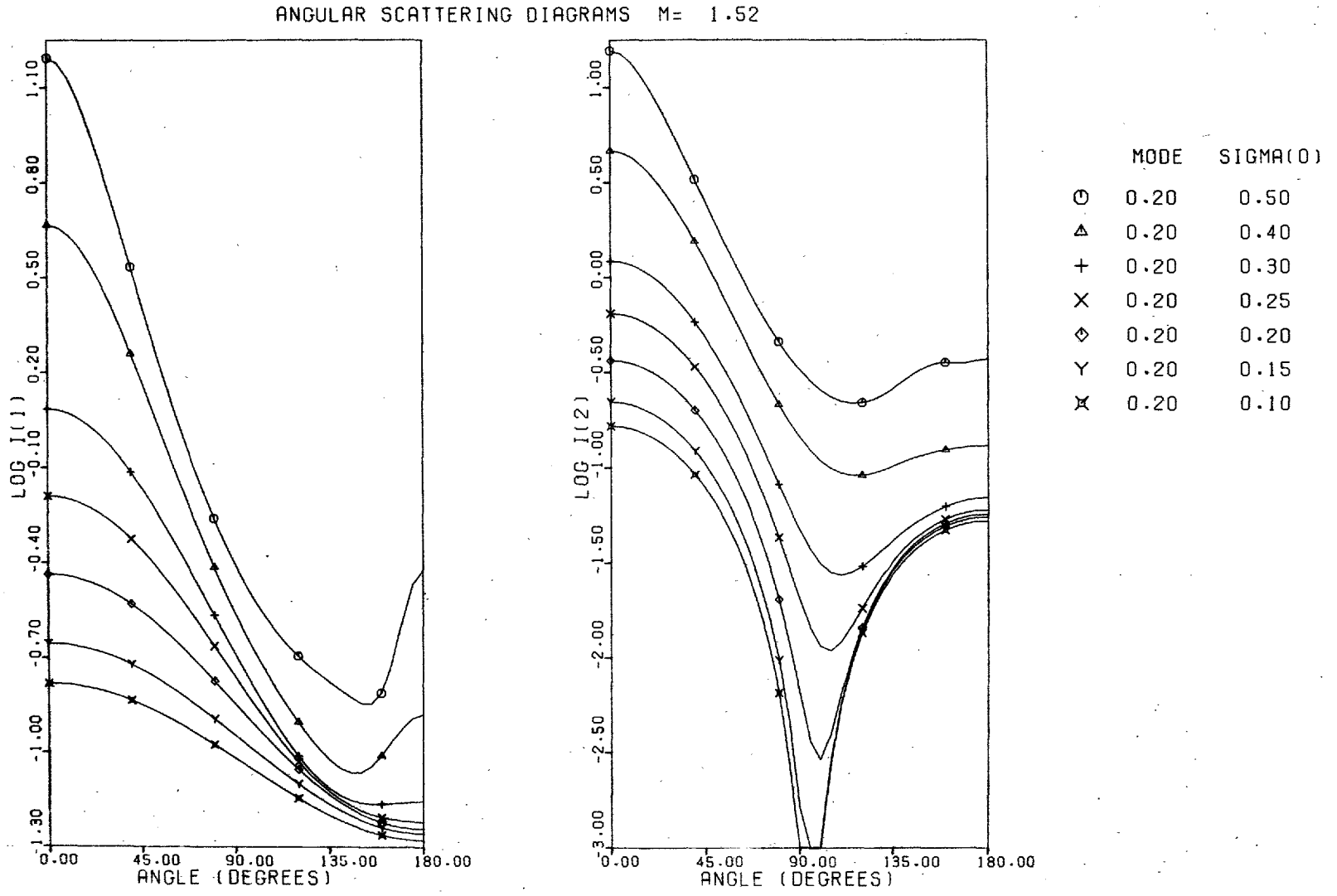

FIG. 4.13 Scattered Intensities for ZOLD Size Functions

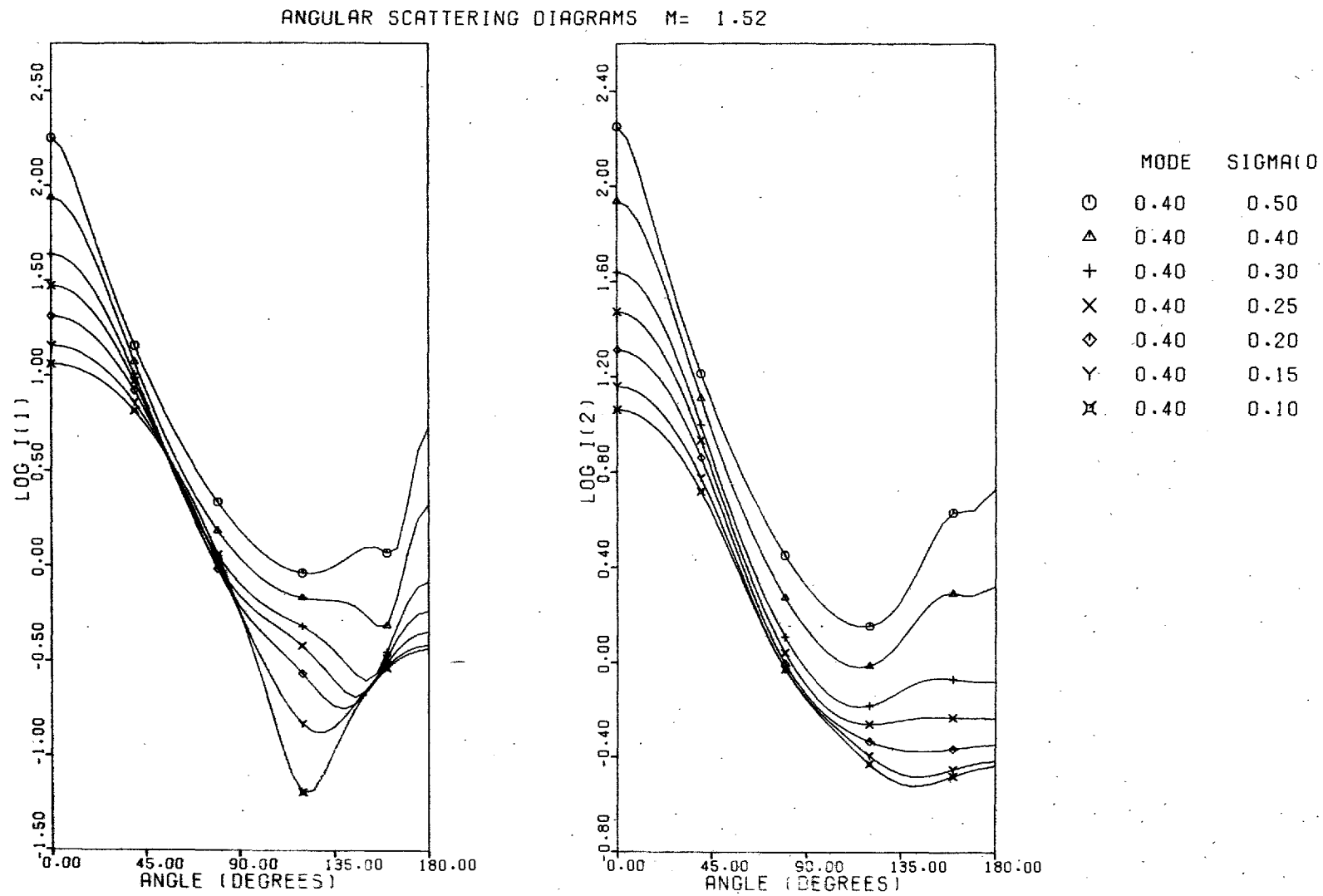

FIG. 4.14 Scattered Intensities for ZOLD Size Functions

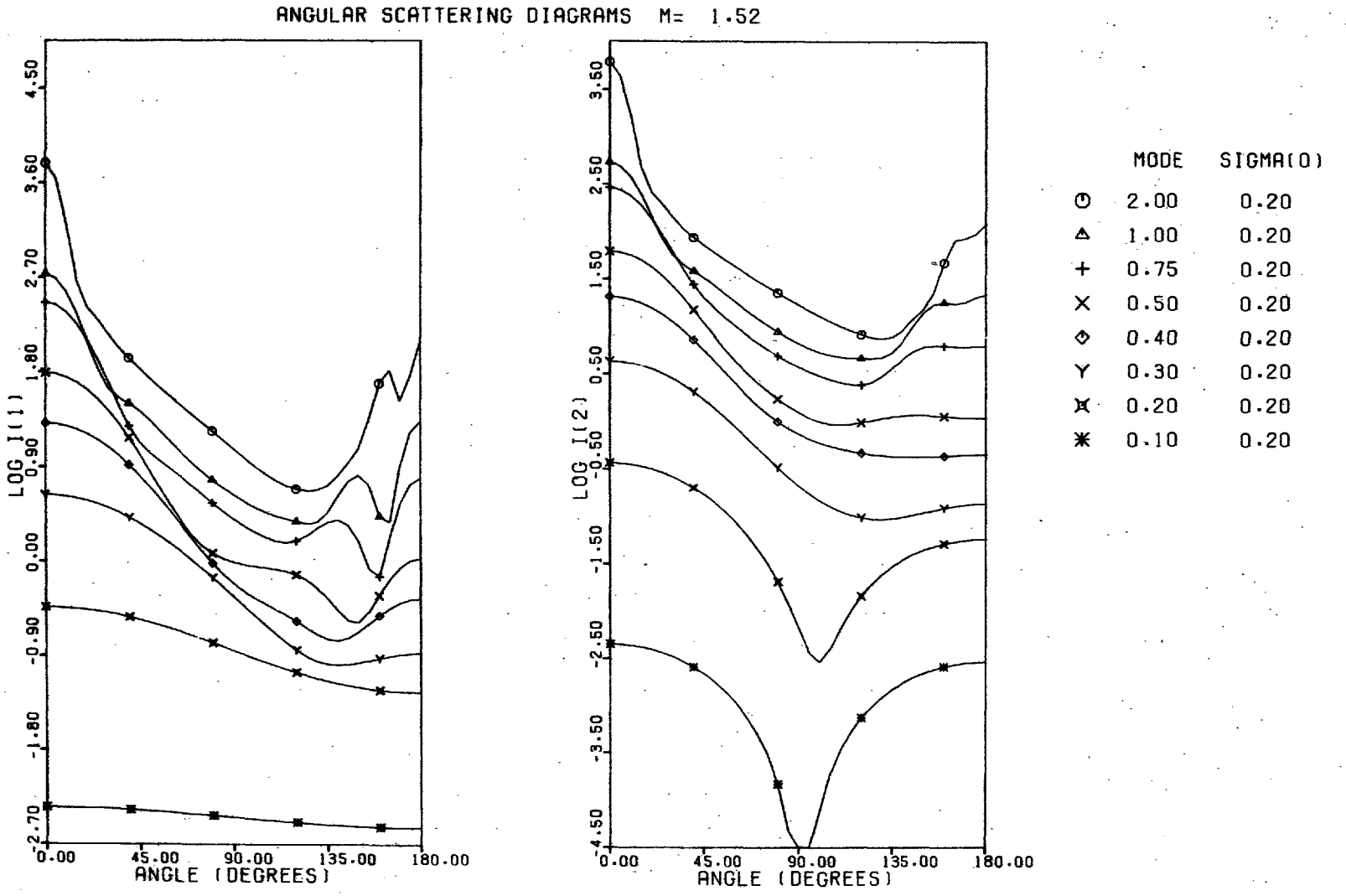

FIG. 4.15 Scattered Intensities for ZOLD Size Functions

The first two figures indicate the variation of scattering intensity as the distribution spread is increased for two constant modal diameters. The smallest size and spreads give the expected similar shaped curves because of the proximity of the Rayleigh regime of scattering. At the larger diameter the intensities in the backward direction (i.e. greater than 90^{o}) are generally more sensitive to changes in size distribution than those in the forward. Unfortunately, as mentioned earlier, backscattering can be affected by reflection problems in measuring. The last diagram (Fig. 4.15) shows a typical set of curves for distributions with a range of modal diameters but constant spread parameter. Although there exists some similarities in several of the curves in these graphs intensity measurements at suitably spaced intervals over the complete angular spectrum should discriminate well between the different distributions.

The first stage of the inversion procedure is to compute the theoretical intensities for an assumed distribution by solving Eqn. (4.2) using numerical integration over a sufficiently broad range so that the integrand reaches a limit. The fractional differences are then found between these values and the corrected experimental data for all angles and the distribution parameters adjusted in successive steps to minimise the sum of squares of these differences, F in Eqn. (4.5), until a final estimate for the dispersion is reached.

$$F = \sum_{\theta} \left\{ \frac{I(\theta) - R(\theta)}{I(\theta)} \right\}^2 \qquad 4.5$$

Rather than use the restrictive grid-type analysis described earlier in Section 3.32, requiring a considerable data store a different approach was adopted aimed at producing a more efficient and flexible

computer analysis. The basis for the new search technique was the 'multivariable minimisation of a sum of squares without derivatives' method put forward by Powell (1965). His algorithm uses conjugate directions and involves a minimisation along each search direction. Since Powell's original routine was written for unconstrained variables a modification was necessary to ensure that the distribution parameters remained in the feasible region, i.e. with values greater than zero. For practical reasons an upper bound was also placed on these parameters which allowed a convenient number of intensity functions (i_1 or i_2) to be calculated and stored on magnetic tape prior to their use in solving Eqn. 4.2.

As performance tests of the search analysis a series of theoretical intensities for pre-selected distributions were computed and used as experimental data, i.e. substituted as $R(\theta)$ in Eqn. (4.5). The final version of the technique, which included a re-arrangement of the Library minimisation subroutines to eliminate conflicting results, was arrived at only after a considerable amount of trial computation using this test data. A more detailed account of the inversion program together with a listing, and a discussion of some of the numerical problems encountered and their method of solution is given in Appendix B.

CHAPTER 5

Experimental Investigations

5.1 Use of the Light Scattering Instrument for Particle Size Analysis

Prior to an experimental run the laser and associated electronic equipment were switched on to warm-up for the manufacturer's recommended period (e.g. 2 hours for the laser). Having aligned the light beams and checked the scattering angles, as outlined in Section 4.33, for the pre-selected scanning sequence, there remained only the setting up of the scattering cell. In the case of the purpose-built cell described earlier, this entailed slotting the combined centre guide and outlet pipe into the hole in the instrument base plate and ensuring that there were no obstructions in the paths of the incident beams or in the direction that the scattered beam was to be measured.

Proving runs were made using latex dispersions of known size, initially in simple thin walled cylindrical glass cells and then with the special cell, before using the system for the aerosol growth study.

5.11 Latex Dispersions

Four different latexes of varying nominal average particle diameters were available for the test runs; polystyrene (0.2 μm), polyvinyl chloride (0.5 μm) and two of polyvinyltoluene (1 and 2 μm). A stock solution of the latex was made up using filtered distilled water prior to each run and then ultrasonically vibrated for a period to break up any aggregates present.

The scattering cell was filled with filtered distilled water to a depth of approximately 4 cm above the height of the laser beam and

the preliminary scans of the background intensity recorded. Measured volumes of the stock latex dispersion were added and three or four scans of the scattered intensity recorded after each addition. This sequence of events was usually continued until the maximum measured intensity approached that equivalent to the recommended photomultiplier current limit for the best dc stability operating conditions.

Initial test runs of the instrument using cylindrical glass cells were stopped as soon as the custom-built cell complete with light trap was available since it was evident during a run that the transmitted part of every incident beam was not being reflected off the opposite glass face back along the incident direction. It was envisaged therefore that it would be impossible to estimate with any accuracy the reflection correction term required when using this type of cell.

Intensity scans, using vertically polarised light, were made with the reference photodiode both in and out of the digital voltmeter measuring circuit. Providing sufficient warm-up time had been allowed, the laser output remained well within the manufacturer's stability specification (noise 0.3%; long term stability better than 5%). Consequently, there was little relative difference in the scattering curves between the ratio and non-ratio measurements involving the laser output reference signal did not seem justified especially as this doubled the time required for the same number of intensity readings. The faster non-ratio measurements were therefore used in all subsequent experiments with the laser output being monitored on a chart recorder.

5.12 Ammonia/Sulphur dioxide Aerosol

Having successfully tested the instrument in sizing stable dispersions of latex particles it was now ready for its originally

designed purpose, i.e. to determine the size distribution as a function of time of an aerosol formed by gaseous chemical reaction. The alignment procedures remain as previously described only in this instance the scattering cell is linked up to a simple glass gas-flow rig.

Ammonia/nitrogen and sulphur dioxide/nitrogen mixtures (approximately 8% by volume) obtained from cylinders were regulated and then filtered before entering the cell. Membrane filters (Millipore Type VF) were used to effectively remove particles approximately 0.01μm in diameter and larger from the gas streams. Flow rates for each gas stream were controlled by needle valves and indicated by rotameters. A mercury manometer and additional filtered nitrogen or air supply was attached to the third inlet. The gas outlet line to the vacuum pump had the same type of membrane filter fitted close to cell exit for sampling purposes and as protection for the vacuum pump. Prior to any experiment, the scattering cell was flushed through with air or nitrogen and several scans of the background intensity recorded.

5.2. Refractive Index Determination

A pre-requisite for size analysis using light scattering is a knowledge of the refractive index of the particles relative to their suspension medium, for the particular wavelength of incident light. An indication of the accuracy that is required can be obtained from Figs. 5.1 - 2 which show intensity against scattering angle curves for the range of relative refractive indices (m) 1.48 (0.02) 1.58. Both vertical and horizontal polarisation are illustrated for two cases, $\alpha = 1$ and $\alpha = 5$ (approximately 0.2μm and 1.0μm diameter spheres at the He-Ne wavelength). At the smaller diameter variation in the refractive index over the range considered has minimal effect on the

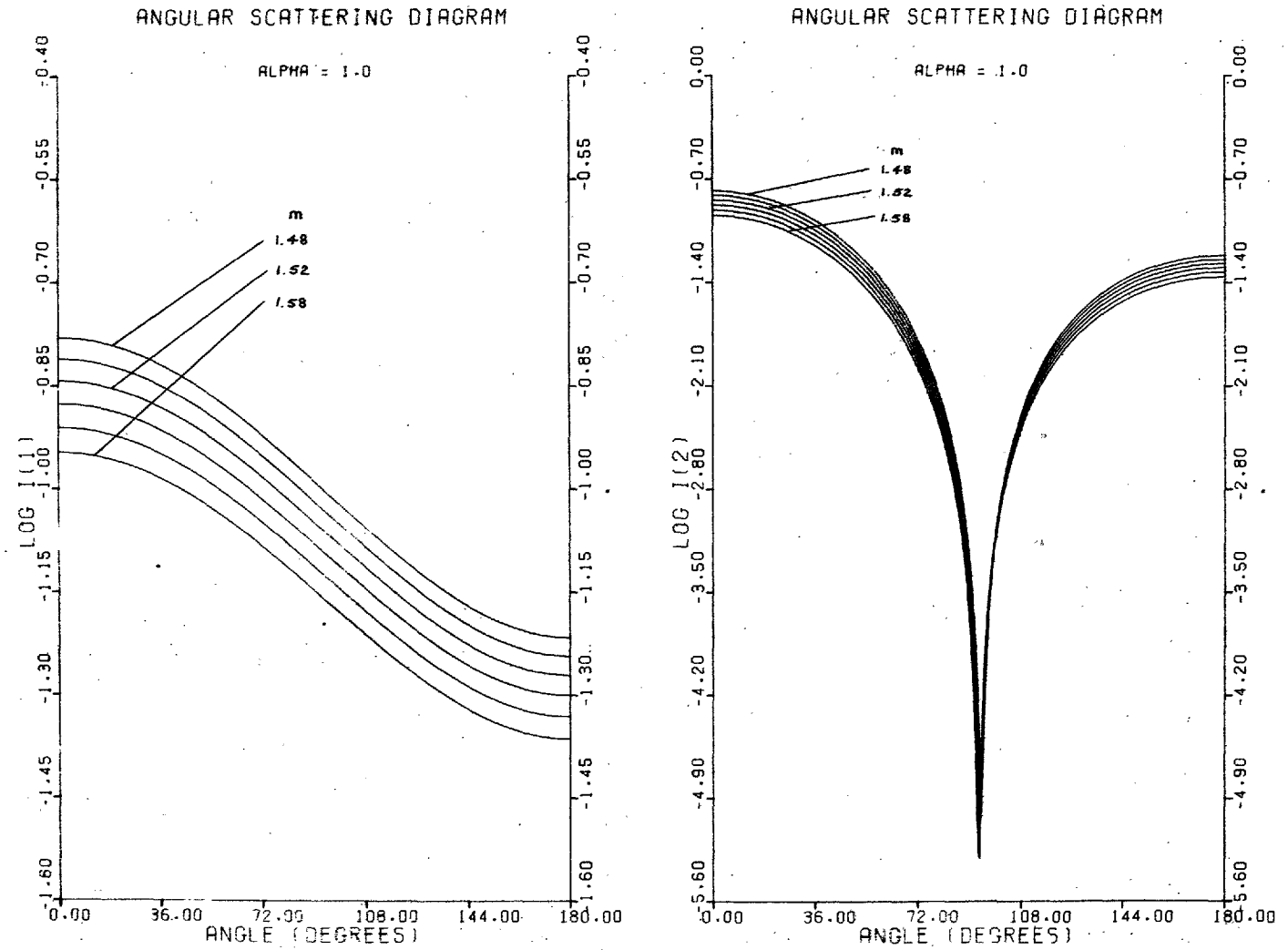

FIG. 5.1 Scattering as a Function of Refractive Index, m = 1.48 (0.02) 1.58

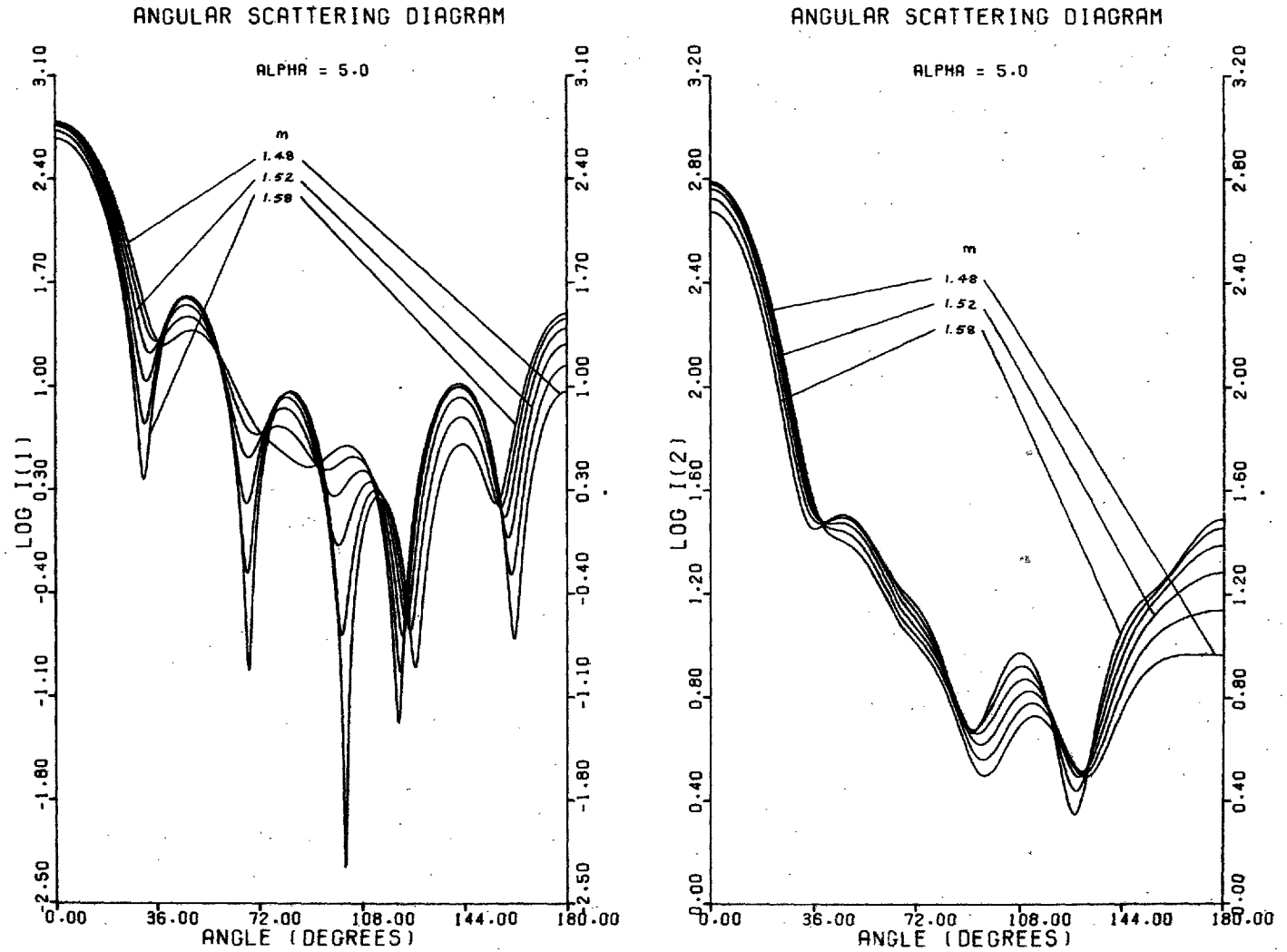

FIG. 5.2 Scattering as a Function of Refractive Index, m = 1.48 (0.02) 1.58

shape of the angular intensity curve, but at the larger size, where the curves are also more complex, the height of the maxima and minima vary considerably especially for the vertically polarised component. An accuracy of .02 in the refractive index is therefore desirable as well as careful choice of the scattering angles so that they do not all correspond to positions of strong maxima or minima.

The determination of the refractive index of a liquid is readily accomplished using the conventional Abbé refractometer. For a gaseous suspension medium the difference of the refractive index from unity is sufficiently small to be neglected.

Table 5.1 Refractive Index of Gases.

Air	1.0003	Ammonia	1.0004
Nitrogen	1.0003	Sulphur dioxide	1.0007
Argon	1.0003	Carbon dioxide	1.0004

However the measurement of the refractive index of samples of aerosol particles presents a more difficult problem. Hanel (1968) determined the real part of the mean refractive index of atmospheric aerosol particles using a technique based on one of the empirical mixture rules (Heller, 1965). Attempts were made to utilise this approach for both NH_4Cl and NH_3/SO_2 aerosol particles but met with little success. This could probably be attributed to difficulties in dispersing the hygroscopic solid, as scraped from the glass collection slide, uniformly throughout the small volumes of liquid that were required.

A different approach was then adopted aimed at matching the particles

refractive index with that of a liquid of known refractive index. The procedure was to deposit the aerosol onto a glass microscope slide divided into a number of small areas. A drop from a series of organic liquid mixtures of varying refractive index was put onto each of these areas in turn and the degree of visibility of the particles assessed when viewed through a microscope. The refractive index of each test liquid was measured at the same time using an Abbé refractometer. It was assumed the particles had the same refractive index as the liquid that rendered them invisible.

Comparative measurements were made using laser light of the He-Ne wavelength and the conventional N_{a_D} light source. It was found that the variation due to the wavelength difference was less than the accuracy that could be achieved in the 'matching' technique. All subsequent measurements were therefore made at the N_{a_D} wavelength which also had the advantage of providing a more identifiable demarcation line in the refractometer and reducing eye strain.

For the sake of completeness the summary of these experimental findings has been kept within this section. Table 5.2 lists the results together with, where available, the refractive index figures from reference tables for the same substance.

Table 5.2 Refractive Index of Solids

Substance	Wavelength	Refractive Index	
		Measured	Previous Work
NH_4Cl	Na_D	1.63 - 1.65	1.6422
	He-Ne	1.62 - 1.65	1.6383
$(NH_4)_2 SO_4$	Na_D	1.51 - 1.52	1.5209
	He-Ne	1.50 - 1.53	1.519
NH_3/SO_2 product	Na_D	i/ 1.54 - 1.57	
a/ fresh samples		ii/ 1.55 - 1.56	
		iii/ 1.53 - 1.54	
b/ exposed to air for 1 hour	Na_D	i/ 1.51 - 1.52	
		ii/ 1.51 - 1.52	
P.V.C. latex	Na_D	1.58 - 1.60	1.585

CHAPTER 6

Results and Discussion

6.1 Inversion of Theoretical Light Scattering Data

The proposed technique for inverting light scattering data to obtain the corresponding ZOLD parameters, outlined in Section 4.4, was first tested using theoretical intensities calculated for a range of known distributions. By using several distributions of varying mode and spread it was hoped to gain an indication of the range of applicability of this particular method. A selection from the scattering patterns of the test distributions are plotted in Fig. 6.1 and 6.2; the refractive index (m = 1.19) corresponding to latex particles in water. Several different initial estimates of the two distribution parameters were made in order to ascertain whether a unique answer was always found. In addition, to provide an indication of the accuracy that would be required in the experimental data, the theoretical test data for the vertically polarised case at m = 1.19 were subjected to $\pm$ 2.5 % and $\pm$ 5% random fluctuations. The results of these various test runs are summarised in Tables 6.1 - 6.4.

Significant features of Table 6.1 are the exact prediction of both parameters for theoretical input data and the very close approximation, in the majority of cases, when random fluctuations were imposed on the input data. Table 6.2 is intended to indicate the prediction accuracy for distributions with parameters close to the limits imposed by either the Rayleigh scattering regime or the range of diameters for which the intensity coefficients had been previously calculated and stored. In these inversions, for vertically polarised light of wavelength 632.8 nm,

diameters up to 0.1 μ m yield intensity distributions very nearly constant and independent of scattering angle, while for $d_M = 2\ \mu m$ the maximum spread before penalty functions are applied is approximately 0.3. Considering these factors it is not surprising that the inversion program stops prematurely in a number of the cases examined in Table 6.2.

A similar set of distribution parameters were used to obtain additional test scattering data for a higher refractive index, m = 1.53, corresponding to the probable value for the NH_3/SO_2 aerosol. The predicted results, as indicated in Table 6.3, again showed excellent agreement except at the largest sizes; the one or two discrepancies that did arise being characterised by an error sum of squares several orders of magnitude higher than normal. Since there is no a priori reason why the inversion analysis should be restricted to vertically polarised light, a similar series of test runs was made using intensities for horizontally polarised light. The predicted size parameters, Table 6.4, were however not as consistent as those obtained with vertically polarised light.

Error contour diagrams have been plotted in several cases to ascertain the overall features of the $d_M - \sigma_o$ domain being searched, e.g. whether there is a global minimum, several local minima, or a broad area where a range of different parameter values would fit the data equally well. These are shown in Figs. 6.3 - 6.8 where the lines join points of equal root mean square deviation,

$$F_{rms} = (F/j)^{\frac{1}{2}} \qquad 6.1$$

where F is the sum of squares as given by Eqn. 4.5 and j is the number of angular readings. In these and in all subsequent error contour diagrams the contour lines are numbered in ascending order of magnitude of F_{rms}. A standard computer routine was employed to draw contours at given levels through a rectangular mesh of data points using linear interpolation based on a method outlined by Dayhoff (1963). The mesh of data points (on average 10 per unit of axis) is scanned row by row for the appropriate contour level which accounts, to some extent, for the 'spikyness' evident in the contour plots.

The presence of any asymmetric steep-sided valleys which curve with the parameters is one of the features likely to cause maximum difficulties within the minimisation subroutines. However, in the examples plotted, a well defined single valley generally leads to the minimum contour level although in some instances the floor of the valley covers a range of both parameters. At the larger diameters there is evidence of secondary valleys leading in some instances to local minima. For a modal diameter of 1 μm (Fig. 6.4) the inversion program required a perturbation for restart in the valley through $d_M = .35$, when the starting point was set at 0.3; 0.3, before finally reaching the correct answer. By the time the mode has increased to 2 μm two distinct valleys either side of a fairly large plateau are clearly visible, one of which leads to a local minimum in the region of 0.1; 0.55. There is also evidence of a further shallow minimum in the area around 2.0; 0.3 close to the constraint limit. Reference to Table 6.2 confirms that it is in these areas that the program stops unless given a starting point reasonably close to the correct answer.

Contour diagrams have also been plotted in two instances for the same size distribution but using respectively vertically and horizontally polarised light (Fig. 6.4 and 6.5). It is evident that the horizontal cases have

secondary valleys and local minima and it is these that are responsible for the incorrect predictions in Table 6.4.

The results thus far obtained from inverting theoretical light scattering data computed for one of the sets of fifteen angles available on the light scattering instrument indicate that distribution widths larger than the suggested 0.3 maximum of Kerker (1969) can be successfully analysed using this technique, providing of course, that the data are sufficiently accurate. The lower size limit appears to be of the order $d_M = 0.1\ \mu m$ and $\sigma_o = 0.1$ due to the predominance of Rayleigh scattering in this size region. An upper limit on the modal diameter was not investigated above 2 μm since this was already as large as the maximum size likely to be encountered in the aerosol experiments. Even at this size problems were starting to arise because the complicated oscillatory scattering pattern of the nearly monodisperse system tends to get "washed out" as soon as the spread parameter becomes significant. The corollary of this as regards experimental measurements is evident from Fig. 6.2. If insufficient scattering angles are used then as the particle diameter approaches 2 μm the characteristic oscillations cannot be singled out, thereby giving the erroneous impression of too large a spread.

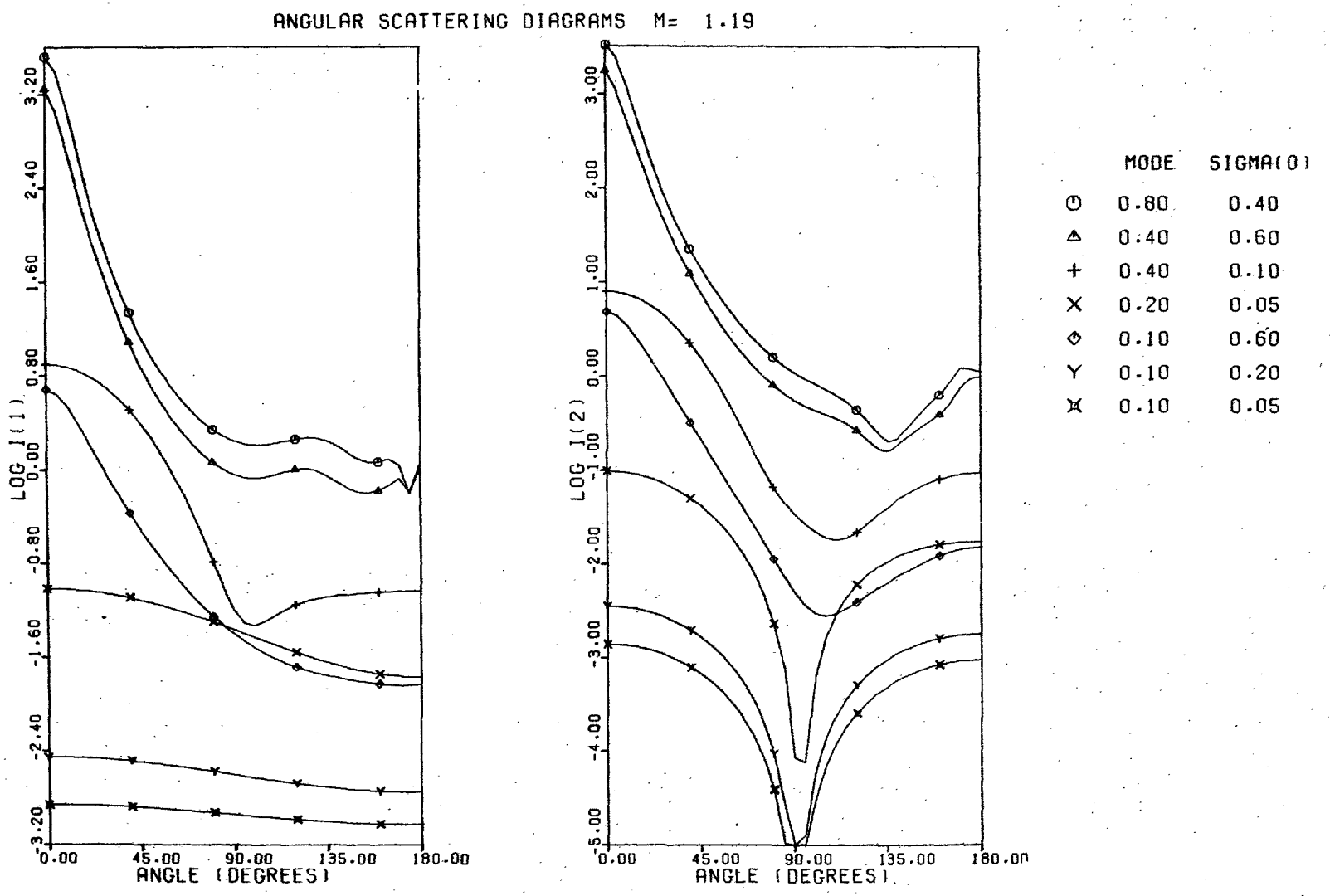

FIG. 6.1 Scattered Intensities Corresponding to the ZOLD Test Functions

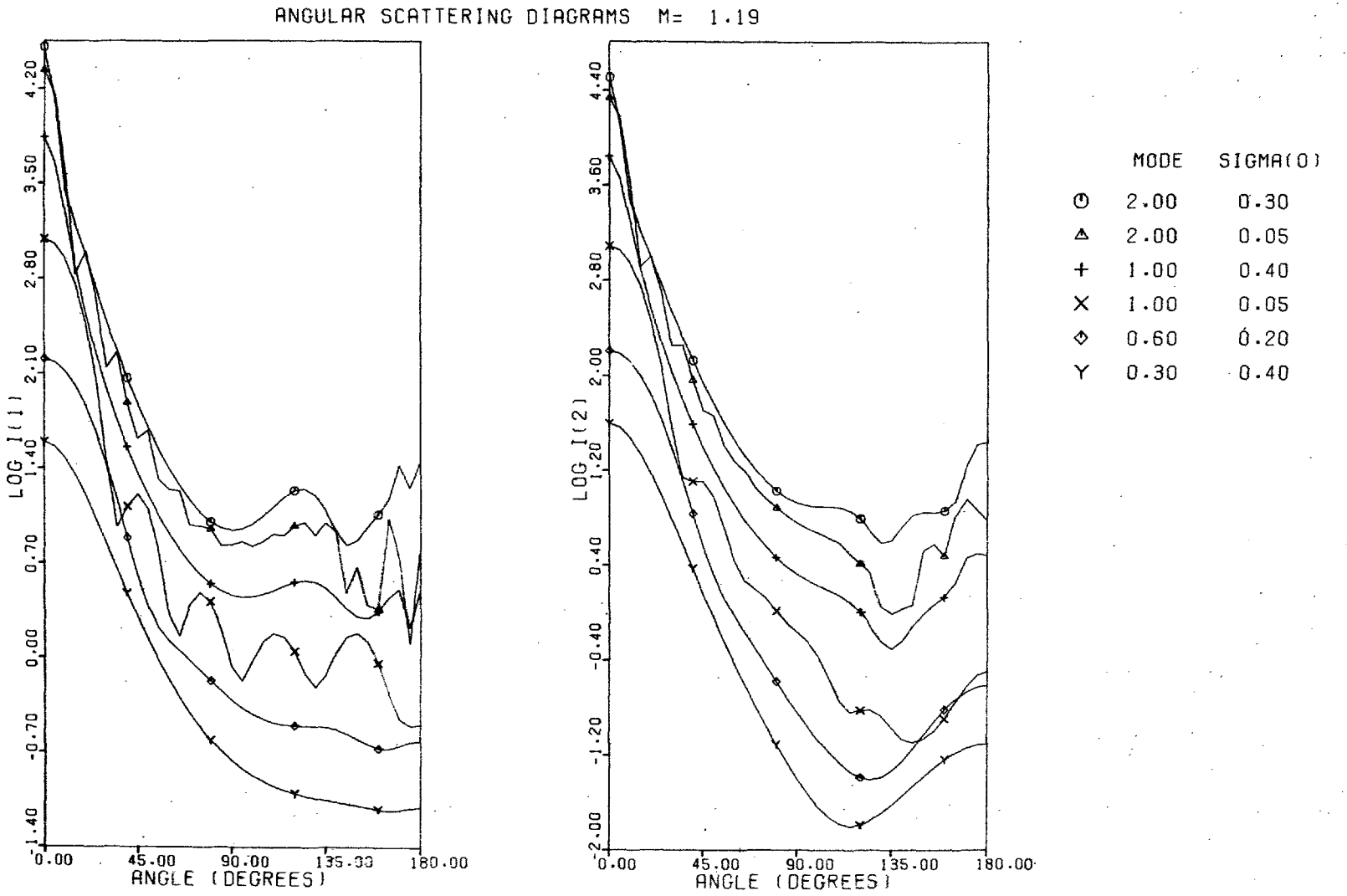

FIG. 6.2 Scattered Intensities Corresponding to the ZOLD Test Functions

Table 6.1 Test data predictions for m = 1.19, vertically polarised light

Size distribution of test data		Results predicted by the search analysis											
		0% fluctuation				± 2.5% fluctuation				± 5% fluctuation			
		i		ii		iii		i		ii		iii	
.1	.2	.099	.203	.100	.199	.100	.199	.115	.146	.109	.168	.101	.197	.123	.110	.115	.146	.126	.093
.1	.6	.100	.600	.100	.600	.100	.600	.102	.590	.102	.590	.102	.590	.104	.579	.105	.579	.105	.579
.3	.4	.300	.400	.300	.400	.300	.400	.291	.406	.291	.406	.291	.406	.282	.411	.283	.410	.283	.410
.4	.1	.400	.100	.400	.100	.400	.100	.399	.100	.399	.100	.399	.100	.399	.100	.399	.100	.399	.100
.4	.6	.400	.600	.400	.600	.400	.600	.352	.637	.353	.636	.451	.227	.303	.676	.302	.677	.303	.678
.6	.2	.600	.200	.600	.200	.600	.200	.593	.201	.593	.201	.593	.201	.581	.202	.581	.202	.585	.199
.8	.4	.800	.400	.800	.400	.800	.400	.856	.384	.854	.385	.855	.385	.552	.516	.542	.520	.552	.516
1.0	.05	1.00	.050	1.00	.050	.086	.527	1.00	.049	1.00	.049	1.00	.049	1.00	.048	1.00	.048	1.00	.048
1.0	.4	1.00	.400	1.00	.400	.449	.104	.954	.405	.954	.405	.954	.405	.918	.406	.918	.406	.920	.406

Starting points for search:- (i) .1 .6 (ii) .3 .3 (iii) .6 .1

In these tables (6.1 to 6.4) the first number of each pair is the modal diameter d_M (μm) and the second σ_0

TABLE 6.2 Test data predictions for m = 1.19, vertically polarised light

Size distribution of test data		Fluctuation %	Results predicted by search analysis from varying start points									
			.1	.6	.3	.3	.6	.1	1.5	.1	1.8	.1
2.0	.3	0	.053	.679	.441	.087	.976	.611	1.95	.305	1.89	.100
2.0	.3	± 2.5	.063	.646	.051	.683	.440	.088	2.15	.275	1.88	.100
2.0	.3	± 5	.050	.682	.050	.682	.440	.090	2.44	.218	1.88	.100
2.0	.05	0	.050	.708	.434	.100	.053	.698	1.96	.265	2.00	.050
2.0	.05	± 2.5	.050	.704	.433	.102	.052	.696	1.96	.265	2.00	.051
2.0	.05	± 5	.051	.699	.078	.614	.050	.699	2.00	.265	1.99	.052
0.2	.05	0	.199	.054	.199	.054	1.86	.005	-		-	
0.1	.05	0	.098	.074	.098	.074	.098	.074	-		-	

TABLE 6.3 Test data predictions for m = 1.53, vertically polarised light

Size distribution of test data		Results predicted by search analysis from varying start points							
		.1	.6	.3	.3	.6	.1	1.5	.2
.1	.2	.100	.201	.100	.201	1.38	.072	-	
.1	.6	.100	.600	.100	.600	.100	.600	-	
.2	.05	.199	.054	.199	.054	1.38	.071	-	
.3	.4	.300	.400	.300	.400	.300	.400	-	
.4	.1	.400	.100	.400	.100	.400	.100	-	
.4	.6	.400	.600	.400	.600	.400	.600	-	
.6	.05	.600	.050	.280	.409	.600	.050	-	
.6	.2	.600	.200	.600	.200	.600	.200	-	
.8	.4	.800	.400	.800	.400	.800	.400	-	
1.0	.05	1.00	.050	1.00	.050	1.00	.050	-	
1.0	.4	.053	.597	.050	.606	1.00	.400	1.00	.400
2.0	.05	.050	.532	.050	.530	1.37	.392	2.00	.050
2.0	.3	.050	.502	.050	.502	.050	.500	2.01	.293

Table 6.4 Test data predictions for m = 1.19, horizontally polarised light

Size distribution of test data		Results predicted by search analysis from varying start points							
		.1	.6	.3	.3	.6	.1	1.5	.2
.1	.05	.090	.110	.097	.056	.598	.003	-	
.2	.05	.200	.009	.200	.006	.599	.005	-	
.1	.2	.100	.200	.397	.007	.598	.004	-	
.1	.6	.100	.600	.100	.600	.596	.040	-	
.3	.4	.300	.400	.300	.400	.300	.400	-	
.4	.1	.400	.100	.400	.100	.400	.100	-	
.4	.6	.400	.600	.400	.600	.640	.005	-	
.6	.2	.600	.200	.600	.200	.600	.200	-	
.8	.4	.800	.400	.800	.400	.654	.005	-	
1.0	.05	1.00	.050	1.00	.050	1.00	.050	-	
1.0	.4	.434	.006	.412	.007	.640	.006	1.01	.396
2.0	.05	.416	.006	1.49	.258	1.49	.258	1.49	.258
2.0	.3	.050	.578	.405	.005	2.03	.291	2.00	.298

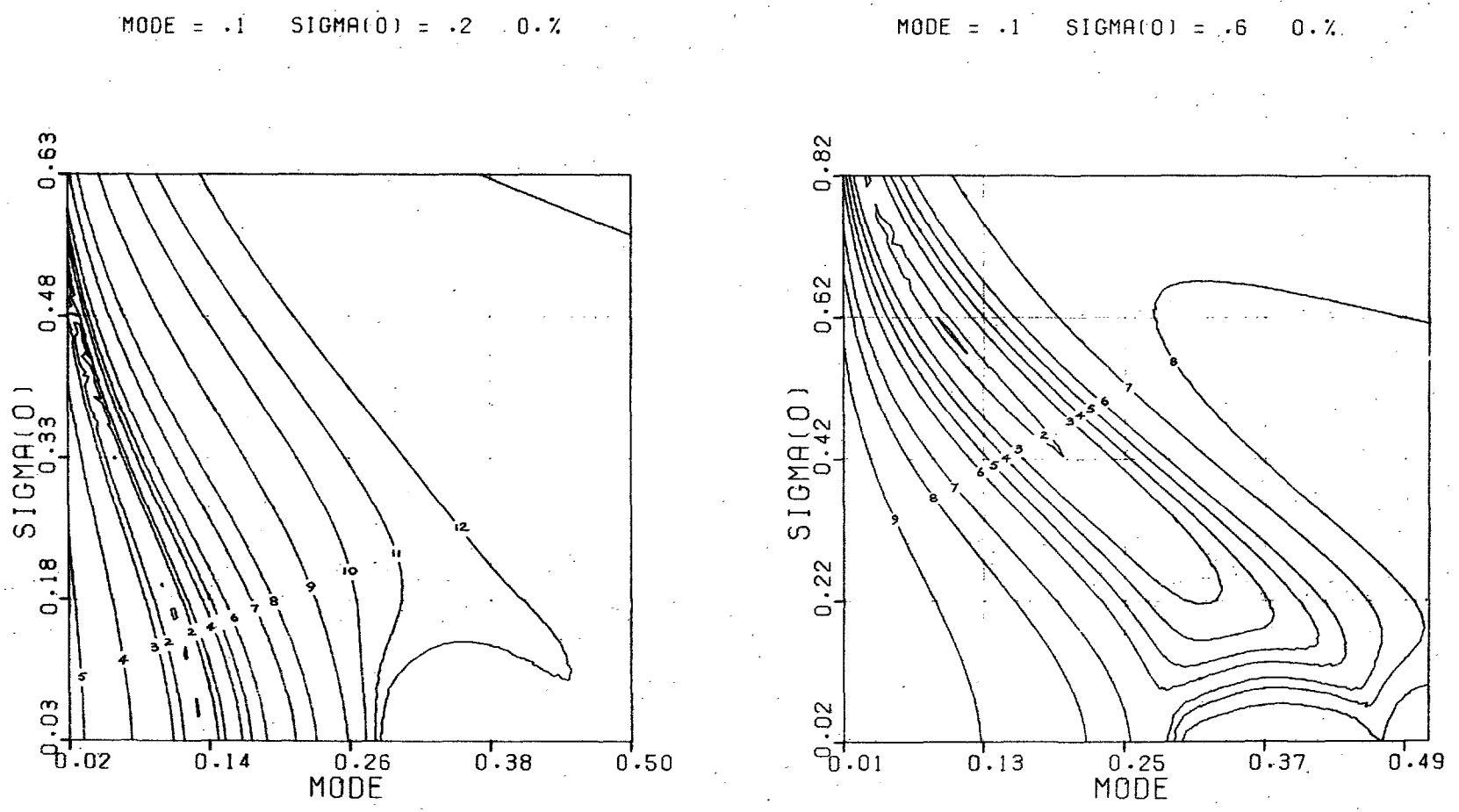

FIG. 6.3 Error Contour Diagrams. Test Data for Vertically Polarised Light at m = 1.19

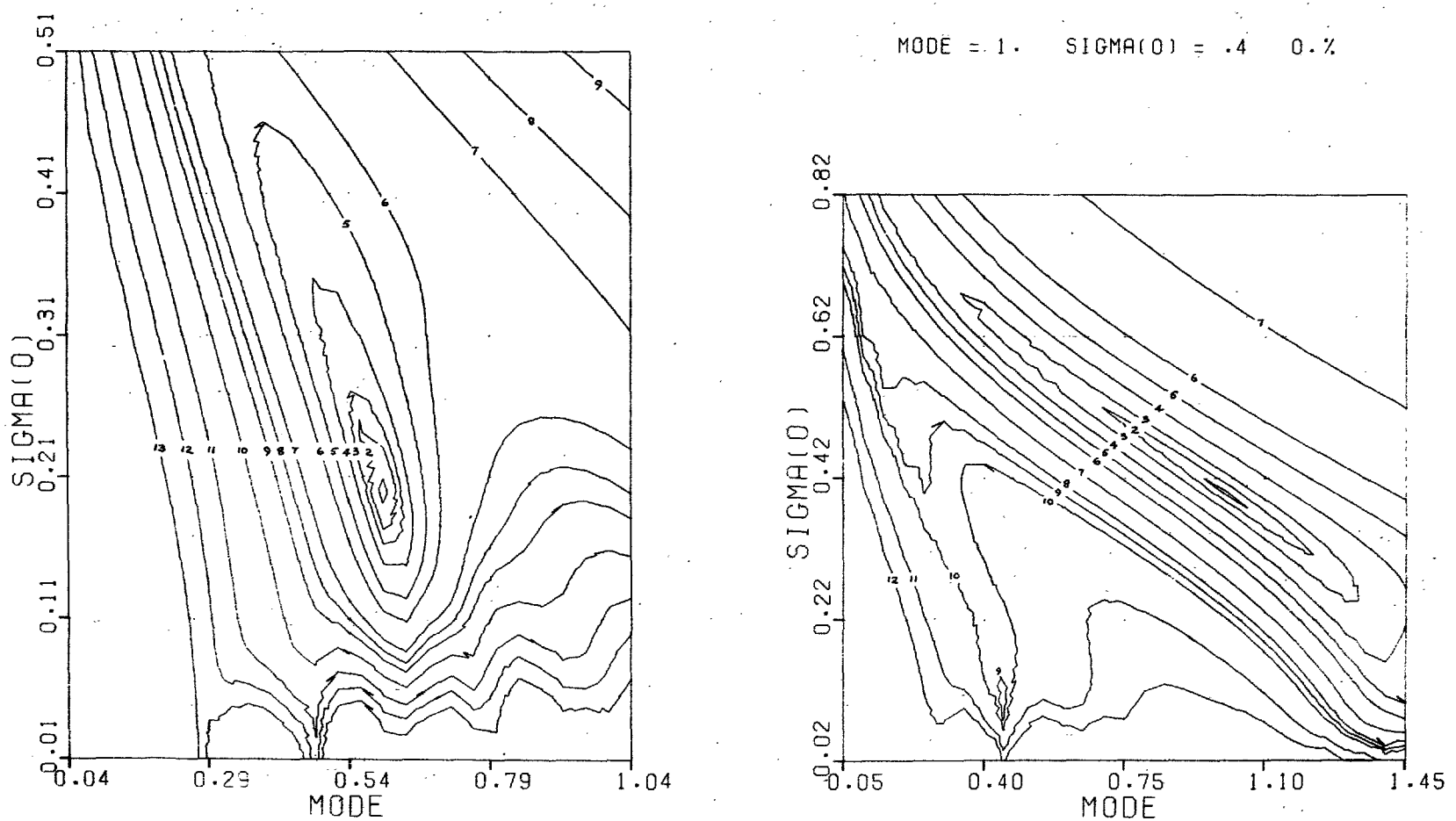

FIG. 6.4 Error Contour Diagrams. Test Data for Vertically Polarised Light at m = 1.19

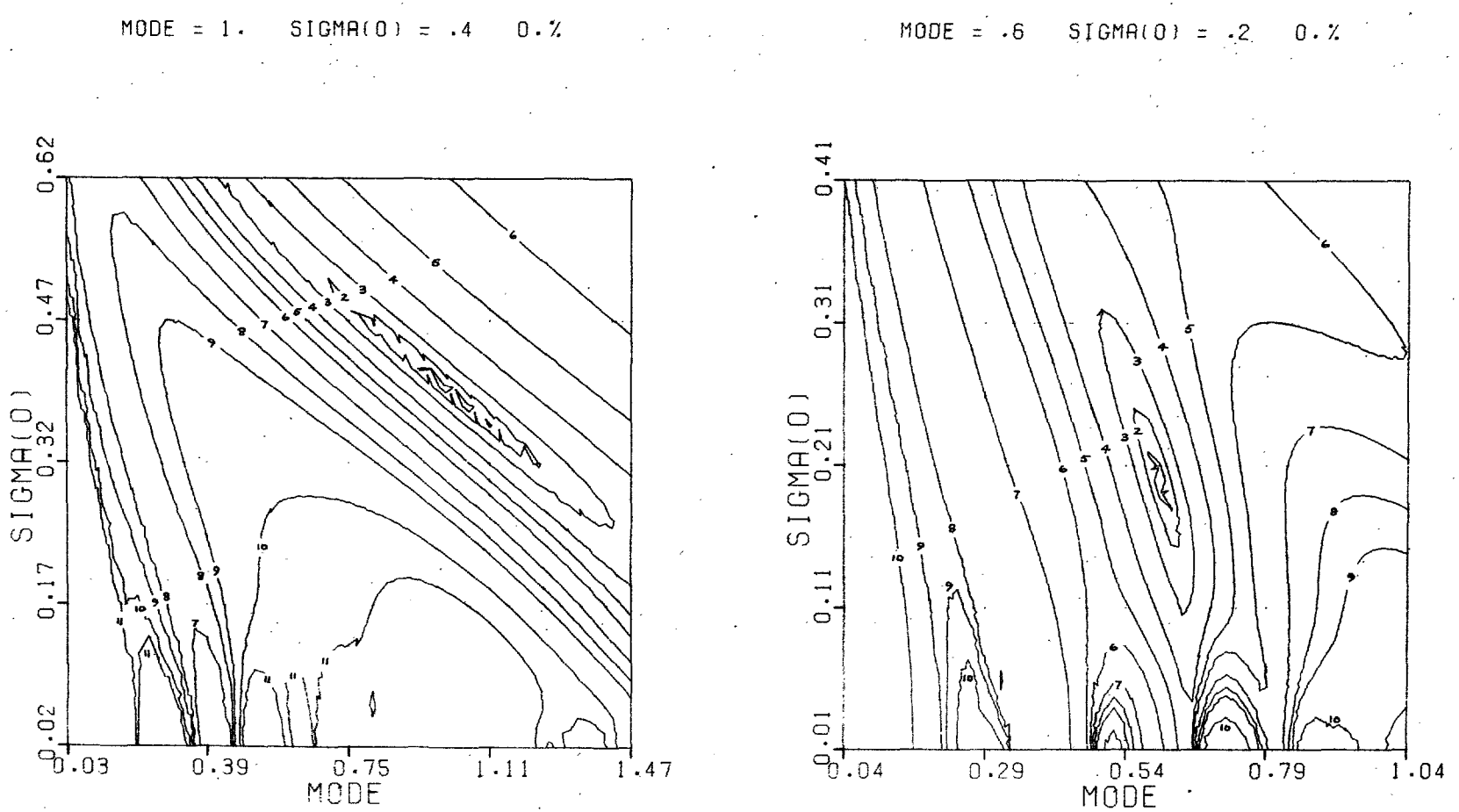

FIG. 6.5 Error Contour Diagrams. Test Data for Horizontally Polarised Light at m = 1.19

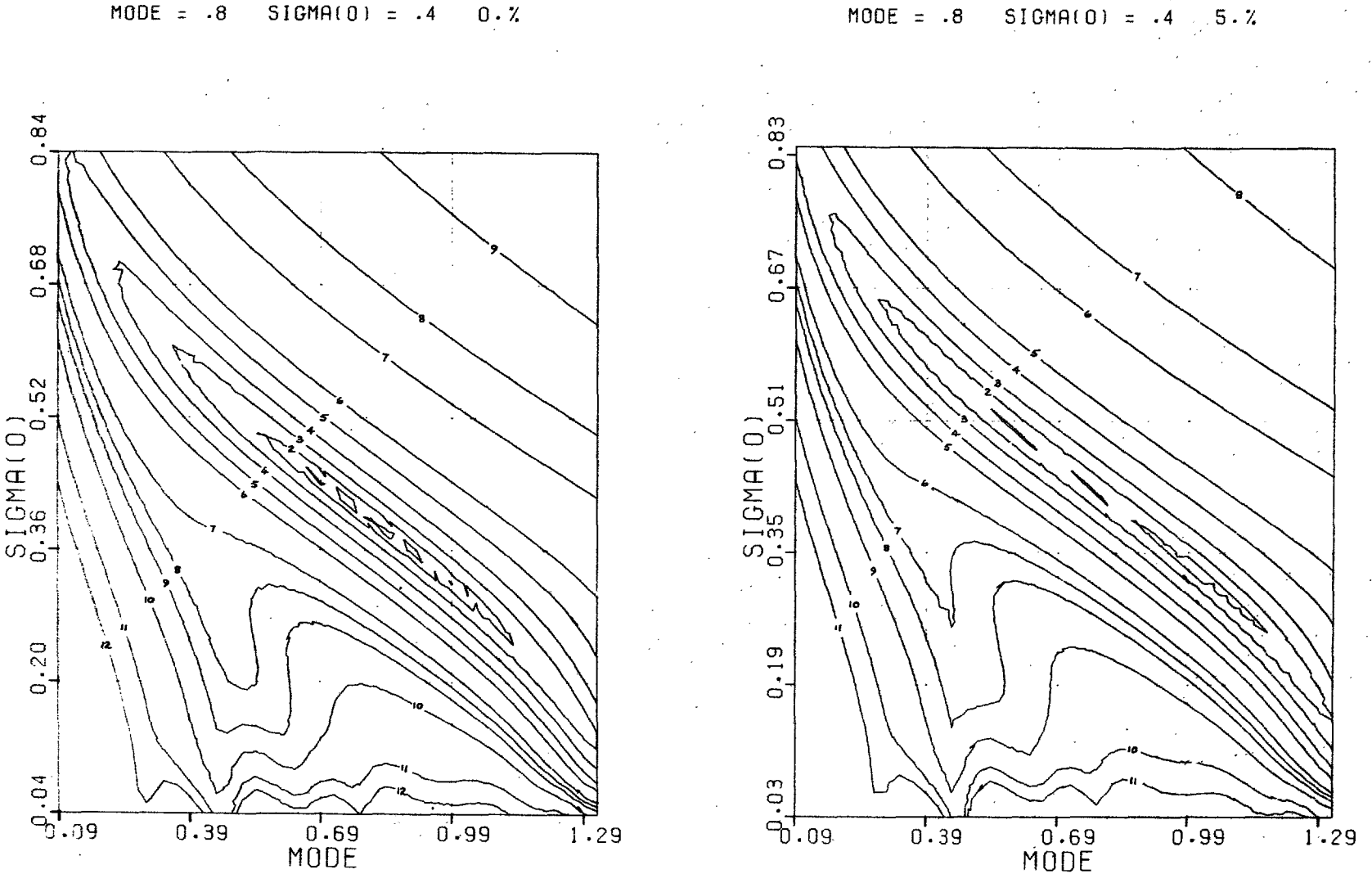

FIG. 6.6 Error Contour Diagrams. Test Data for Vertically Polarised Light at m = 1.19

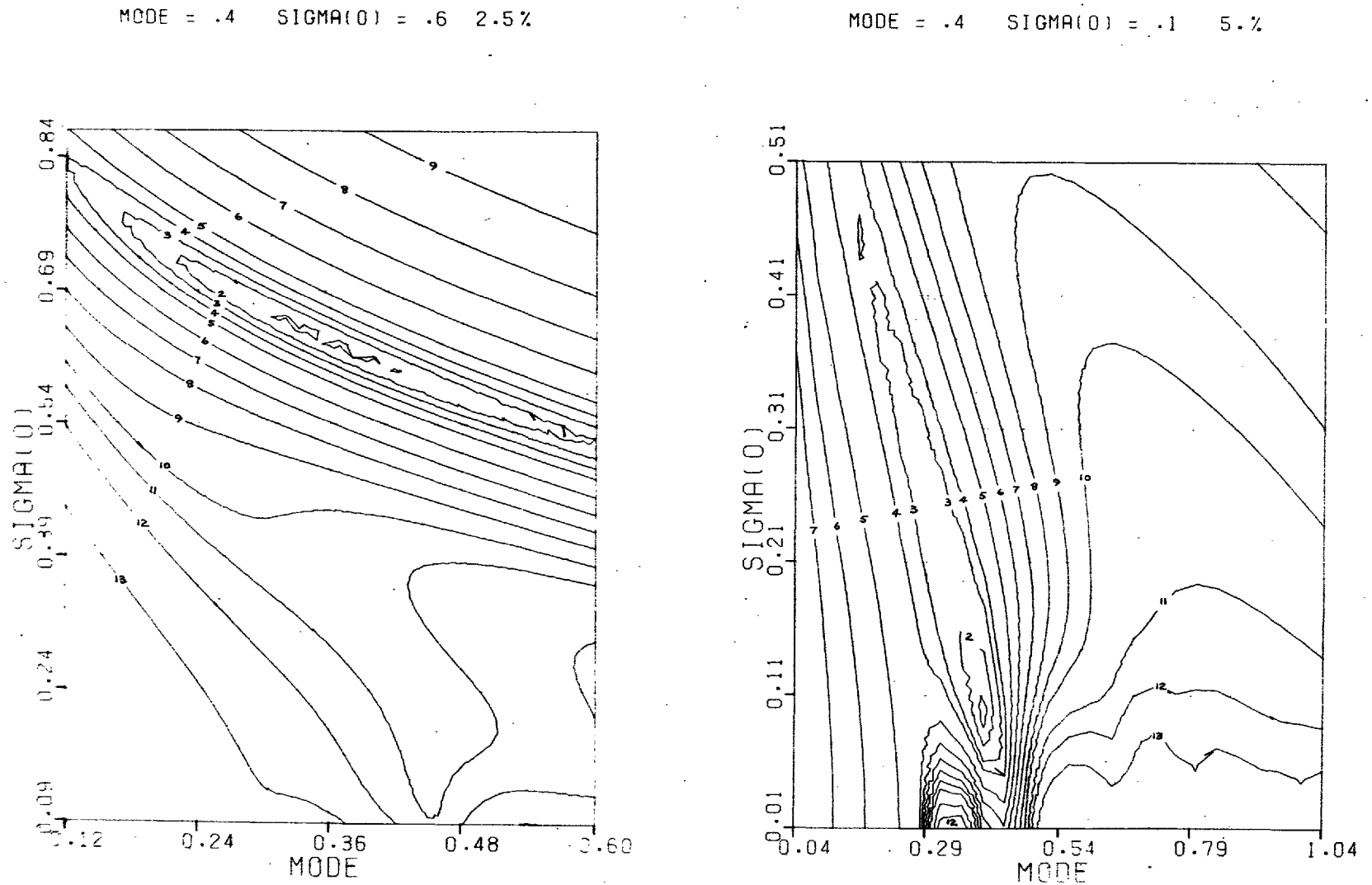

FIG. 6.7 Error Contour Diagrams. Test Data for Vertically Polarised Light at m = 1.19

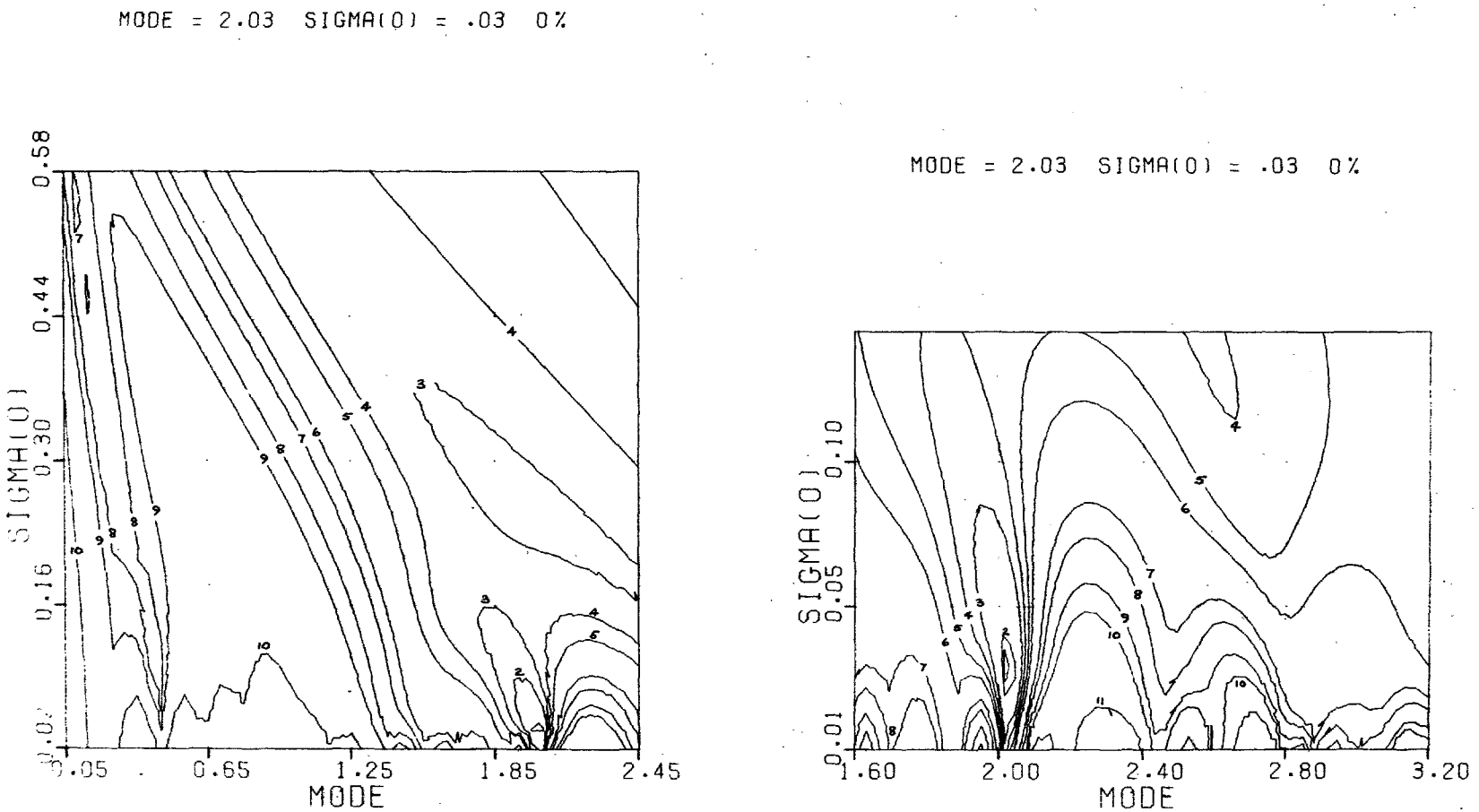

FIG. 6.8 Error Contour Diagrams. Test Data for Vertically Polarised Light at m = 1.19

6.2 Size Analysis of Latex Dispersions

Four different latexes were available having, according to the manufacturers, mean diameters in the range 0.2 - 2 μm and a fairly narrow size range (coefficient of variation 6 - 8%), as indicated in Table 6.5. Samples of the stock solutions used in each of the light scattering experiments were taken for examination by electron microscopy, resulting in the four size distribution plots shown in Fig. 6.9. The indicated curves for the best fitting Z O L D function confirm the validity of using this particular distribution function in the light scattering analysis. It should also be pointed out that, despite several attempts, the particles inthe micrographs of the polystyrene latex appeared hazy and out of focus making them difficult to measure and those in the P. V. C. latex showed some evidence of shrinkage and slight distortions from sphericity.

The measured scattered intensities for each latex are shown in Figs. 6.10 and 6.11. Each set of symbols denotes a different experimental condition, usually a change in particle concentration, and the continuous line joins the intensities calculated for the best fitting size distribution at the same set of angles. The experimental scattering patterns were all analysed using the inversion program 'SEARCH' and the predicted distribution parameters are tabulated in Table 6.6 together with the root mean square value of the difference between the scaled experimental readings and the intensities corresponding to the best fitting size distribution.

An error contour diagram has been constructed for one set of data from each latex sample (Figs. 6.12 - 6.14). It is evident that the

inversion program has predicted an answer within the lowest contour level in each case although for the P. V. T. (2) latex (Fig. 6.14) there are two other local minima within the depicted domain. These do not necessarily arise from experimental error in the light scattering measurements since on comparing the contour diagram with one for theoretical data corresponding to a similar distribution (Fig. 6.8) the same local minima can be seen.

The results from the two size analysis methods are summarised, together with manufacturer's data for comparison, in the table below. The light scattering size distributions are an average of the best fitting ones from the intensity scans at different particle concentrations. For the most part there is excellent concordance between the size distribution predicted from light scattering and that from electron microscopy bearing in mind that the error in size determination from electron micrographs could be up to 20% too low (Davidson and Collins, 1972).

Table 6.5 Latex Particle Size Distributions

Latex	Size Distribution					
	Manufacturer (* estimate)		Electron Microscopy		Light Scattering	
	d_M	σ_o	d_M	σ_o	d_M	σ_o
Pstyrene	.2*	-	.21	.29	.19	.06
P. V. C.	.45	.05	.37	.09	.50	.08
P. V. T. (1)	1.15	.07*	1.14	.02	1.20	.04
P. V. T. (2)	2.03	.07*	2.03	.013	2.07	.02

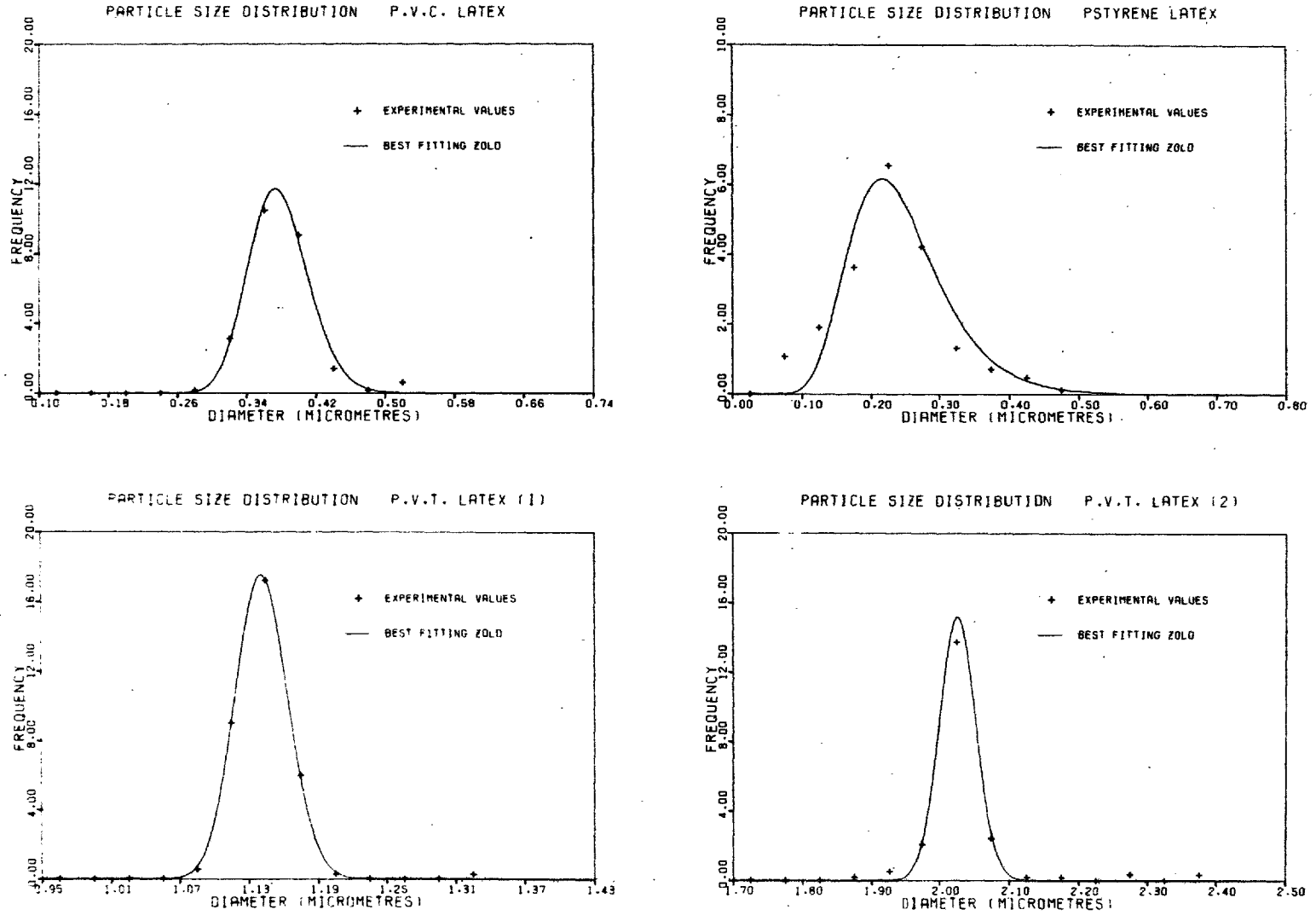

FIG. 6.9 Latex Size Distributions Obtained from Electron Microscope Analysis

Table 6.6 Latex distributions predicted from experimental light scattering data

Latex	Symbol	d_M	σ_o	F_{rms}	Latex	Symbol	d_M	σ_o	F_{rms}
Pstyrene		.195	.059	.091	P.V.T.(1)		1.628	.112	.360
	⊡	.189	.067	.070		⊡	1.197	.054	.382
	⊙	.195	.060	.098		⊙	1.195	.045	.245
	△	.193	.069	.171		△	1.197	.040	.208
	+	.085	.361	.062		+	1.197	.037	.157
	×	.194	.063	.113		×	1.200	.035	.130
	◇	.186	.068	.107		◇	*1.201	.035	.127
P.V.C. a		.500	.071	.094					
(2 runs)a		.505	.071	.117	P.V.T.(2)		1.821	.038	.370
b	⊡	.521	.081	.247			1.857	.005	.497
b	⊙	.265	.377	.366		⊡	1.862	.079	.368
b	△	.250	.391	.359		⊙	2.071	.024	.190
b	+	.498	.084	.106		△	2.060	.282	.387
b	×	*.256	.388	.357		+	*2.070	.022	.229
b	◇	.494	.087	.096		×	3.228	.034	.378
b		*.283	.365	.348		◇	2.069	.018	.219
b	⊕	.498	.081	.109					
b	⊠	*.494	.087	.102					

Symbols relate to Figs. 6.10 and 6.11. Results are in order of increasing concentration except where indicated by * which is for the same concentration but measured after a lapse in time (ca. 30 mins).

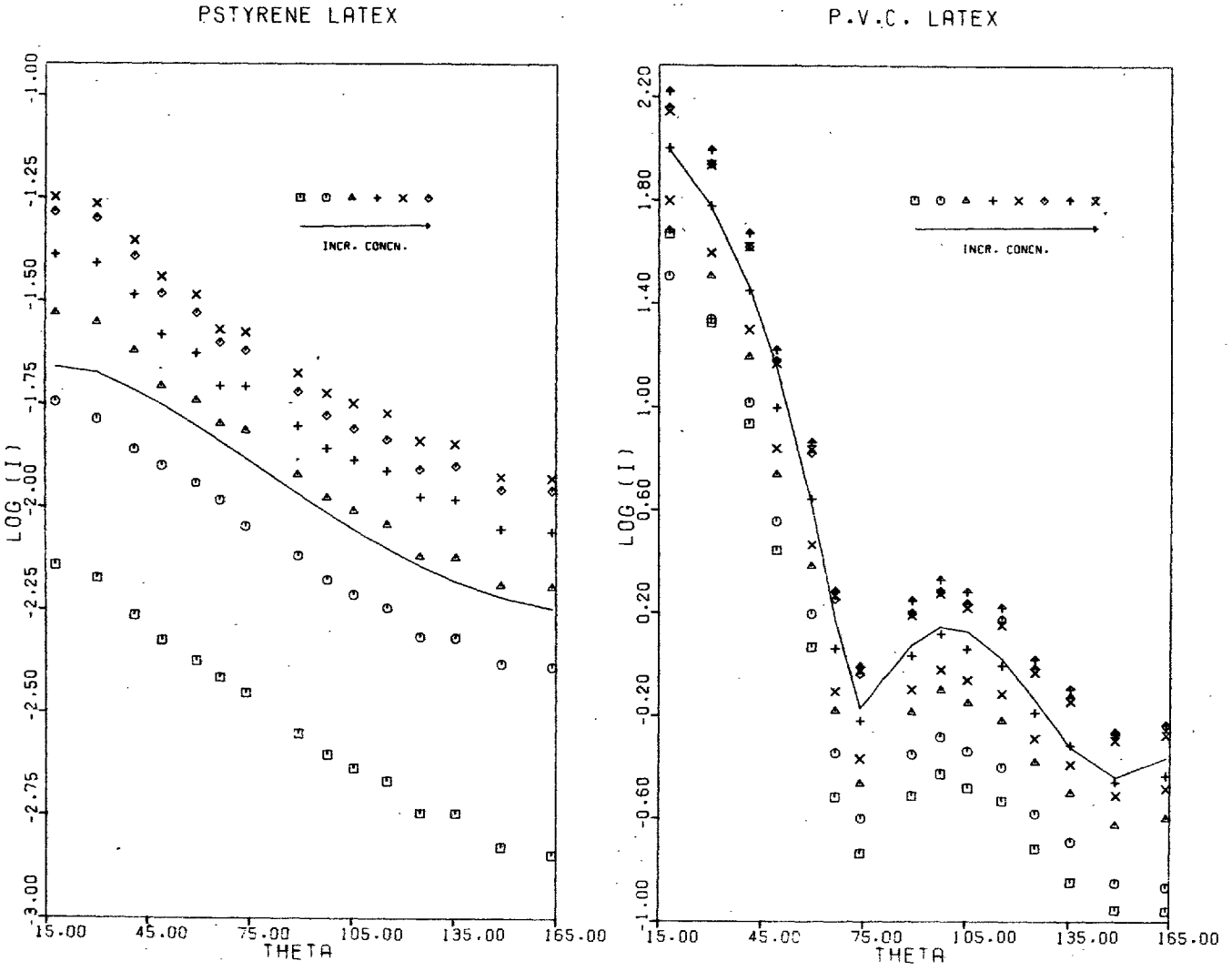

FIG. 6.10 Experimental Light Scattering Results for Latex Dispersions (solid line corresponds to the predicted best fitting size distribution)

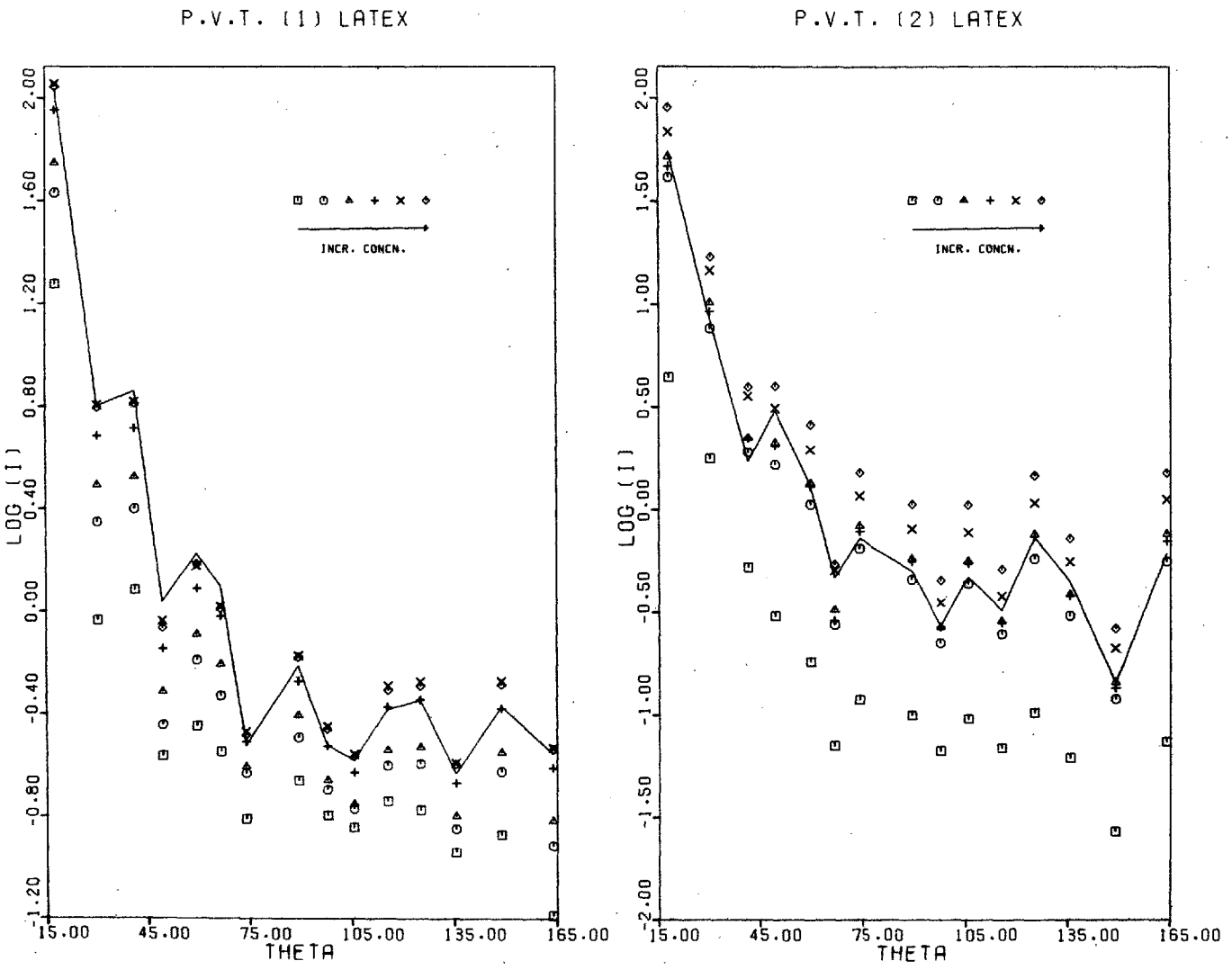

FIG. 6.11 Experimental Light Scattering Results for Latex Dispersions (solid line corresponds to the predicted best fitting size distribution)

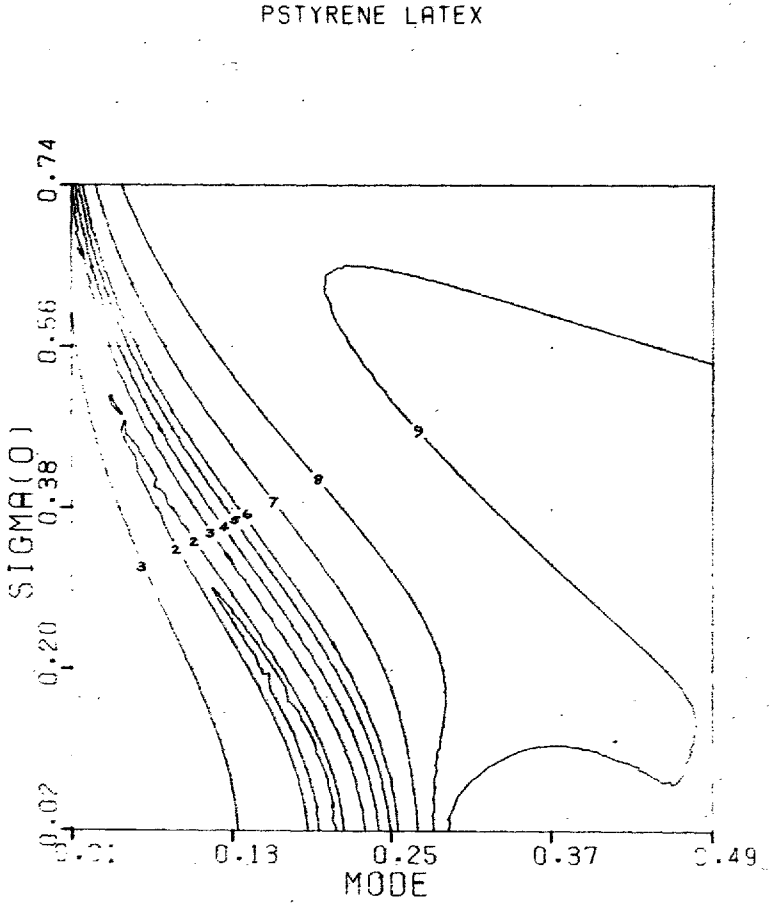

FIG. 6.12 Error Contour Diagram. Experimental Data for Vertically Polarised Light

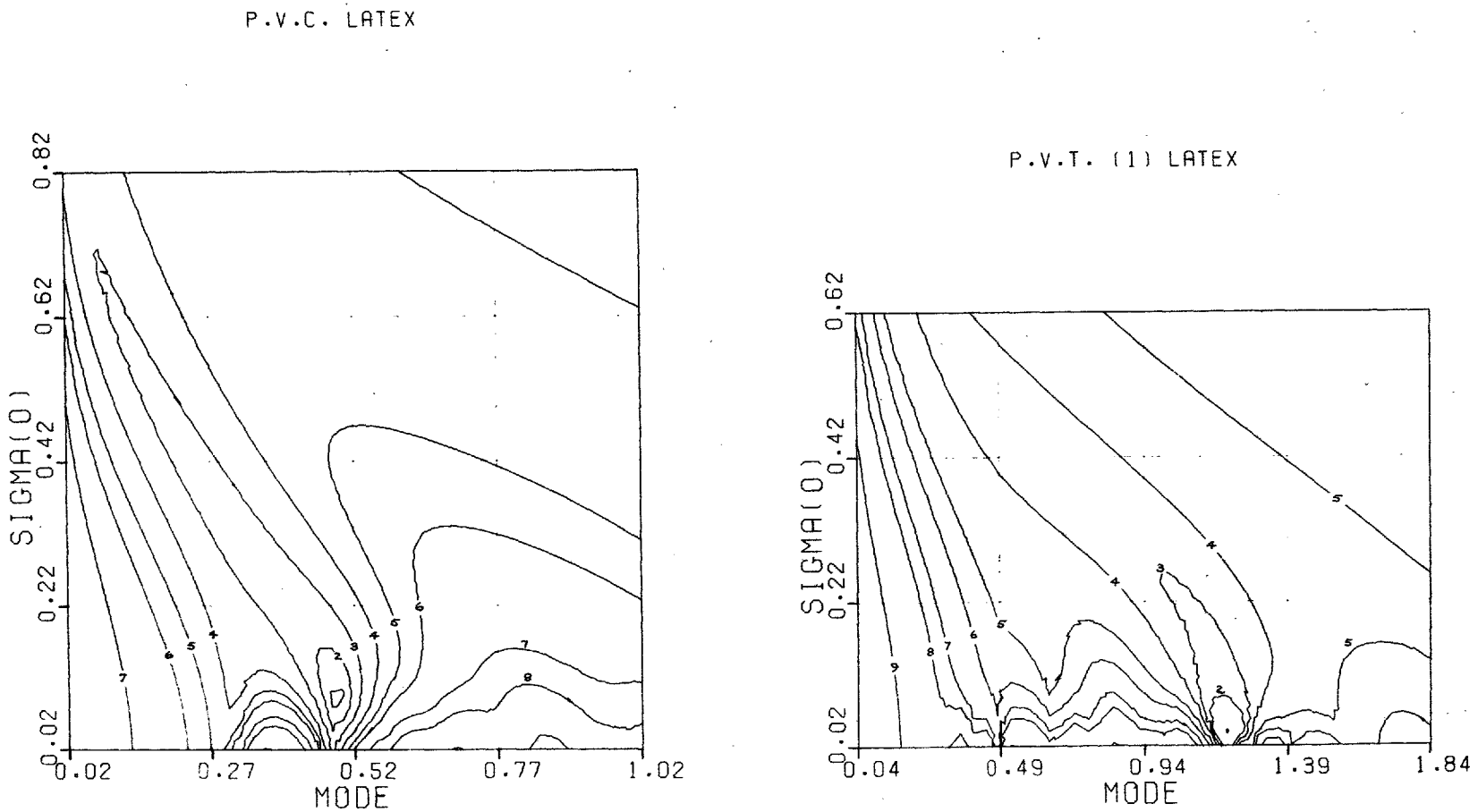

FIG. 6.13 Error Contour Diagrams. Experimental Data for Vertically Polarised Light

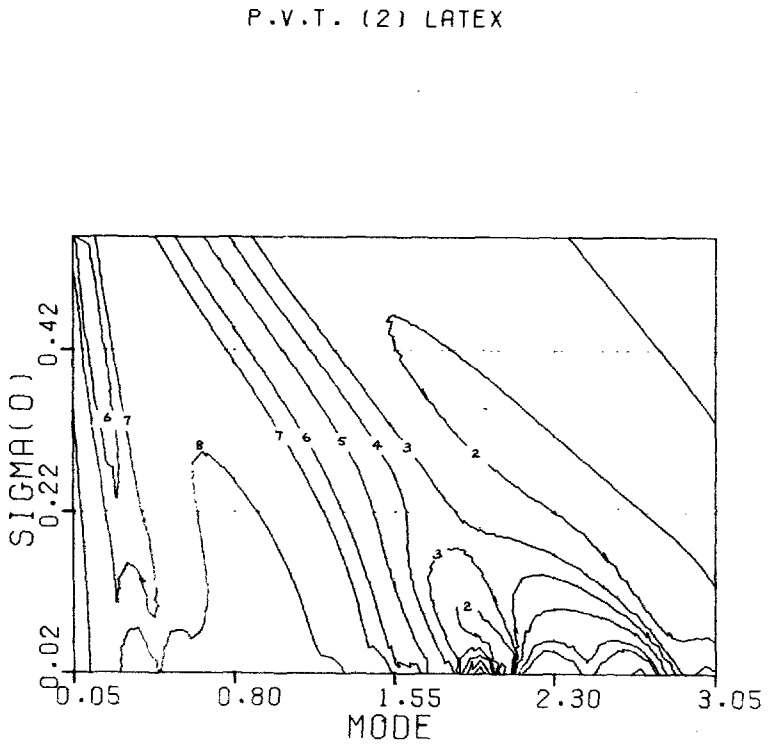

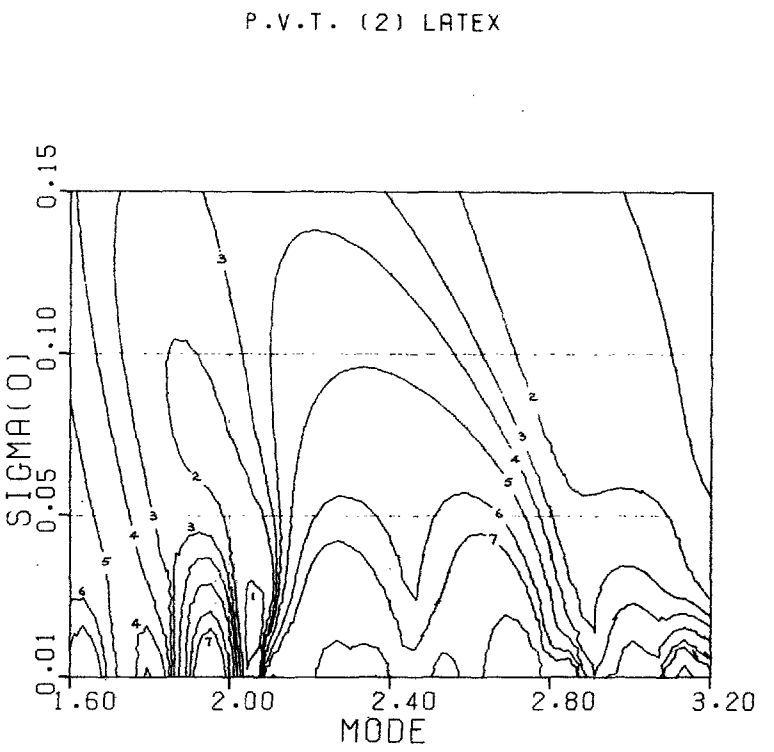

FIG. 6.14 Error Contour Diagrams. Experimental Data for Vertically Polarised Light

6.3 Size Analysis of the Ammonia/Sulphur Dioxide Aerosol

6.31 Electron Microscopy

Since little was known about the particle shape of the NH_3/SO_2 aerosol; apart from work by Heard and Whiffen (1969) on ammonium sulphate particles sampled from the atmosphere which were predominatly spherical and had a median diameter of 0.3 μm; a short series of experiments was conducted prior to the light scattering study. A simple experimental arrangement analogous to that described by Maddock (1970) was used to flow the two gas mixtures from glass storage bulbs to a spherical glass reaction vessel, evacuated before each run. Samples of the aerosol were withdrawn onto Type VF Millipore membrane filters and specimens prepared for examination by an electron microscope using a similar technique to that of Larner (1964).

Sample electron micrographs, including one of an unused Millipore filter for background comparison purposes, are shown in Fig. 6.15 and size distribution curves in Fig. 6.16. The small particles of aerosol I resulted from the rapid dilution with dry nitrogen of an initial mixture at low pressure containing approximately 4% ammonia and 4% sulphur dioxide in nitrogen. Micrograph (d) is of a rather heavy deposit from aerosol IV and shows a number of agglomerates of near spherical particles which may or may not have been present in the original aerosol prior to sampling. Also apparent is the partial decomposition of the particles after only a short, approximately 10 second, exposure to the electron beam. The large particle in micrograph (c) is the consequence of injecting a small quantity of water into a reaction mixture similar in concentration to those already described.

FIG. 6.15 Electron Micrographs of NH_3/SO_2 Aerosol Particles

Magnification x 10000

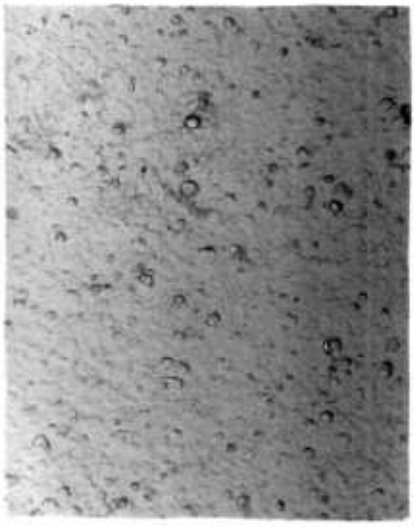

a) Millipore Type VF Filter - unused

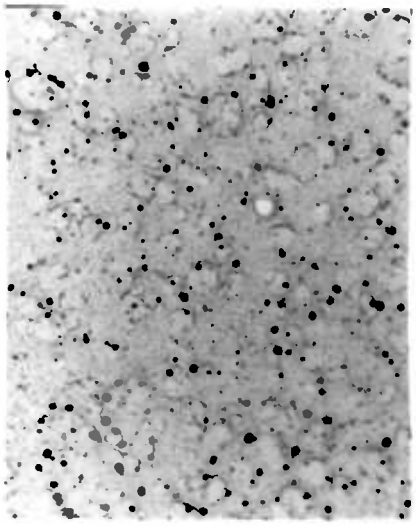

b) Aerosol I

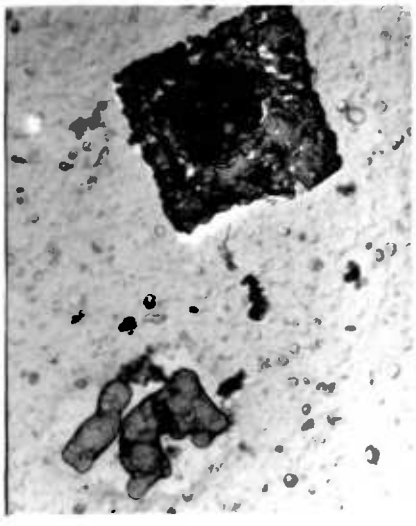

c) Aerosol V
One of Several Large Particles Formed

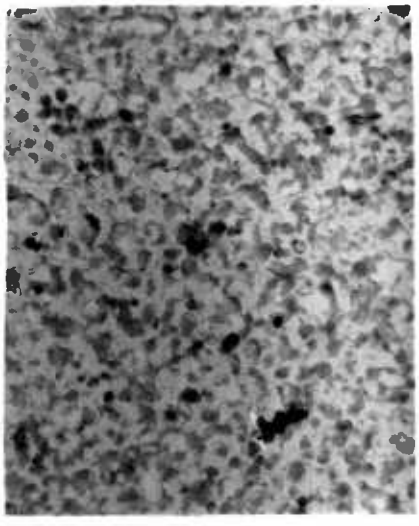

d) Aerosol IV
Heavy deposit showing partial decomposition by electron beam

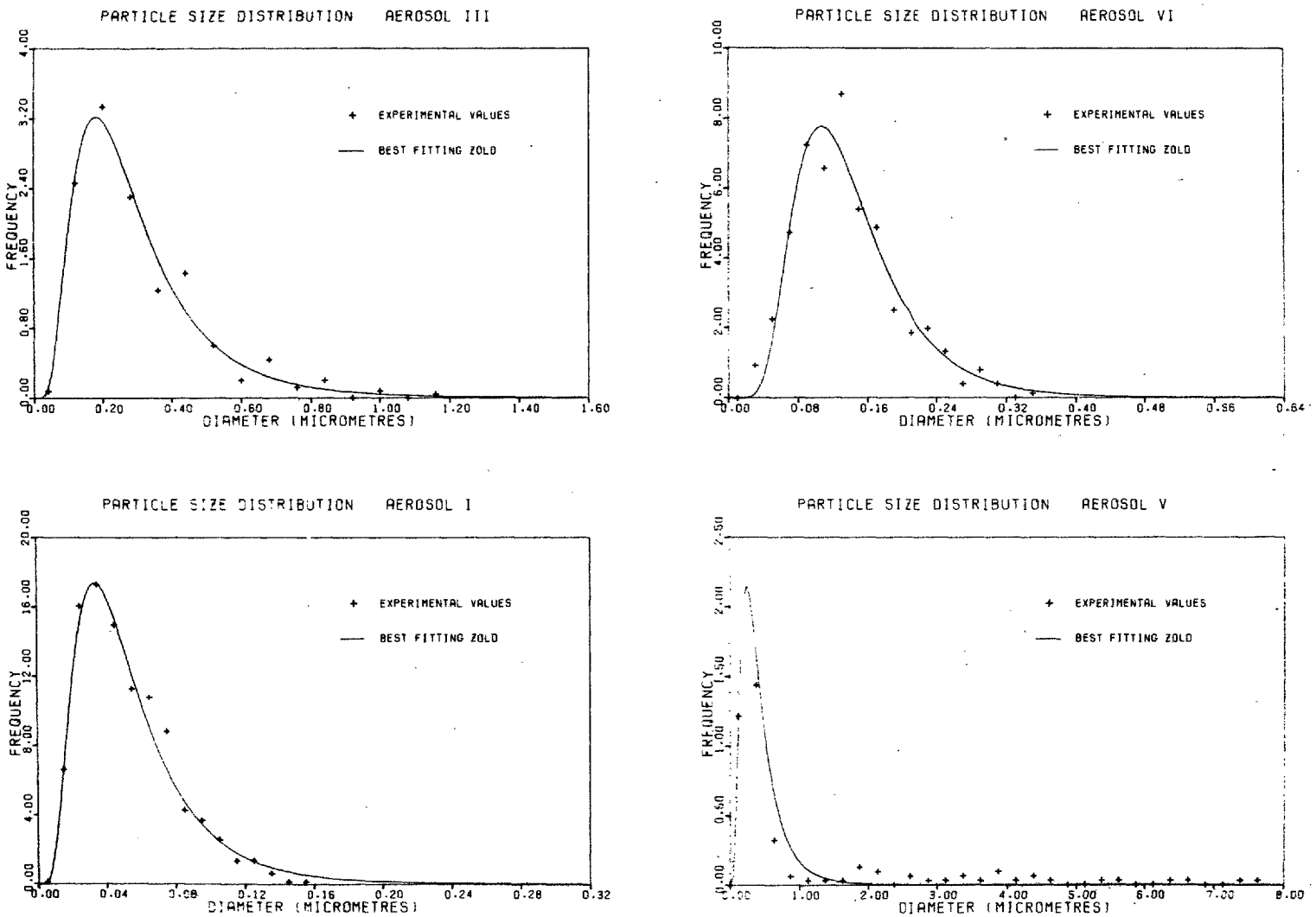

FIG. 6.16 NH_3/SO_2 Aerosol Size Distributions Obtained from Electron Microscopy

An overall appraisal of the micrographs and size distribution curves indicated that individual particles were generally spherical in shape, provided the specimens had not been allowed to absorb moisture, and conformed to a ZOLD size function. The aerosols should therefore be amenable to the proposed light scattering inversion analysis, which is based on these two assumptions, unless the aggregation apparent in several micrographs was not a direct result of the sampling method.

6.32 Light Scattering

The investigation of the NH_3/SO_2 aerosol forming reaction using the light scattering instrument had to be limited to a preliminary study owing to the time available. Six experimental runs were made, in half the scattering cell was flushed through with filtered laboratory air and the remainder with filtered cylinder nitrogen (oxygen free). The flows of the two reactant gas mixtures were each approximately 50cc/min (or a 50 to 25 split to achieve a 2:1 concentration ratio for either reactant) with an outflow sufficient to keep the pressure in the cell at atmospheric. The incoming gas streams were stirred gently on entry to encourage mixing and the maintenance of a reasonably steady aerosol concentration within the scattering volume. In the latter stages of a run all the flows and stirring were stopped and the aerosol allowed to develop without any further external influence. In all the studies the only radiation present in the reaction cell was the laser beam itself.

An aerosol formed in all cases, usually within about 30 seconds of starting the gas flows into the scattering cell, which corresponded to an initial rapid increase in the measured intensities. The time per scan, with four readings per station, was 17.8 seconds which was

reduced to 10.9 seconds when only two readings were selected per station. However, even at these speeds the change in intensity at a particular angle on successive scans was still relatively high, sometimes double, in the first stages of aerosol formation. Since this effect could be caused by fluctuations in the number concentration owing to varying the gas flow patterns through the scattering volume as well as increasing particle size, there was little to be gained by interpolating amongst the recorded intensities to establish an intensity pattern at a particular instant in time. It was possible to see the movement of the particles in the laser beam quite clearly by viewing through the small observation window in the side of the scattering cell.

All the experimental intensity scans were analysed using the SEARCH inversion program with intensity coefficients for a relative refractive index of 1.53. Almost without exception the size distributions predicted were either $d_M \simeq 0.05\ \mu m\ \ \sigma_o \simeq 0.6$ or $d_M \simeq 1.4\ \mu m\ \ \sigma_o \simeq 0.1$ and characterised by a fairly high error sum (at least an order of magnitude above the latex results). Several different starting points were used in the data analysis and in a number of cases the choice between the two alternative distributions depended on the actual starting point chosen. Even when there was little relative change in intensity on successive scans, contrasting with the rapid changes during aerosol formation, there was little variation in the predicted size distributions throughout the whole time period, although there was a greater tendency towards the distribution with the larger of the two modes as the answer at the later times.

Two examples of the recorded variations in the scattered intensity are shown in Fig. 6.17 where each set of symbols corresponds to a particular scan of the instrument, the scans ranging from the one following the first indications of aerosol formation until after all flows had been stopped. Aerosol LS3 is one produced when filtered air had been used

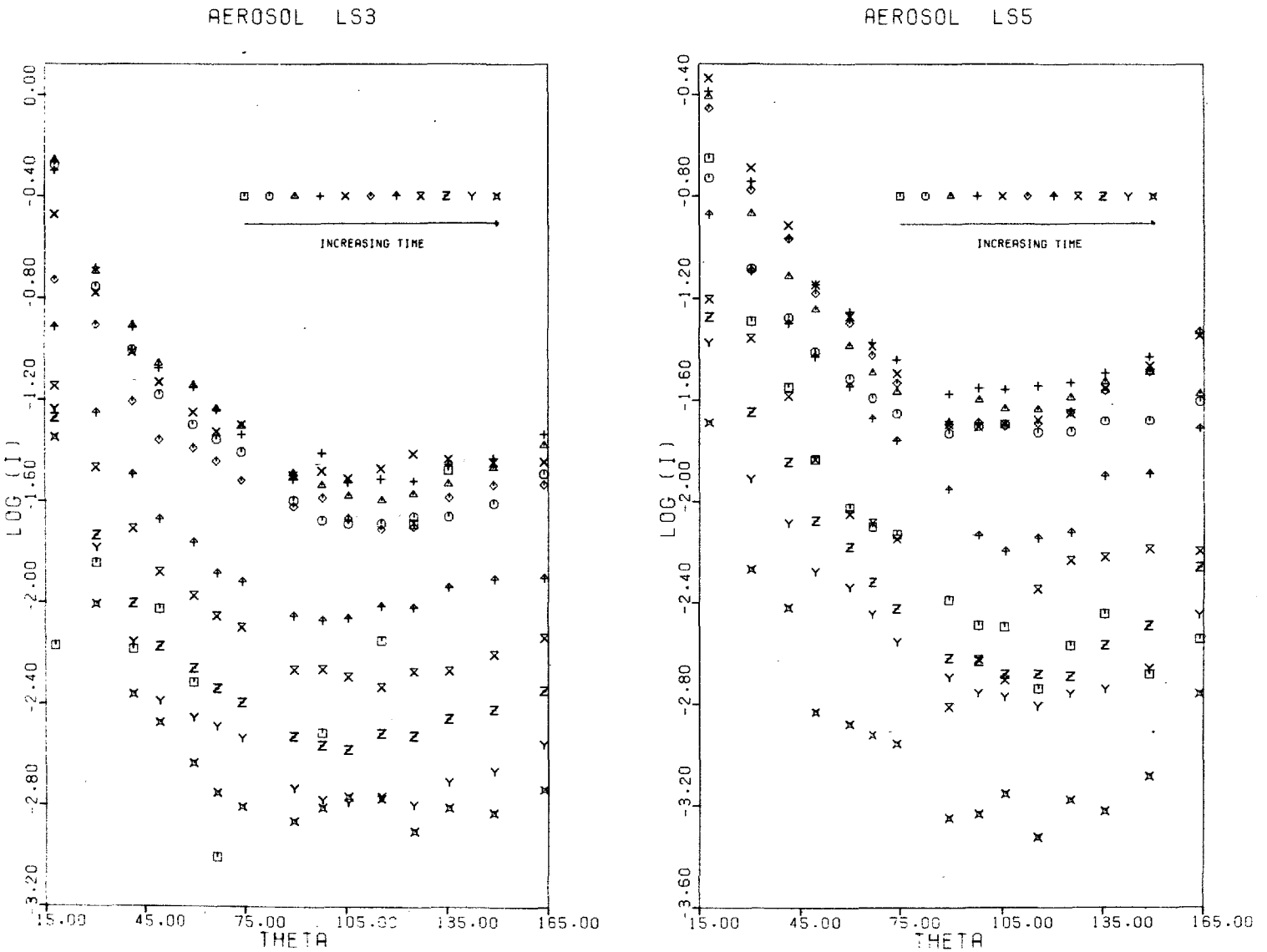

FIG. 6.17 Experimental Light Scattering Results for NH_3/SO_2 Aerosol

as the flushing medium together with equal flows of the reactant gases. The alternative using nitrogen as the flushing and diluent gas is typified by Aerosol LS5 and here equal reactant gas flows have again been used. In both examples the scattering intensities can be seen to increase rapidly and then start to diminish once the gas flows have stopped. There are also several common features shared between the curves for the two runs possibly indicating similarities in size distribution development.

Further to this point it was observed in two other runs that aerosol still remained in the cell, despite continual flushing with inert gas, some two hours after cessation of the reactant gas flows. Inversion of intensity scans taken at this time gave similar size distributions ($d_M \simeq 0.7\,\mu m$, $\sigma_o \simeq 0.2$) with error sums much lower than all the other aerosol inversions and comparable to the earlier latex results. In view of these two results it may be that in other cases the particle concentration was too high and that multiple scattering was predominant.

Although this preliminary study failed to produce any significant particle size information the time scale of the initial formation of the aerosol is in agreement with Megaw and Cox (1969). They reported that the aerosol observed downwind of a pair of stacks emitting respectively ammonia and sulphur dioxide must have been formed within 10 seconds or so of the mixing of the two effluents. Experiments by Friend et al (1972) on the reactant system air - H_2O (trace) - SO_2 (~ 1 ppm) - NH_3 (~ 1 ppm) indicated a rapid production of Aitken nuclei ($d \leq 0.2\ \mu m$) followed within a few minutes by the production of large particles in measurable concentrations up to $2\,\mu m$ diameter. However, they found that this reaction only occurred in the presence of light (U.V. radiation) there being no significant change from the

background nuclei count if the gases were mixed in the darkness or alternatively if nitrogen was used instead of air as the diluent gas whether in the light or not. The results of this investigation, although using much higher ammonia and sulphur dioxide concentrations, contradict these observations, an aerosol always rapidly forming in the dark even when using nitrogen as the diluent.

No indication is given by Friend et al (1972) as to the shape of the larger particles, for example, if they were agglomerates of the smaller nuclei. Even assuming that their particles were spherical throughout the size range up to 2 μ m considerable difficulties would be encountered in a light scattering study, as they were here, because of the width of distribution and the complicated oscillatory nature and greater magnitude of the scattering intensities at the larger sizes. The more likely explanation to account for the relative failure of the light scattering study is a combination of nucleation and growth with coagulation resulting in aggregates that give an angular intensity distribution far removed from those calculated assuming spherical particles following a logarithmic size distribution. It would seem likely therefore that the aggregates predominant on several electron micrographs taken from aerosols produced under not too dissimilar conditions from those prevailing in the light scattering study were not formed on the membrane sampling filter as thought previously but were already present in the aerosol cloud.

An analysis based on the assumption of Brownian coagulation with say an additional input term to account for the continuing formation of new particles would not be productive in this instance. Even if it was possible to predict the number and size of particles in the clusters as a function of time, there is still the problem of evaluating the light scattering

properties which are themselves functions of the arrangement of the particles within the cluster. At present, as mentioned in earlier chapters, this is only possible if the particle refractive index relative to the suspension medium is close to one. Hence, for the NH_3/SO_2 aerosol where this ratio (m) is approximately 1.53 the approach would not be feasible.

CHAPTER 7

Conclusions and Suggestions for Future Work

Light scattering has been shown to be a powerful tool for in situ measurement of the size distribution of dispersions of particles. It should be borne in mind when applying these techniques that the present scattering theory is rigorous only for spheres of arbitrary size and refractive index, although, under certain limiting conditions referred to in Section 2.3, it is quite possible to analyse particles of a non-spherical shape.

The scanning light scattering instrument developed during the course of this work employs a linearly polarised He - Ne laser as the light source and allows, in its present design phase, for the measurement of up to fifteen different angular intensities per scan. For use in conjunction with the instrument a computer technique, based on the assumption that the scatterers were spherical and satisfied a zeroth-order logarithmic distribution (ZOLD), was devised to invert the measured scattering data and predict the best-fitting distribution parameters. Inversion of test data evaluated at two refractive indices ($m = 1.19$ and 1.52) and for a number of different ZOLD functions was shown in Section 6.1 to be feasible over the range of modal diameters 0.1 to 2 μm with spreads in some cases of up to 0.6. In each case the data corresponded to the same set of fifteen scattering angles and radiation wavelength that were to be used in later experiments.

Even with the advent of extremely high-speed computers it would still be extremely costly and time consuming to completely evaluate the range of applicability of this technique as a function of refractive index, wavelength of the incident light, different combinations of scattering angles, particle size and width of distribution. The size range quoted

above should however provide a reasonable estimate of the size determination capabilities of this particular instrument when used in conjunction with the data inversion computer program, SEARCH.

Among the advantages to be gained in using measured intensities at only one orientation of the polarisation plane (vertical in this instrument) over the alternate polarisation method are an increase in data acquisition speed, based on using the same number of scattering angles, and an extended size range of applicability, as indicated Section 6.1. Whereas the polarisation ratio tends to become invariant with scattering angle as the size and expecially the spread increase the angular intensity curves for vertical polarisation have been shown to retain sufficient structure for the inversions to be successfully completed.

The light scattering instrument has provided data on several latex dispersions which have subsequently been successfully inverted to yield size distribution parameters close to those obtained from an electron microscope analysis. Since it is quite probable that there are errors in both these methods, there is no 'absolute' standard to which to compare the results.

Using the instrument to investigate the reaction of gaseous ammonia and sulphur dioxide showed that particles were produced in detectable numbers within about fifteen seconds of the gases mixing. The measured angular scattering data, however, rarely produced consistent size distributions with a low sum of squares error term from the inversion analysis. Several possible reasons have been put forward for this relative failure; the presence of significant numbers of agglomerates or non-spherical particles in the aerosol thereby invalidating the basic assumptions behind the inversion program, the initial rapid increase and subsequent fluctuations in the particle number concentration within the scattering volume, and too high a particle concentration which would negate the assumption of single particle scattering. Evidence of aggregate formation had been found in several electron micrographs of aerosol samples.

Recalling the consistent results obtained for the stable latex dispersions and the inversion of theoretical scattering data it would appear that the basic design of the light scattering instrument is sound. The problems in the aerosol formation study could have arisen from combining the reaction chamber and scattering cell as one unit thereby allowing insufficient control over the movement and number of aerosol particles within the scattering volume. In future studies of this nature it would seem advantageous to have the reaction vessel as a separate item and then flow a sample stream of the aerosol with an inert gas sheath through the light beam, as mentioned earlier in Section 4.34. From the pollution view point it is also perhaps worth considering reducing the concentrations of ammonia and sulphur dioxide from the relatively high levels used here to levels approaching those to be found in the atmosphere. This could be achieved for example by using permeation membranes and would possibly have the added advantage, as far as light scattering is concerned, of reducing the resulting aerosol particle concentration.

Experience in using the light scattering instrument has revealed one or two areas which would benefit from minor design changes. Ideally the scan completion time of the instrument, at present limited by the sampling rate of the digital voltmeter, needs to be decreased to follow particle growth more accurately. Large changes, which sometimes occur at present, between the scattering intensities recorded at the same angle on successive scans should be reduced but it may be found necessary to interpolate between measurements at successive scans in order to obtain a complete angular scattering distribution at a particular instant in time. A further design improvement would be to include a pre-selectable time delay at the end of a scan. This would provide a single fast scan capability at prescribed time intervals, useful for monitoring purposes where rapid and continued size changes are not expected. Introduction of a narrow band passfilter (e.g. 0.0005 μm)

at the front of the light-tight photomultiplier housing would enable the instrument to be operated in full roomlights or daylight with only a marginal increase in the recorded background light levels.

Implementation of these improvements would increase the potential of this instrument for particle size analysis. Its time resolution would be commensurate with that required for studies on Brownian coagulation and condensation growth. (Carabine and Moore, 1973; see Appendix C). This would be of particular interest in systems involving liquid droplets where particle sphericity is likely to be retained thereby allowing the use of the rigorous Mie theory of light scattering. Further scope for in situ particle size measurement, using an instrument based on the prototype developed here, lies for example in the field of monitoring pollution in the atmosphere or size and quality control in the manufacture of particulate products.

REFERENCES

Bateman, J.B., Weneck, E.J. and Eshler, D.C. (1959) J. Colloid Sci. 14, 308

Benoit, H., Ullman, R., de Vries, A.J. and Wippler, C. (1962) J. Chim. Phys. 59, 889

Born, M. and Wolf, E. (1964), "Principles of Optics" Pergamon Press, Oxford.

Cadle, R.D. (1972) J. Colloid Interface Sci. 39, 25

Cadle, R.D. and Robbins, R.C. (1960) Faraday Soc. Discussion No. 30, 155

Carabine, M.D. (1972) Chem. Soc. Rev. 1, 411

Chao-Ming Huang, Kerker, M. and Matijevic, E. (1970) J. Colloid Interface Sci. 33, 529

Chin, J.H., Sliepcevich, C.M. and Tribus, M. (1955) J. Phys. Chem. 59, 841

Coutarel, L, Matijevic, E. and Kerker, M. (1967) J. Colloid Interface Sci. 24, 338

Dayhoff, M.O. (1963) Comm. A.C.M. 6, 620

Davidson, J.A. and Collins, E.A. (1972) J. Colloid Interface Sci. 40, 437

Debye, P. (1909) Ann. Physik, 30, 57

Debye, P. (1915) Ann. Physik, 46, 809

Debye, P. (1930) Physik Z. 31, 419

Debye, P. (1947) J. Phys. & Colloid Chem. 51, 18

Dezelic, G. and Kratohvil, J. P. (1961) J. Colloid Sci. 16, 561

Eggleton, A.E.J. and Atkins, D.H.F. (1969) Atmospheric Environment 3, 355

Espenscheid, W.F., Kerker, M. and Matijevic, E. (1964a) J. Phys. Chem. 68, 3093

Espenscheid, W.F., Matijevic, E. and Kerker, M. (1964b) J. Phys. Chem. 68, 2831

Friend, J.P., Leifer, R. and Trichon, M. (1972) submitted to J. Atmos. Sci.

Gans, R. (1925) Ann. Physik, 76, 29

Gladkova, E. and Natanson, G. (1958) in "Aerosol Science" ed. Davies, C.N. Academic Press, London

Gledhill, R.J. (1962) J. Phys. Chem. 66, 458

Gumprecht, R.O. and Sliepcevich, C.M. (1951) "Tables of Light Scattering Functions for Spherical Particles". Univ. of Michigan Press. Ann. Arbor, Michigan

Gumprecht, R.O. and Sliepcevich, C.M. (1953) J. Phys. Chem. 57, 95

Hanel, G. (1968) Tellus 20, 371

Harris, F.S. (1969) Tellus 21, 223

Harris, F.S., Sherman, G.C. and Morse, F.L. (1967) IEEE Trans. Antennas Propagation AP-15, 141

Hata, T. and Kinumaki, S. (1964) Nature 203, 1378

Healy, T.V., McKay, H.A.C., Pilbeam, A. and Scargill, D. (1970) J. Geoph. Res. 75, 2317

Heard, M.J. and Wiffen, R.D. (1969) Atmospheric Environment 3, 337

Heller, W. (1965) J. Phys. Chem. 69, 1123

Heller, W. and Nakagaki, M. (1959) J. Chem. Phys. 31, 1188

Heller, W. and Wallach, M.L. (1963) J. Phys. Chem. 67, 2577

Heller, W. and Wallach, M.L. (1964) J. Phys. Chem. 68, 931

Heller, W., Wada, E. and Papazian, L.A. (1961) J. Polymer Sci. 47, 481

Hodkinson, J.R. (1966) Appl. Optics 5, 839

Jacobsen, R., Kerker, M. and Matijevic, E. (1967) J. Phys. Chem. 71, 514

Johnson, I. and La Mer, V.K. (1947) J. Am. Chem. Soc. 69, 1184

Johnstone, H.F. and Coughanowr, D.R. (1958) Ind. and Eng. Chem. 50, 1169

Junge, E.C. (1954) J. Met. 11, 323

Kerker, M. (1950) J. Colloid Sci. 5, 164

Kerker, M. (1969) "The Scattering of Light and Other Electromagnetic Radiation" Academic Press, New York

Kerker, M. (1972) J. Colloid Interface Sci. 39, 2

Kerker, M. and La Mer, V.K. (1950) J. Am. Chem. Soc. 72, 3516

Kerker, M. and Hampton, M.I. (1953) J. Opt. Soc. Am. 43, 370

Kerker, M. and Matijevic, E. (1960) J. Opt. Soc. Am. 50, 722

Kerker, M., Daby, E., Cohen, G.L., Kratohvil, J.P. and Matijevic, E. (1963) J. Phys. Chem. 67, 2105

Kerker, M., Krathovil, J.P. and Matijevic, E. (1962) J. Opt. Soc. Am. 52, 551

Kerker, M., Matijevic, E., Expenscheid, W.F., Farone, W.A. and Kitani, S. (1964) J. Colloid Sci. 19, 213

Kiang, C.S., Stauffer, D. and Mohnen, V.A. (1973) submitted to Nature

Kitani, S. (1960) J. Colloid Sci. 15, 287

Kratky, O. and Porod, G. (1949) J. Colloid Sci. 4, 35

Kratohvil, J.P. (1964) Anal. Chem. 36, 458R

Kratohvil, J.P. (1966) Anal. Chem. 38, 517R

Kratohvil, J.P. (1966) J. Colloid Interface Sci. 21, 498

Kratohvil, J.P. and Smart, C. (1965) J. Colloid Sci. 20, 875

Larner, E.E. (1964) Atomic Weapons Research Establishment, Unclassified Report No. 0-84/64

Lips, A., Smart, C. and Willis, E. (1971) Trans. Faraday Soc. 67, 2979

Maddock, J.E.L. (1970) M.Sc. Thesis, Univ. of London

Maron, S.H. and Elder, M.E. (1963a) J. Colloid Sci. 18, 107

Maron, S.H. and Elder, M.E. (1963b) J. Colloid Sci. 18, 199

Maron, S.H., Elder, M.E. and Pierce, P.E. (1963a) J. Colloid Sci. 18, 733

Maron, S.H., Pierce, P.E. and Elder, M.E. (1963b) J. Colloid Sci. 18, 391

Maron, S.H., Pierce, P.E. and Ulevitch, I.N. (1963c) J. Colloid Sci. 18, 470

Matijevic, E., Kitani, S. and Kerker, M. (1964) J. Colloid Sci. 19, 223

Maxim, L.D., Klein, A., Meyer, M.E. and Kuist, C.H. (1966) Abstracts, Am. Chem. Soc. Meeting, Sept. 1966, New York

Meehan, E.J. and Beattie, W.H. (1960) J. Phys. Chem. 64, 1006

Megaw, W.J. and Cox, L.C. (1969) Proceedings of Seventh International Conference on Condensation and Ice Nuclei, Prague and Vienna, page 92

Mie, G. (1908) Ann. Physik 25, 377

Müller, H. (1928) Kolloidchem. Beihefte 26, 257

Nakagaki, M. and Heller, W. (1960) J. Chem. Phys. 32, 835

Nakagaki, M. and Shimoyama, T. (1964) Bull. Chem. Soc. Japan 37, 1634

Napper, D.H. and Ottewill, R.H. (1963) J. Colloid Sci. 18, 262

Napper, D.H. and Ottewill, R.H. (1964) Trans. Faraday Soc. 60, 1466

Neugebauer, T. (1943) Ann. Phys. 42, 509

Nicolaon, G., Kerker, M., Cooke, D.D, Matijevic, E. (1972) J. Colloid Interface Sci. 38, 460

Ottewill, R.H. and Shaw, J.N. (1966) Disc. Faraday Soc. 42, 154

Picot, C. Weill, G. and Benoit, H. (1968) J. Colloid Interface Sci. 27, 360

Pierce, P.E. and Maron, S.H. (1964) J. Colloid Sci. 19, 658

Powell, M.J.D. (1965) Computer J. 7, 303

Rayleigh, Lord (1881) Phil. Mag. 12, 81

Rayleigh, Lord (1918) Proc. Roy. Soc. A94, 296

Rowell, R.L., Wallace, T.P. and Kratohvil, J.P. (1968) J. Colloid Interface Sci. 26, 494

Sargent, R.W.H. (1973) "Numerical Optimisation Techniques" Dept. Chem. Eng. & Chem. Tech. Imperial Coll., London

Scott, W.D., Lamb, D. and Duffy, J. (1969) J. Atmos. Sci. 26, 727

Sherman, G.C., Franklin, S., Harris, F.S. and Morse, F.L. (1968) Appl. Optics 7, 421

Sinclair, D. and La Mer, V.K. (1949) Chem. Rev. 44, 245

Smoluchowski, M. (1917) Z. Physik. Chem. (Leipzig) 92, 129

Stevenson, A.F., Heller, W. and Wallach, M.L. (1961) J. Chem. Phys. 34, 1789

Stratton, J. (1941) "Electromagnetic Theory" McGraw-Hill, New York

Tabibian, R.M. and Heller, W. (1958) J. Colloid Sci. 13, 6

Urone, P. and Schroeder, W.H. (1969) Environmental Sci. and Technology. 3, 436

Van de Hulst, H.C. (1957) "Light Scattering by Small Particles", Wiley, New York

Van den Heuvel, A.P. and Mason, B.J. (1963) Quart. J. Roy. Meteorol. Soc. 89, 271

Wallace, T.P. and Kratohvil, J.P. (1967) J. Polymer Sci. B5, 1139

Wallach, M.L. and Heller, W. (1964) J. Phys. Chem. 68, 924

Wallach, M.L., Heller, W. and Stevenson, A.F. (1961) J. Chem. Phys. 34, 1796

Walton, A.G. and Hlabse, T. (1963) Talanta 10, 601

Willis, E., Kerker, M. and Matijevic, E. (1967) J. Colloid Interface Sci. 23, 182

Wippler, C. de Vries, A.J. and Benoit, H. (1959) IUPAC Symp. Macromol, Communication III C8 Verlag Chemie, Wiesbaden, Germany

Yajnik, M., Witeczek, J. and Heller, W. (1968) J. Polymer Sci. C25, 99

APPENDIX

A. Computation of Light Scattering Data

The computer print-out at the end of this appendix is of the programme which evaluates, using the Mie theory, the efficiencies for extinction, scattering, absorption and radiation pressure, and the angular intensity functions for both horizontally and vertically polarised radiation. The data required are the particle diameter, the radiation wavelength, the refractive index of both particle and medium (which must be real in this instance) and the increment of change in the scattering angle at which the intensities are to be computed. The mathematical methods used to evaluate the various scattering quantities are as follows:-

(i) the scattering coefficients a_n and b_n

These coefficients are expressed in terms of the parameters m and α , and the relevant Ricatti-Bessel function.

$$a_n = \frac{\psi_n(\alpha)\,\psi_n'(\beta) - m\,\psi_n(\beta)\,\psi_n'(\alpha)}{\zeta_n(\alpha)\,\psi_n'(\beta) - m\,\psi_n(\beta)\,\zeta_n'(\alpha)} \qquad \text{A.1}$$

$$b_n = \frac{m\,\psi_n(\alpha)\,\psi_n'(\beta) - \psi_n(\beta)\,\psi_n'(\alpha)}{m\,\zeta_n(\alpha)\,\psi_n'(\beta) - \psi_n(\beta)\,\zeta_n'(\alpha)} \qquad \text{A.2}$$

The Ricatti-Bessel functions $\psi_n(z)$, $\chi_n(z)$, $\zeta_n(z)$ are related respectively to the half integral order spherical Bessel, Neumann and the second kind of Hankel functions.

$$\psi_n(z) = z\,j_n(z) \qquad \chi_n(z) = z\,n_n(z) \qquad \text{A.3}$$

$$\zeta_n(z) = z\,h_n^{(2)}(z) = \psi_n(z) + i\,\chi_n(z) \qquad \text{A.4}$$

The addition of a prime to these functions in A.1 and A.2 denotes differentiation with respect to their arguments. By using the following general recurrence relationships the appropriate Ricatti-Bessel function and its derivative can be readily calculated.

$$f_{n+1}(z) = \frac{2n+1}{z} f_n(z) - f_{n-1}(z) \qquad \text{A.5}$$

$$f_n'(z) = \frac{d}{dz} f_n(z) = \frac{n}{z} f_n(z) - f_{n+1}(z) \qquad \text{A.6}$$

The first two orders of each function are calculated directly from simple trigonometric expressions,

$$\psi_o(z) = \sin z \qquad \psi_1(z) = \frac{\sin z}{z} - \cos z \qquad \text{A.7}$$

$$\chi_o(z) = \cos z \qquad \chi_1(z) = \frac{\cos z}{z} + \sin z \qquad \text{A.8}$$

Repeated use of the recursion formula A.5 may cause severe accumulation of rounding errors especially if the order n becomes much larger than the argument z. In order to obviate this difficulty the sub-program evaluating these functions was written in double precision arithmetic which on the CDC 6400/6600 computers means the use of approximately 29 significant digits. The computed values of $\psi_n(z)$ and $\chi_n(z)$ agreed with those published in the National Bureau of Standards Handbook of Mathematical Functions to at least ten significant figures for values n and z up to 100 and 50 respectively. These values of order and argument are sufficiently large to enable the calculation of efficiency factors (using values of a_n and b_n in so doing as explained below) to a precision of 8 significant figures for size parameter (α) up to 50.

The routines were further checked by comparing values of a_n and b_n with those published by Gumprecht and Sliepcevich (1951) for various m and α .

(ii) the efficiency factors Q_{sca}, Q_{ext}, Q_{abs}, Q_{pr}

The calculation of these factors is accomplished by the summation of infinite series involving the scattering coefficients a_n and b_n.

$$Q_{sca} = \frac{2}{\alpha^2} \sum_{n=1}^{\infty} (2n + 1) \left\{ |a_n|^2 + |b_n|^2 \right\} \qquad A.9$$

$$Q_{ext} = \frac{2}{\alpha^2} \sum_{n=1}^{\infty} (2n + 1) \left\{ \mathrm{Re}\,(a_n + b_n) \right\} \qquad A.10$$

$$Q_{pr} = Q_{ext} - \overline{\cos\theta} \cdot Q_{sca} \qquad A.11a$$

where

$$\overline{\cos\theta} \cdot Q_{sca} = \frac{4}{\alpha^2} \sum_{n=1}^{\infty} \left\{ \left[n(n + 2)/(n + 1) \right] \mathrm{Re}(a_n^* a_{n+1} + b_n^* b_{n+1}) + \left[(2n + 1)/n(n + 1) \right] \mathrm{Re}\, a_n^* b_n \right\} \qquad A11b$$

The asterisk indicates that the complex conjugate is to be taken.

The method used was to progressively increase the summation limit n, from an initial estimate related to particle size, until the fractional change in Q_{sca}, Q_{ext} and the asymmetry function

$\overline{\cos\theta}$. Q_{sca} were all less than 10^{-9}. A simple computational check can be made of Eqns. A.9 and A.10 since for dielectric spheres there is no absorption i.e.

$$Q_{ext} = Q_{sca} \quad \text{and} \quad Q_{abs} = Q_{ext} - Q_{sca} = 0$$

The values of Q_{abs} obtained in such checks were all less than 10^{-13} which is very near the limit of precision for the difference of two single precision numbers with nearly identical values in the range 1 - 10. For values of α up to 50 and several refractive indices the computed scattering efficiencies were checked against tables compiled by Gumprecht and Sliepcevich (1951).

(iii) the intensity functions i_1 and i_2

These were evaluated by summing infinite series involving the scattering coefficients and the Legendre functions. The series were terminated at the same value of n that satisfied the convergence criteria for the efficiency factors.

$$i_1 = \left| \sum_{n=1}^{\infty} \frac{2n+1}{n(n+1)} \left\{ a_n \pi_n(\cos\theta) + b_n \tau_n(\cos\theta) \right\} \right|^2 \qquad \text{A.12}$$

$$i_2 = \left| \sum_{n=1}^{\infty} \frac{2n+1}{n(n+1)} \left\{ a_n \tau_n(\cos\theta) + b_n \pi_n(\cos\theta) \right\} \right|^2 \qquad \text{A.13}$$

The angular functions $\pi_n(\cos\theta)$ and $\tau_n(\cos\theta)$ are related to the associated Legendre polynomials of the zero or first degree.

$$\pi_n(\cos\theta) = \frac{P_n^{(1)}(\cos\theta)}{\sin\theta} = \frac{d}{d\theta} P_n(\cos\theta) \qquad \text{A.14}$$

$$\tau_n(\cos\theta) = \frac{d}{d\theta} P_n^{(1)}(\cos\theta) \qquad \text{A.15}$$

Hence

$$\tau_n(\cos\theta) = \cos\theta\ \pi_n(\cos\theta) - \sin^2\theta\ \pi_n'(\cos\theta) \qquad \text{A.16}$$

The first three values of $\pi_n(\cos\theta)$ and its derivative $\pi_n'(\cos\theta)$ are:-

$$\pi_o(\cos\theta) = 0 \qquad \pi_o'(\cos\theta) = 0 \qquad \text{A.17}$$

$$\pi_1(\cos\theta) = 1 \qquad \pi_1'(\cos\theta) = 0 \qquad \text{A.18}$$

$$\pi_2(\cos\theta) = 3\cos\theta \qquad \pi_2'(\cos\theta) = 3 \qquad \text{A.19}$$

Higher orders can then be obtained using the following recursion formulae:-

$$\pi_n(\cos\theta) = \cos\theta \left[(2n-1)/(n-1) \right] \pi_{n-1}(\cos\theta) - \left[n/(n-1) \right] \pi_{n-2}(\cos\theta) \qquad \text{A.20}$$

$$\pi_n'(\cos\theta) = \cos\theta \left[(2n-1)/(n-2) \right] \pi_{n-1}'(\cos\theta) + \left[(n+1)/(n-2) \right] \pi_{n-2}'(\cos\theta) \qquad \text{A.21}$$

Computed values of i_1 and i_2 were compared with published tables by Heller and Nakagaki (1959) and by Kerker and Matijevic (1960) for $\theta = 45^\circ$ and 135°, $m = 1.20$ and α up to 7. Agreement was found with both sets of published data in almost all cases to within 0.1%. Where there was a discrepency between the two published tables (9 cases out of the 70) my results agreed with Kerker's work except in one instance at $\alpha = 6.2$ where the results were very much nearer to Heller's answers.

```
      PROGRAM MIE (INPUT, OUTPUT, TAPE 5=INPUT, TAPE 6=OUTPUT)
C     THIS PROGRAM COMPUTES, USING THE MIE THEORY, THE
C     SCATTERING FUNCTIONS FOR HOMOGENOUS SPHERES HAVING
C     REAL REFRACTIVE INDEX
C     THE QUANTITIES EVALUATED ARE.. ..
C     1)  THE SCATTERING COEFFICIENTS A(N), B(N)
C     2)  THE EFFICIENCIES FOR EXTINCTION (QEXT), ABSORPTION
C         (QABS) AND SCATTERING (QSCA), AND THE RADIATION
C         PRESSURE (QPR)
C     3)  THE INTENSITY FUNCTIONS I(1), I(2) AS A FUNCTION
C         OF THE SCATTERING ANGLE (THETA)
C
C     MAIN PROGRAM EVALUATES EFFICIENCY FACTORS BY
C     SUMMATION OF INFINITE SERIES INVOLVING THE SCATTERING
C     COEFFICIENTS A(N) AND B(N)
C
C     RIP-REFRACTIVE INDEX OF PARTICLE
C     RIG-REFRACTIVE INDEX OF MEDIUM
C     RLAMDA-WAVELENGTH OF RADIATION
C     D-DIAMETER OF PARTICLE (SAME UNITS AS RLAMDA)
C     THETA-SCATTERING ANGLE IN DEGREES MEASURED FROM THE
C           FORWARD TO THE SCATTERED DIRECTION
C     DELTA-INTERVAL OF ANGLE (THETA)
C           SET DELTA=0.  IF INTENSITY FUNCTIONS NOT REQUIRED
C     N-NUMBER OF TERMS USED IN SERIES SUMMATION
C     SET LK POSITIVE ON LAST DATA CARD OTHERWISE LK NEGATIVE
C
C     SUBSCRIPTS USED IN THIS PROGRAM ARE ALL ONE GREATER
C     THAN THOSE IN MIE THEORY EQUATIONS

          COMPLEX A, B, AAC, BB C, F5, F4
          DIMENSION A(202), B(202)
          COMMON N, NN, N1, N2, N3, N4
    1     READ (5, 100) D, RIP, RIG, DELTA, RLAMDA, LK
          RIPTG=RIP/RIG
          X=3. 14159265*D/RLAMDA

C         COMPUTE ALPHA ---DIMENSIONLESS SIZE PARAMETER
          ALPHA=X*RIG
          ALPHA2=ALPHA*ALPHA
          BETA=RIPTG*ALPHA
          WRITE (6, 101) D, ALPHA, RIP, RIG

C         ESTIMATE NUMBER OF TERMS REQUIRED IN SERIES SUMMATION
          N=2.*X+2.
          IF (N-60) 3, 3, 2
    2     N=X

    3     N1=2
          N2=1
          N3=2
          N4=1

C         INITIALISE TEST VARIABLES FOR CONVERGENCE CRITERIA
          TSTEX=0.
          TSTSC=0.
          TSTAS=0.
```

```
C           INITIALISE STARTING VALUES FOR SERIES SUMMATION
                SCA=0.
                EXT=0.
                ASYM=0.

    4           NN=N+1
                CALL ABMIE (A, B, RIPTG, ALPHA, BETA)

C           SUM SERIES FOR SCA, EXT, ASYM
                DO 5 K=N1, N
                EN=K-1
                F1=2.*EN+1.
                F2=EN*(EN+2)/(EN+1.)
                F3=F1/(EN*(EN+1.))
                SA=A(K)*CONJG(A(K))
                SB=B(K)*CONJG(B(K))
                SCA=SCA+F1*(SA+SB)
                EXT=EXT+F1*(REAL(A(K)) + REAL(B(K)))
                AAC=CONJG (A(K+1))
                BBC=CONJG(B(K+1))
                F4=A(K)*AAC+B(K)*BBC
                F5=A(K)*CONJG(B(K))
    5           ASYM=ASYM+F2*REAL(F4)+F3*REAL(F5)

C           COMPUTE EFFICIENCES FOR SCATTERING (QSCA), EXTINCTION
C           (QEXT) AND ASYMMETRY FUNCTION (ASYMFN)
                QSCA=2./ALPHA2*SCA
                QEXT=2./ALPHA2*EXT
                ASYMFN=4./ALPHA2*ASYM

C           TEST FOR CONVERGENCE IN SERIES SUMMATIONS
                ATST=ABS(TSTEX./QEXT)
                BTST=ABS(ATST-1.)
                IF (BTST-.1E-08) 6, 6, 8
    6           ATST=ABS(TSTSC/QSCA)
                BTST=ABS(ATST-1.)
                IF (BTST-.1E-08) 7, 7, 8
    7           ATST=ABS(TSTAS/ASYMFN)
                BTST=ABS(ATST-1.)
                IF (BTST-.1E-08) 9, 9, 8

C           RESET TEST VARIABLES TO CURRENT ESTIMATES OF SERIES
C           SUMS
    8           TSTEX=QEXT
                TSTSC=QSCA
                TSTAS=ASYMFN

                N1=N+1
                N2=N+2
                N3=N2
                N4=N+3

C           IF THE RELATIVE ACCURACIES OF QSCA, QEXT, ASYMFN ARE
C           NOT ALL WITHIN .000000001 INCREASE N BY 5, RETURN TO
C           STEP 4AND ADD NEW TERMS TO THE RESPECTIVE SERIES SUM

                N=N+5
                GO TO 4
```

```
C           COMPUTE EFFICIENCIES FOR ABSORPTION (QABS) AND
C           RADIATION PRESSURE (QPR)
    9           QABS=QEXT-QSCA
                QPR=QEXT-ASYMFN

                WRITE (6, 102)
                WRITE (6, 103) QEXT, QSCA, QABS, QPR

                IF (DELTA) 10, 11, 10
   10           CALL POLAR (A, B, DELTA)
   11           CONTINUE

C           IF LK IS LESS THAN ONE RETURN TO START TO READ NEXT
C           SET OF DATA OTHERWISE STOP
                IF (LK) 1, 1, 12
   12           CONTINUE

C           FORMAT STATEMENTS FOR INPUT AND OUTPUT
   100          FORMAT (5F10.4, I3)
   101          FORMAT (1X, 2HD=, F7.4, 5X, 6HALPHA=, F7.4, 5X, 4HRIP=, F6.4,
               1 4HRIG=, F6.4)
   102          FORMAT (1X, 18HEFFICIENCY FACTORS/8X, 4HQEXT, 13X,
               1 4HQSCA, 13X, 4HQABS, 13X, 3HQPR)
   103          FORMAT (4(2X, E15.8))

                STOP
                END
```

```
      SUBROUTINE ABMIE (A, B, RIPTG, ALPHA, BETA)
C     TO EVALUATE SCATTERING COEFFICIENTS A(N) AND B(N) FROM
C     RICATTI-BESSEL FUNCTIONS PSI(N) AND CHI(N)
        COMPLEX A, B, AB, BB
        DIMENSION PSIS(2, 102), DPSI(2, 102),CHIS(102), DCHI(102),
     1 A(202), B(202)
        COMMON N, NN, N1, N2, N3, N4
        NNN=NN+1
        L=1
        CALL PSICHI (ALPHA, L, PSIS, CHIS)
        L=2
        CALL PSICHI (BETA, L, PSIS, CHIS)

        DO 2 K=N2, NN
        RK=K
C     DERIVATIVE FUNCTIONS DPSI(N) AND DCHI(N)
        DPSI(1, K)=RK/ALPHA*PSIS(1, K)-PSIS(1, K+1)
        DPSI(2, K)=RK/BETA*PSIS(2, K)-PSIS(2, K+1)
        DCHI(K)=RK/ALPHA*CHIS(K)-CHIS(K+1)
C     SCATTERING COEFFICIENTS A(N) AND B(N)
        AT=PSIS(1, K)*DPSI (2, K)-RIPTG*PSIS(2, K)*DPSI(1, K)
        ABR=AT
        ABI=CHIS(K)*DPSI(2, K)-RIPTG*PSIS(2, K)*DCHI(K)
        AB=CMPLX(ABR, ABI)
        A(K)=AT/AB
        BT=RIPTG*PSIS(1, K)*DPSI(2, K)-PSIS(2, K)*DPSI(1, K)
        BBR=BT
        BBI=RIPTG*CHIS(K)*DPSI(2, K)-PSIS(2, K)*DCHI(K)
        BB=CMPLX(BBR, BBI)
   2    B(K)=BT/BB

        RETURN
        END
```

```
      SUBROUTINE PSICHI (ZZ, L, PSIS, CHIS)

C     TO EVALUATE RICATTI-BESSEL FUNCTIONS PSI(Z) AND CHI(Z)
C     METHOD USES RECURSION FORMULA WITH DOUBLE PRECISION
C     ARITHMETIC

          DOUBLE PRECISION Z, CHI, PSI
          DIMENSION PSI(2, 102), CHI(102), PSIS(2, 102), CHIS(102)
          COMMON N, NN, N1, N2, N3, N4
          Z=ZZ
          IF (N1-2) 1, 1, 2

C     FIRST TWO ORDERS FROM SIMPLE TRIGONOMETRIC
C     EXPRESSIONS
    1     PSI(L, 1) = DSIN(Z)
          CHI(1)=DCOS(Z)
          PSI(L, 2)=DSIN(Z)/Z-DCOS(Z)
          CHI(2)=DCOS(Z)/Z+DSIN(Z)

    2     GO TO (3, 6), L
    3     CONTINUE

C     PSI(Z) AND CHI(Z) REQUIRED FOR Z=ALPHA
          DO 4 K=N3, NN
          RK=2*K-1
          PSI(L, K+1)=RK/Z*PSI(L, K)-PSI(L, K-1)
    4     CHI (K+1)=RK/Z*CHI(K)-CHI(K-1)

C     CONVERT TO SINGLE PRECISION FOR TRANSFER TO ABMIE
          DO 5 K=N4, NNN
          PSIS(L, K)=PSI(L, K)
    5     CHIS(K)=CHI(K)
          RETURN

    6     CONTINUE

C     PSI(Z) ONLY REQUIRED FOR Z=BETA
          DO 7 K=N3, NN
          RK=2*K-1
    7     PSI(L, K+1)=RK/Z*PSI(L, K)-PSI(L, K-1)

C     CONVERT TO SINGLE PRECISION FOR TRANSFER TO ABMIE
          DO 8 K=N4, NNN
    8     PSIS(L, K)=PSI(L, K)

          RETURN
          END
```

```
      SUBROUTINE POLAR (A, B, DELTA)

C     TO EVALUATE INTENSITY FUNCTIONS I(1) AND I(2) BY THE
C     COMBINATION OF SCATTERING COEFFICIENTS AND LEGENDRE
C     FUNCTIONS
C
C     THETA --- SCATTERING ANGLE IN DEGREES MEASURED FROM
C     THE FORWARD TO THE SCATTERED DIRECTION
C     S1, S2 - AMPLITUDE FUNCTIONS
C     SS1, SS2 - INTENSITY FUNCTIONS PERPENDICULAR (I1) AND
      PARALLEL (I2) TO THE SCATTERING PLANE
C     RHO ----- POLARISATION RATIO
C     DEGPOL -- DEGREE OF POLARISATION

          COMPLEX A, B, S1, S2
          DIMENSION A(202), B(202), PI(101), TAU(101)
          COMMON N, NN, N1, N2, N3, N4
          WRITE (6, 100)
          THETA=0.

C         CONVERT DEGREES TO RADIANS
    1     RAD=THETA*0.01745329252

          S1=0
          S2=0
          CALL PITAU (RAD, PI, TAU)
          DO 2 K=2, NN
          CAY = K-1
          PROD=(2.*CAY+1.)/(CAY*(CAY+1.))
          S1=S1+PROD*(A(K)*PI(K)+B(K)*TAU(K))
    2     S2=S2+PROD*(A(K)*TAU(K)+B(K)*PI(K))
          SS1=S1*CONJG(S1)
          SS2=S2*CONJG(S2)
          RHO=SS2/SS1
          DEGPOL=(SS2-SS1)/(SS2+SS1)
          WRITE (6, 101) THETA, SS1, SS2, RHO, DEGPOL
          THETA=THETA+DELTA
          IF (THETA-180.) 1, 1, 3
    3     CONTINUE

C         FORMAT STATEMENTS FOR OUTPUT
  100     FORMAT (/6H ANGLE, 9X, 2HI1, 15X, 2HI2, 14X, 5HI2/I1, 7X,
         1 15H(I2-I1)/(I2+I1))
  101     FORMAT (1X, F5.1, 4(2X, E15.8))

          RETURN
          END
```

```
      SUBROUTINE PITAU (THETA, PI, TAU)
C     TO CALCULATE LEGENDRE FUNCTIONS PI(COS) AND TAU(COS)
C
C     METHOD USES RECURSION FORMULAE TO EVALUATE PI(COS)
C     AND ITS DERIVATIVE DPI(COS)
          DIMENSION PI(101), DPI(101), TAU(101)
          COMMON N, NN, N1, N2, N3, N4
          COTH=COS(THETA)
          SITH=SIN(THETA)
          SITH2=SITH*SITH
C         FIRST THREE ORDERS OF PI(COS) AND ITS DERIVATIVE DPI(COS)
          PI(1)=0.
          PI(2)=1.
          PI(3)=3.*COTH
          DPI(1)=0.
          DPI(2)=0.
          DPI(3)=3.
C         HIGHER ORDERS DETAINED USING RECURSION FORMULAE
          DO 1 K=3, N
          CAY=K-1
          PI(K+1)=(2.*CAY+1.)*PI(K)*COTH-(CAY+1.)*PI(K-1)
          PI(K+1)=PI(K+1)/CAY
          DPI(K+1)=(2.*CAY+1.)*COTH*DPI(K)-(CAY+2.)*DPI(K-1)
    1     DPI(K+1)=DPI(K+1)/(CAY-1.)
C         CALCULATE TAU(COS)
          DO 2 K=1, NN
    2     TAU(K)=COTH*PI(K)-SITH2*DPI(K)
          RETURN
          END
```

B. Inversion of Light Scattering Data

The inversion procedure involves successively comparing the angular intensity distribution for assumed size distributions with the experimental scattering data until the criterion of 'best-fit' is satisfied. The technique can be conveniently divided into two sections, the computation of the angular intensity distribution, and the method of finding the size distribution parameters.

i) Computation of Angular Intensity Distribution

The scattered intensity at a particular angle θ and orientation of polarisation is given by :

$$I(\theta) = \int_0^\infty i(\alpha, \theta)\, p(\alpha)\, d\alpha \qquad \text{B.1}$$

where $p(\alpha)$ - ZOLD size function (normalised)

$i(\alpha, \theta)$ - intensity coefficients, calculated as shown in Appendix A

For computation the above integral was expressed as a summation and the particle diameter (μm) used as the characterising size dimension

$$I(\theta) = \sum_0^{d_{max}} i(d, \theta)\, p(d)\, \Delta d \qquad \text{B.2}$$

where Δd - step length

d_{max} - the cut-off point for the summation

a) Choice of step length , Δd

Step sizes of .001; .0025; .005; and .01 μm were tried and the results compared over a series of angles for distributions of varying mode and spread. For a step size

below .005 μm there was no significant difference in the answers, except for very narrow distributions at small modes, only an increase in computing time. A step size of .001 was therefore used for the diameter range 0 - 0.6 μm and .005 for the range 0.6 - 6.6 μm. The Mie intensity functions for the required set of angles were calculated at each of these diameters, using PROGRAM MIE as the basis, and the results stored on magnetic tape for subsequent use.

b) cut-off point for integration , d_{max}

Since, in general, the magnitude of $i(d, \theta)$ increases with size d but oscillates as θ varies, the cut-off point for the integration was taken as a function of p(d) only and not the product $p(d)\, i(d, \theta)$. Yajnik et al (1968) found that the three-figure accuracy of scattering functions was not affected if the cut-off in the distribution was taken when $p(d) < 10^{-5}$. Their results were confirmed over a range of distributions; in fact four figure accuracy was attainable in many cases. This test was therefore used as the cut-off criterion when $d > d_M$.

ii) To find the Best-Fitting Size Parameters

a) Changes required in the Library minimisation routines.

Details of the library routines VA02A, VD01A, MINIM referred to in this section are available from the Chemical Engineering Computer Library, Imperial College, London, SW7.

The basis of the search method is Powell's (1965) program VA02A. This program, incorporating another Library routine VD01A, is a quadratic unconstrained multivariable minimisation of a sum of squares without derivatives. In this

particular case there were only two variables, d_M and σ_o of the size distribution, but constraints were needed since values of zero or less were obviously not valid.

According to Sargent (1973) there are two convenient ways of introducing constraints, either by defining dummy variables or by using penalty functions. The use of dummy variables was considered first; thus for x(n) with positive values only the dummy variables y(n) where $[\, y(n) \,]^2 = x(n)$ were used for the minimisation in VAO2A. This proved fairly successful in test runs with theoretical data similar to those described in Section 4.4 but on a number of occasions the programme "crashed" due to numerical problems at a particular point either in VAO2A or VDO1A. Since constraints were also needed on a practical basis to limit for example the maximum spread of the distribution the dummy variables were replaced by the use of penalty functions.

However, this still did not overcome the occasional failure inside VDO1A. At this stage it was decided to substitute VDO1A with a later and more rigorously tested univariable minimisation routine MINIM. This necessitated a rearrangement of the calling programme VAO2A and the insertion of a function subroutine consisting of part of VAO2A. The changes are shown in the programme listing where the statement numbers in the library routines refer to the original versions.

b) <u>difference functions and application of penalty functions.</u>

The functions $F(\theta)$ required by the VAO2A routine for use in the sum of squares calculation are evaluated in the subroutine CALFUN according to:

$$F(\theta) = 1 - R(\theta) / I(\theta) \qquad \text{B.3}$$

where $R(\theta)$ is the corrected experimental scattering intensity at the angle θ and $I(\theta)$ the theoretical intensity at the same angle calculated for the current estimate of the two distribution parameters.

The four constraint tests for using penalty functions are also applied within this routine. Their area of application lies outside the enclosed area illustrated in Fig. B.1

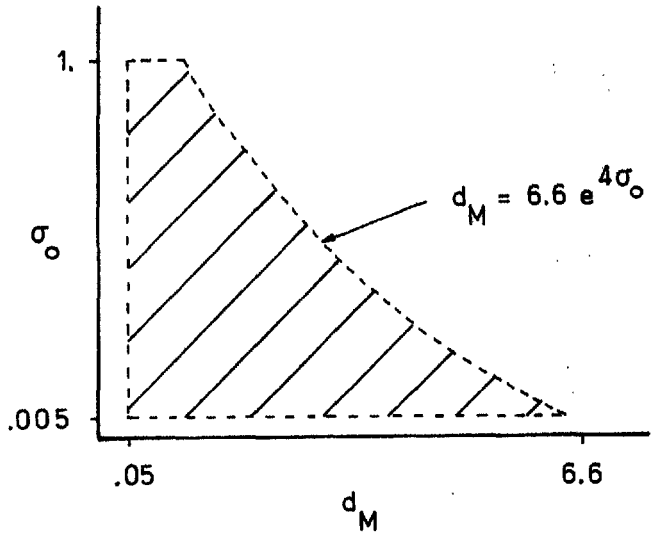

FIG. B.1 Constraints for distribution parameters.

The penalty function was simply taken as the distance outside the constraint limit multiplied by a weighting factor of 10000. This was then added to the difference functions $F(\theta)$ calculated as in Eqn. B.3 for each angle using the violated boundary condition when evaluating $I(\theta)$.

c) convergence criteria

Convergence is assumed when the distribution parameters

have been found within specified absolute accuracies. Numerical results indicated that setting these accuracies much above .0001 caused premature termination of the programme on several occasions. This may have been caused by local irregularities in the error contour surface. The conjugate directions which are then set up with respect to the local quadratic approximation to the error contour function could result in the step taken to the 'minimum' being less than the specified accuracy. Alternatively a local minimum may have been found. Setting the accuracies less than .0001 considerably increased the number of function evaluations and hence the computing time.

The accuracies were therefore set at .0001 and a test introduced that perturbs, by two different increments in each of the co-ordinate directions, the best-fit values of the variables returned to the main programme. If a decrease in the sum of squares function was found the search was restarted from the new point.

Simplified Flow Chart for SEARCH

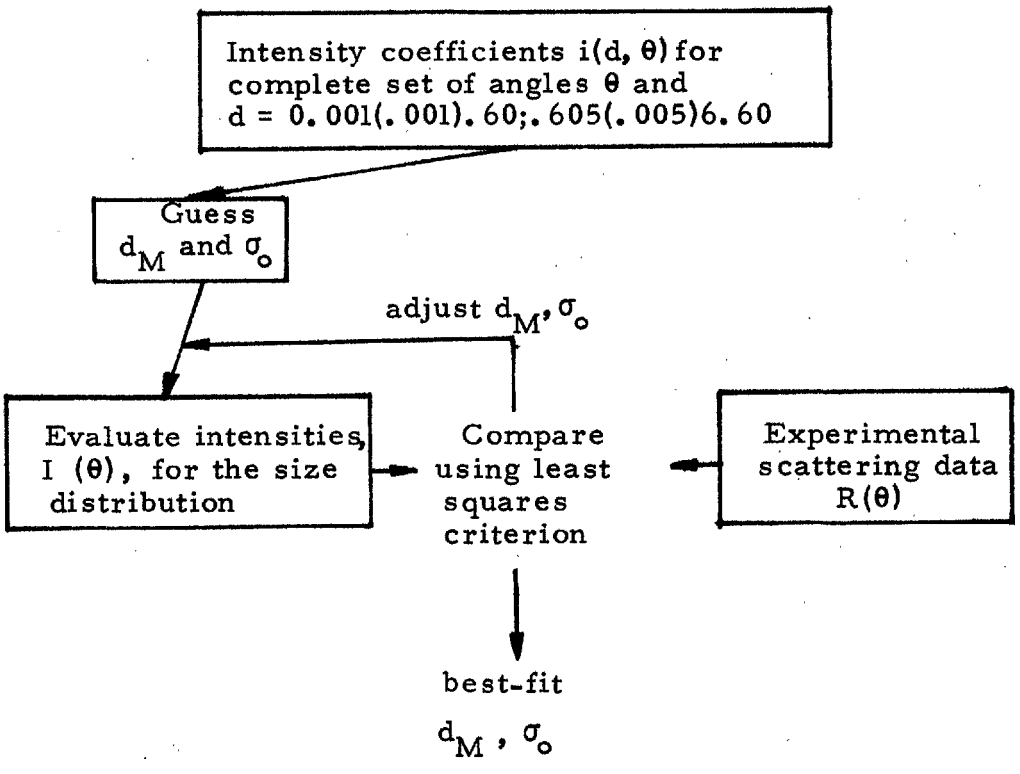

```
      PROGRAM SEARCH (INPUT,OUTPUT,IDATA,TAPE5=INPUT,
     1 TAPE6=OUTPUT,TAPE7=IDATA)
C
C     THIS PROGRAM INVERTS EXPERIMENTAL LIGHT SCATTERING
C     DATA TO GIVE THE TWO PARAMETERS OF THE BEST FITTING
C     ZOLD PARTICLE SIZE FUNCTION
C     THESE PARAMETERS ARE CALCULATED BY MINIMISING THE
C     SUM OF SQUARES OF THE DIFFERENCES BETWEEN THE
C     EXPERIMENTAL DATA AND THE THEORETICAL INTENSITIES,
C     CALCULATED USING THE MIE THEORY, FOR THE ASSUMED
C     DISTRIBUTION
C
C     JMAX-NUMBER OF FUNCTIONS (I.E. NO. OF SCATTERING
C     ANGLES)
C     NVAR-NUMBER OF VARIABLES
C     XX-FUNCTION VARIABLES (I.E. DMODE AND SIG)
C     E-ABSOLUTE ACCURACY PARAMETERS FOR XX
C     F-DIFFERENCE FUNCTIONS EVALUATED IN SUBROUTINE CALFUN
C     MAXFUN-LIMITS MAXIMUM NUMBER OF FUNCTION EVALUATIONS
C     IPRINT-PRINT CONTROL INSIDE ROUTINE, SET TO ZERO FOR
C     NO PRINT
C     W-WORKING SPACE IN LIBRARY ROUTINES
C     THETA-SCATTERING ANGLE
C     FF-SUM OF SQUARES OF DIFFERENCES
C     DSTEP-INTEGRATION STEPLENGTH (ALSO DST5)
C     LK-DATA INDICATOR LK = +IVE STOP
C                 LK=0  READ NEW SET OF SCATTERED INTENSITIES
C                 LK=-IVE "   "   "   "  BACKGROUND VALUES

      DIMENSION THETA(15),EXPVAL(15),BLANK(15),FS(15),E(2),
     1 SAVE(15),SV(15)
      COMMON/BLOCK1/PIE,DSTEP,DST5,SUMB,SUM1(15),COREX
     1 (15), SL(15),JJ(15)
      COMMON/VAPAR/JMAX,NVAR,XX(2),F(15),W(60)
      COMMON SS1 (15,1680)
      EXTERNAL CALFUN
      DATA E/.0001,.0001/,MAXFUN/200/,IPRINT/0/,RLAMDA/.
     1 6328/
      DSTEP=0.005
      PIE=SQRT(6.2831853)
      DST5=DSTEP/5.

C     READ INPUT CONSTANTS FOR RUN. REFRACTIVE INDICES,
      ANGLES ETC,
          READ (5,100) RIP,RIG,RLAMDA,JMAX
          READ (5,101) (THETA(J),J=1,JMAX)
          READ (5,102) (JJ(J),J=1,JMAX)

C     READ INTENSITY COEFFICIENTS STORED ON MAGNETIC TAPE
          READ (7) SS1

          NVAR=2
          NM3N=3*JMAX+14

C     READ EXPERIMENTAL BACKGROUND AND SCATTERED INTENSITY
      VALUES
    1     READ (5,103) (BLANK(J),J=1,JMAX)
    2     READ (5,103) (EXPVAL(J),J=1,JMAX)

C     READ INITIAL ESTIMATE OF ZOLD PARAMETERS
          READ (5,104) DMODE,SIG,LK

          WRITE (6,200) RIP,RIG
```

```
C           SUBTRACT BACKGROUND INTENSITY AND MAKE SCATTERING
C           CORRECTION

                SUMB=0.
                DO 3 J=1,JMAX
                RAD=THETA(J)*0.01745329252
                SINTH=SIN(RAD)
                COREX(J)=EXPVAL(J)-BLANK(J)
                COREX(J)=COREX(J)*SINTH
   3            SUMB=SUMB+COREX(J)

                WRITE (6,201)
                WRITE (6,202) ((THETA(J),BLANK(J),EXPVAL(J),COREX(J)),
               1 J=1,JMAX)
   4            XX(1)=DMODE
                XX(2)=SIG
                ITEST=0

C           CALL LEAST SQUARES MINIMISATION ROUTINE *VA02A*
                CALL VA02A (E,IPRINT,MAXFUN,CALFUN,NM3N)

                STEPX=E(1)*40.
                FO=0.

C           STORE CURRENT BEST FIT VALUES PRIOR TO PERTURBATION
C           TESTS
                DO 5 J=1,JMAX
                SV(J)=SL(J)
                SAVE(J)=SUM1(J)
                FS(J)=F(J)
   5            FO=FO+F(J)*F(J)

C           TEST WHETHER AT LOCAL STOPPING POINT BY MAKING SMALL
C           PERTURBATIONS ON EACH VARIABLE IN TURN
                DO 10 I=1,2
                XO=XX(I)
                JJX=1
                DO 9 JX=1,2
                DO 8 J=1,3,2
                TURB=FLOAT((J-2)*JJX)
                XX(I)=XO+TURB*STEPX
                CALL CALFUN (JMAX,NVAR,F,XX)
                FF=0.
                DO 6 IJ=1,JMAX
   6            FF=FF+F(IJ)*F(IJ)

C           IF FF REDUCED RESTART MINIMISATION FROM THE NEW POINT
                IF (FF-FO) 7,8,8
   7            WRITE (6,203) XX,FF
                DMODE=XX(1)
                SIG=XX(2)
                FO=FF
                ITEST=1
   8            CONTINUE
                JJX=JJX*20
   9            CONTINUE
   10           XX(I)=XO
                IF (ITEST.EQ.1) GO TO 4
```

```
      DMODE=XX(1)
      SIG=XX(2)
      RMS=SQRT(FO/JMAX)
      WRITE (6, 204) DMODE, SIG, FO, RMS

C     CHECK WHETHER MODAL DIAMETER IS IN RAYLEIGH REGIME
C     AND PRINT WARNING IF REQUIRED
      RAYDM=0. 1*RLAMDA
      IF (DMODE-RAYDM) 11, 11, 12
11    WRITE (6, 205)

12    WRITE (6, 206)
      WRITE (6, 207) ((THETA(J), SV(J), SAVE(J), FS(J)), J=1, JMAX)
      IF (LK) 1, 2, 13
13    CONTINUE

C     FORMAT STATEMENTS FOR INPUT AND OUTPUT
100   FORMAT (3F10. 5, 14)
101   FORMAT (8F10. 5)
102   FORMAT (15I5)
103   FORMAT (8E10. 4)
104   FORMAT (2F10. 6, I5)
200   FORMAT (1H1, * REFRACTIVE INDEX... PARTICLES=*, F7. 3,
     1 5X, *MEDIUM=*, F7. 3)
201   FORMAT (* THETA BACKGROUND SCATTERED *,
     1 *CORRECTED*)
202   FORMAT (1X, F8. 1, 5X, F10. 6, 5X, F10. 6, 5X, F10. 6)
203   FORMAT (1X, *RESTART AT XX(1)=*, F8. 3, * XX(2)=*, F8. 3,
     1 * FF=*, E14. 5)
204   FORMAT (/* MODE...*, F5. 3, * SIGMA(0)...*, F5. 3, 10X,
     1 *SUM OF SQUARES (FF)...*, E14. 6, * RMS ERROR...*, E14. 6)
205   FORMAT (/* MODAL DIAM IS IN RAYLEIGH REGIME*)
206   FORMAT (/* THETA EXPTL. SHIFTED MIE INTENSITIES
     1 FRACTIONAL DIFFERENCE*)
207   FORMAT (1X, 0PF8. 1, 5X, 1PE15. 5, 5X, 1PE15. 5, 8X, 1PE15. 5)
      STOP
      END
```

```
      SUBROUTINE CALFUN (JMAX,NVAR,F,XX)

C     COMPUTES DIFFERENCE FUNCTIONS REQUIRED BY SUBROUTINE
C     *VA02A*

      DIMENSION F(JMAX),XX(NVAR)
      COMMON/BLOCK1/PIE,DSTEP,DST5,SUMB,SUM1(15),
     1 COREX(15), SL(15),JJ(15)
      COMMON SS1(15,1680)

      DATA DMDMAX/6.6/,DMDMIN/.05/,SIGMIN/0.005/,SIGMAX/
     1 1.0/,RR/10000./

C     SET ZOLD PARAMETERS TO LOCAL VARIABLES
      DMODE=XX(1)
      SIG=XX(2)

      PENF1=0.
      PENF2=0.

C     TEST WHETHER VARIABLES ARE WITHIN BOUNDS. IF OUTSIDE
C     SET LOCAL VARIABLE TO APPROPRIATE BOUNDARY AND APPLY
C     PENALTY FUNCTION
      IF (XX(2).GT.SIGMIN) GO TO 10
      SIG=SIGMIN
      PENF2=SIG-XX(2)
      GO TO 11
10    IF (XX(2).LT.SIGMAX) GO TO 11
      SIG=SIGMAX
      PENF2=XX(2)-SIG

11    IF (XX(1).GT.DMDMIN) GO TO 12
      DMODE=DMDMIN
      PENF1=DMODE-XX(1)
      GO TO 13
12    TESTD=DMODE*EXP(4.*SIG)
      IF (TESTD.LT.DMDMAX) GO TO 13
      DMODE=DMODE*DMDMAX/TESTD
      PENF1=XX(1)-DMODE
13    PENF=(PENF1+PENF2)*RR

C     CALCULATE THEORETICAL SCATTERED INTENSITIES FOR
C     ESTIMATED ZOLD AT THE REQUIRED ANGLES
      DO 14 J=1,JMAX
14    SUM1(J)=0.
      DENZ=PIE*DMODE*SIG*EXP(SIG*SIG/2.)
      DEXP=2.*SIG*SIG
      DSTMD=DST5/DMODE
      DO 16 LL=1,600
      XL=LL
      DD=ALOG(XL*DSTMD)
      PZ=EXP(-DD*DD/DEXP)/DENZ
      DO 15 J=1,JMAX
      KJ=JJ(J)
15    SUM1(J)=SUM1(J)+SS1(KJ,LL)*PZ*DST5
16    CONTINUE
```

```
C           INCREASE INTEGRATION STEP FOR DIAMETERS GREATER
C           THAN 0.6
                DSTMD=DSTEP/DMODE
                DO 20 LL=601,1680
                XL=LL-480
                DD=ALOG(XL*DSTMD)
                PZ=EXP(-DD*DD/DEXP)/DENZ
                IF (DD) 18,18,17
   17           IF (PZ-.1E-04) 21,18,18
   18           CONTINUE
                DO 19 J=1,JMAX
                KJ=JJ(J)
   19           SUM1(J)=SUM1(J)+SS1(KJ,LL)*PZ*DSTEP
   20           CONTINUE

   21           SUMT=0.
                DO 22 J=1,JMAX
   22           SUMT=SUMT+SUM1(J)

C           SCALE EXPERIMENTAL READINGS TO MAGNITUDE OF
C           THEORETICAL INTENSITIES JUST CALCULATED
                ADV=SUMT/SUMB
                DO 23 J=1,JMAX
                SL(J)=COREX(J)*ADV

C           CALCULATE FRACTIONAL DIFFERENCES AND ADD PENALTY
C           FUNCTION (IF ANY)
   23           F(J)=1.-SL(J)/SUM1(J)+PENF

                RETURN
                END
```

```
      SUBROUTINE VA02A (E, IPRINT, MAXFUN, CALFUN, NM3N)

C     QUADRATIC UNCONSTRAINED MULTIVARIABLE MINIMISATION
C     OF A SUM OF SQUARES WITHOUT DERIVATIVES.  LISTING OF
C     CHANGES MADE TO VERSION AVAILABLE ON ICLIB.

          DIMENSION E(2)
          COMMON/VAPAR/M, N, X(2), F(15), W(60)
          COMMON VAPAS/IS, MC, K, KSTORE, FMIN, FSEC, FF, XL
          EXTERNAL FNCN

C     ROUTINE CONTINUES AS PER LIBRARY VERSION *VA02A* TO
C     STATEMENT 49

   49     CONTINUE
          FC=FF
          ACC=0.1/CHANGE
          IT=3
          XC=0.
          XL=0.
          IS=3
          XSTEP=0.5
          IF (CHANGE-1.) 50, 50, 51
   50     ICONT=2
   51     IND=3

C     CALL SINGLE VARIABLE MINIMISATION ROUTINE *MINIM*
          CALL MINIM (FC, XC, XSTEP, ACC, 2, IND, 8, IPRINT, FNCN)

          IF (MC-MAXFUN) 53, 53, 55
   55     WRITE (6, 56) MAXFUN
   56     FORMAT (5X, 5HVA02A, 16, 16H CALLS OF CALFUN)
          ISS=2
   53     K=KSTORE

C     ROUTINE CONTINUES AS PER LIBRARY VERSION *VA02A*
      TO END


          END
```

```
      SUBROUTINE MINIM (YY, XX, STEP, ERROR, ISTOP, INDL,
     1 MAXFN, IPRINT, F)

C     SINGLE VARIABLE MINIMISATION ROUTINE
C     F - FUNCTION SUBROUTINE

          REAL DX(3), Y(3)
          DATA ACC, RED/0.01, 0.02/

C     SINCE CONDITIONS AT FIRST INITIAL POINT ARE KNOWN ON
C     ENTRY SET Y0=YY.  THIS REPLACES Y0=F(X) LINE MIN0 104
C     THEREBY SAVING ONE FUNCTION EVALUATION PER CALL OF
C     *MINIM*

          Y0=YY

C     ROUTINE CONTINUES AS PER LIBRARY VERSION OF *MINIM*
C     TO END

          END
```

N. B. The subroutine above replaces VD01A, the single variable minimisation routine which formed part of the original least squares routine VA02A. This change also requires the addition of the function subroutine shown overleaf, which was formerly part of VA02A.

```
      FUNCTION FNCN (XC)
C     ROUTINE REQUIRED BY *MINIM* TO EVALUATE THE FUNCTION
C     AT THE NEWLY PREDICTED POINT (XC)
          COMMON/VAPAR/M, N, X(2), F(15), W(60)
          COMMON/VAPAS/IS, MC, K, KSTORE, FMIN, FSEC, FF, XL
C     ROUTINE AS PER LIBRARY VERSION *VA02A* FROM STATEMENT
C     52 TO 68 INCLUSIVE
68        CONTINUE
51        FNCN=FC
          RETURN
          END
```

C Papers Published During This Research

'Particle Size Distributions in Aerosols formed from Gaseous Reactants'

M. D. Carabine, J. E. L. Maddock and A. P. Moore

Nature, Physical Science 231, 18, (1971)

'Light Scattering Instrument for Kinetic Measurements in Aerosols with Changing Particle Size Distributions'

M. D. Carabine and A. P. Moore

Faraday Symposium 'Fogs and Smokes'

Annual Chemical Congress Swansea March 1973

'Particle Size Analyser'

M. D. Carabine and A. P. Moore

Patent: Provisional Specification 11209/73: 7th March 1973

(Reprinted from Nature Physical Science, Vol. 231, No. 18, pp. 18–19, May 3, 1971)

Particle Size Distributions in Aerosols formed from Gaseous Reactants

LIGHT scattering is a technique whereby the size of suspended particles can be measured *in situ*, and the experiments reported here show its validity for polydisperse aerosols of moderate concentration. Unresolved problems emphasizing the practical importance of finding kinetic data for systems where submicron sized particles are formed by, or react with, gases include the involvement of gaseous pollutants in the formation of ammonium sulphate particles in the air[1], the influence of residence time in the lung on the dilution of an inhaled acid droplet, and the effect on the pigment quality of titanium dioxide of its residence time in the reactors in which it is produced. Angular scattering patterns have been calculated, using the Mie theory[2], for distributions of spherical particles. The inverse procedure, the deduction of size distributions from

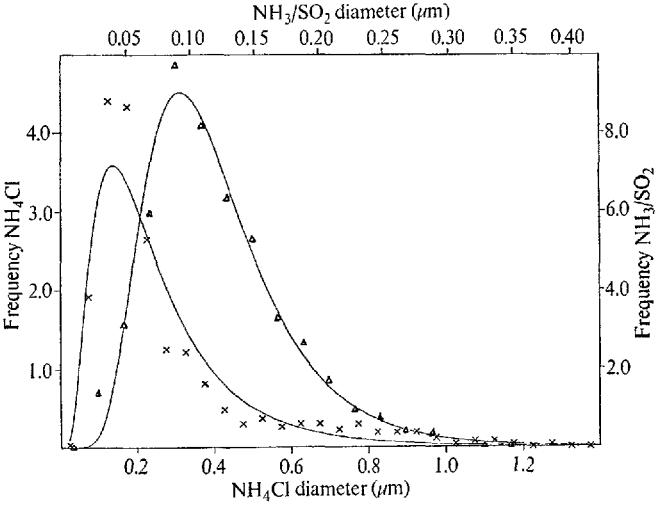

Fig. 1 Particle diameter distributions for the aerosols. Points are data from electron micrographs, solid lines are best fitting ZOLDs. ×, NH_4Cl aerosol, modal diameter 0.14 μm, spread parameter $\sigma_0 = 0.65$; △, NH_3/SO_2 aerosol, modal diameter 0.09 μm, spread parameter $\sigma_0 = 0.46$.

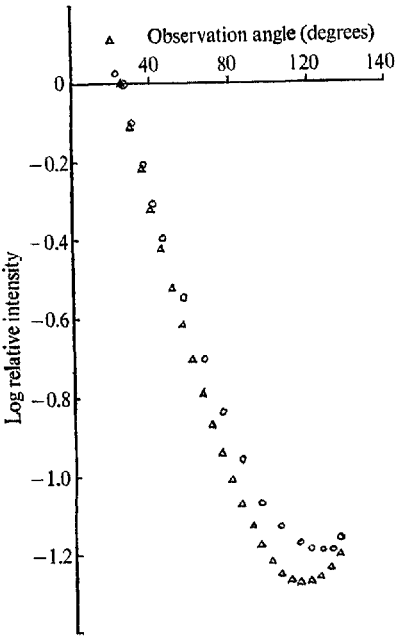

Fig. 2 Angular scattering diagram for the NH_4Cl aerosol of Fig. 1, parallel polarization, wavelength 632.8 nm. ○, Measured intensity; △, intensity calculated for the distribution in Fig. 1.

scattering intensities, will be feasible with the present instrumental precision of 4% in cases where (*a*) the dispersity is not too large (e.g., if the spread parameter (σ_0) in the "zeroth order logarithmic distribution" (ZOLD)[3] is below 0.7 when the modal diameter is of the order 0.2 μm) and (*b*) the particle size is comparable with or greater than the wavelength of the scattered radiation.

A logarithmic distribution function has been proved applicable by electron micrographic sizing of particles collected from two aerosols derived from gases as follows. (1) Ammonia and hydrogen chloride reacting at equal partial pressures (0.01–0.03 kN m^{-2}), with product collected on glass slides in the reaction vessel. (2) Ammonia and sulphur dioxide (equimolar at about 5 kN m^{-2}) yielding particles which were collected on 'Millipore' filters (pore size 0.02 μm) and prepared for sizing as described by Lamer[4].

Each gas was premixed with dry nitrogen at normal pressures and the resulting aerosols contained typically 10^{10}–10^{11}

particles/m^3. Specimen size distributions are shown in Fig. 1, together with the ZOLD curves which fit the data.

In Fig. 2 angular scattering measurements, using an He–Ne laser light source, are compared for an ammonium chloride aerosol with those calculated for the known size distribution in Fig. 1. For these particles below 1 μm the agreement is good in spite of their aspherical (cubic) shape. The present experimental accuracy gives the modal diameter within 20% and the spread parameter within 5%. Time resolved studies are being made of the development of particles in such aerosols.

M. D. CARABINE
J. E. L. MADDOCK
A. P. MOORE

Imperial College,
London SW7

Received February 26; revised March 17, 1971.

[1] Heard, M. J., and Wiffen, R. D., *Atmospheric Environment*, **3**, 337 (1969).
[2] Mie, G., *Ann. Physik.*, **25**, 377 (1908).
[3] Espenscheid, W. F., Kerker, M., and Matijevic, E., *J. Phys. Chem.*, **68**, 3093 (1964).
[4] Lamer, E. E., *Atomic Weapons Research Establishment Unclassified Report* No. 0–84/64 (1964).

Printed in Great Britain by Fisher, Knight & Co., Ltd., St. Albans.

PATENTS FORM NO. 2

PATENTS ACT 1949

PROVISIONAL SPECIFICATION

11209/73
7 MAR 1973

PARTICLE SIZE ANALYSER

We, MICHAEL DENNIS CARABINE, of 6 Evelyn Gardens, London, S.W.7, and ALAN PETER MOORE, of 28 Parkway, Dorking, Surrey, both British subjects, do hereby declare this invention to be described in the following statement:-

The present invention concerns a device for measuring particle size distribution in aerosol systems such as those produced by aerosol canisters, sprays and atomisers, and sources of dust and droplets.

The required information can be derived from the variation of intensity of light scattered from the aerosol system with either the angle of scattering, polarisation or wavelength.

In accordance with the present invention there is provided a device for analysing particle size distribution in an aerosol system, the device comprising a rotatable mirror, a plurality of static mirrors in the plane of rotation of the rotatable mirror so that as the rotatable mirror rotates it can reflect light from a light source sequentially on to individual static mirrors, and a photosensitive device arranged to receive light which has been reflected from said rotatable mirror on to one of the static mirrors and which after reflection by the static mirror has been scattered by the particles of an aerosol system so that light from the static mirrors strikes the aerosol system at a variety of angles of incidence.

Preferably the static mirrors are arranged on an ellipse with the rotating mirror at one of the principal foci, and the centre of the aerosol system at the other principal focus.

According to a further feature the stepping means may be provided for rotating the rotatable mirror step-wise through a predetermined sequence of steps. Further, the

static mirrors may be replaced by a single curved reflector and the means for step-wise rotation by the means for continuous rotation.

Thus although the light source and the photomultiplier remain stationary it is possible to obtain in a short space of time the measurements of intensity of light scattered by the aerosol system over a wide range of angles of incidence. Each time this range is scanned the particle size distribution is thus recorded, and so temporal variations in the distribution can be measured with appropriate time-resolution.

An embodiment of the present invention will now be described by way of example and with reference to the accompanying drawings in which Figure 1 is a diagrammatic view of a particle size analyser constructed in accordance with the present invention and Figure 2 is a block diagram of the electronic control system for the device of Figure 1.

As shown in Figure 1 the particle size analyser comprises a light source 1. The part of the aerosol system the particles of which are to be analysed is shown at 2 whilst 3 is a photomultiplier for detecting light from the laser 1 scattered by the aerosol system.

Light from the source 1 impinges on a plane mirror 4 which can be rotated by a stepping motor which is not shown so as to reflect the beam from the source 1 sequentially on to a series of static plane mirrors at the positions marked 5. Each of the mirrors is so positioned that when light is

reflected on to it by the plane mirror 4 the beam is directed back to the location 2 in the aerosol system. As there is a slight divergence of the light beam over the optical path the mirrors 5 are positioned on an ellipse the principal foci of which are at the plane mirror 4 and the location in the aerosol system 2.

In the present embodiment a helium-neon laser with a continuous 15mW output at 632. 8nm is used as the light source. The photomultiplier has a modified S-20 spectral response yielding a high quantum efficiency at this wavelength compared with other photocathodes. Plane front surface mirrors are used throughout, and precise adjustment of the static ones is effected by three-point spring mountings. A special light trap can be used made from black glass fibre reinforced resin, to minimise back reflections from the transmitted light beams. Based on the conventional Rayleigh horn, but having a wide curving aperture, it traps any light entering within an angular range of 174°. In this apparatus it is attached directly to a gas-tight scattering cell, opposite to a thin semi-circular glass window which admits the incident beams with negligible distortion.

Figure 2 shows a control system for the device of Figure 1.

The control circuitry shown in Figure 2 comprises a stepping motor 9 of known kind under the control of a motor control gate 10 receiving a train of 100 Hz mains derived clock pulses from a clock source 11, the output of which is in turn

controlled by a clock inhibiting gate 12 having a pair of inputs to control the starting and stopping of the clock train and thus the stepping motor 9.

The circuit also includes a divider 13 dividing the clock train by 10 and a divider 14 for dividing the resultant train by 2. The output from the divider 13 is taken via a delay selector 15 together with the output of the stage 14 to a counter 16. The clock train is then taken via a selector 17 which selects the number of readings per static mirror to the motor control gate 10. A switch 18 provides for an unlimited number of readings at one static mirror. The motor control gate 10 has four further inputs, namely 19, 20, 21 and 22. The input 19 is a switch enabling the stepping motor to be reversed whilst 20 enables the motor to be advanced in single steps. Input 21 is taken from a counter 23 counting steps between static mirrors and counter 23 is in turn controlled by a switch 24 which determines which set of mirror positions are to be used; that is assuming the static mirrors to be numbered consecutively switch 24 determines whether the even or the odd mirrors are to be used. The counter 23 also has a control switch 25 which determines the number of mirrors to be used in a single full scan and hence also determines the number of steps between stations.

At input 22 a signal from a counter 26 allows free rotation in search of the start position after readings have been taken at all the required mirror positions. Alternatively a command to inhibit the clock at this point can be selected by a switch 29.

A start position locator 27 determines when the stepping motor has reached its start position, and resets counter 26. A control switch 28 determines whether a full or a half scan of the static mirrors is to be made.

Naturally the present invention could also be utilised to examine particle size of particles suspended in a liquid; in such a case a sample of the suspension to be examined could be placed in an optically inert container at one of the principal foci of the ellipse.

I.A.R. MACKENZIE,
Chartered Patent Agent,
Agent for the Applicants.

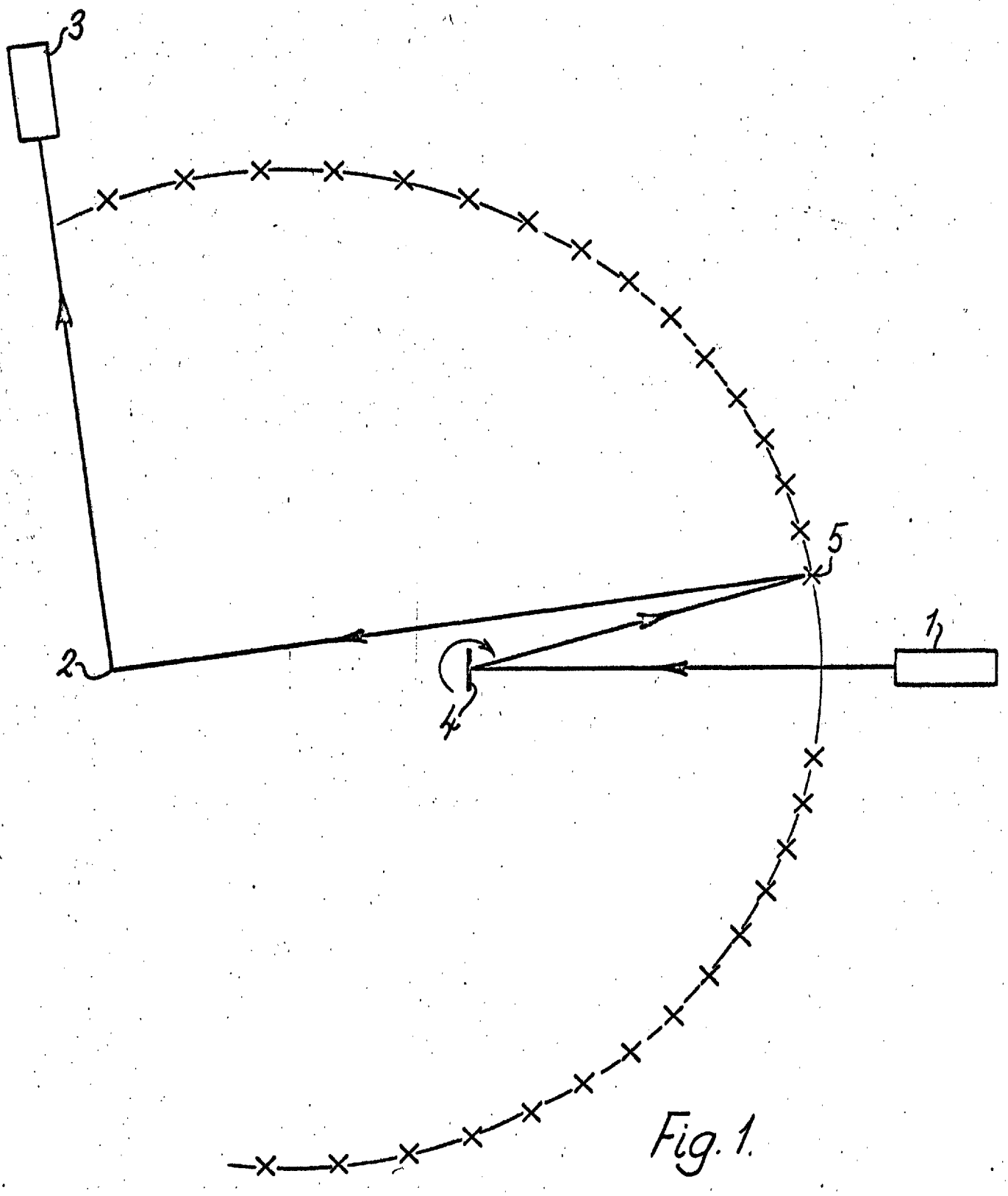

Fig. 1.

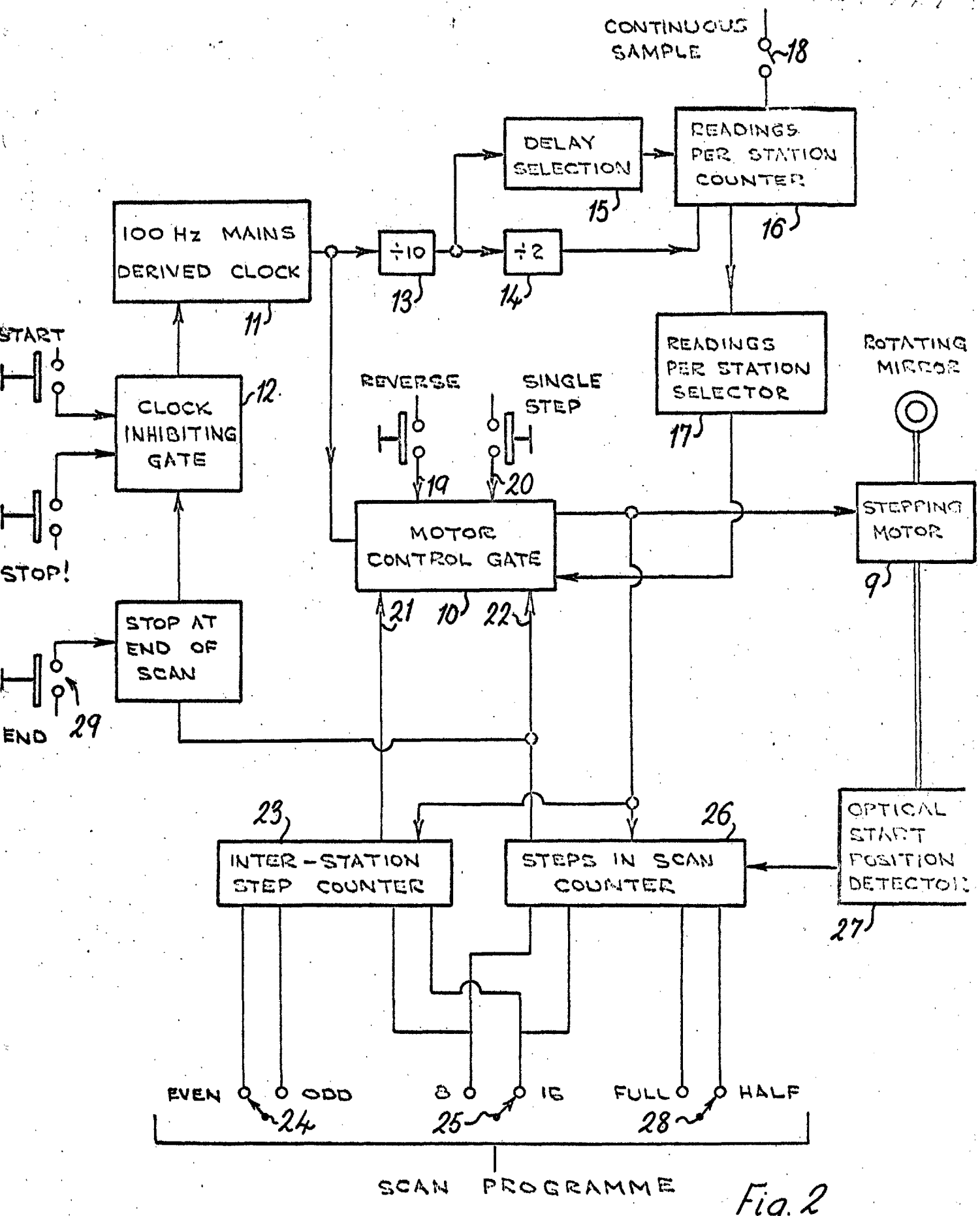
CONTINUOUS SAMPLE
18
DELAY SELECTION
15
READINGS PER STATION COUNTER
16
100 Hz MAINS DERIVED CLOCK
11
÷10
13
÷2
14
START
CLOCK INHIBITING GATE
12
READINGS PER STATION SELECTOR
17
ROTATING MIRROR
REVERSE
19
SINGLE STEP
20
STOP!
MOTOR CONTROL GATE
21
10
22
STEPPING MOTOR
9
STOP AT END OF SCAN
END
29
23
INTER-STATION STEP COUNTER
26
STEPS IN SCAN COUNTER
OPTICAL START POSITION DETECTOR
27
EVEN
ODD
24
8
16
25
FULL
HALF
28
SCAN PROGRAMME

Fig. 2

Light-Scattering Instrument for Kinetic Measurements in Aerosols with Changing Particle Size Distributions

By M. D. Carabine and A. P. Moore

Department of Chemical Engineering and Chemical Technology, Imperial College, Prince Consort Road, London S.W.7.

Received 13*th December*, 1972

The construction and use are described of a laser light-scattering instrument for kinetic measurements of the particle size distribution in a developing aerosol. In the present stage of development, the time resolution (of the order of seconds) is adequate for the study of aerosols which are developing by growth and by coagulation. Such an *in situ* measurement is preferable for particles, and for kinetic studies. The systems investigated are of importance in atmospheric pollution, namely, the formation of solid particles by interaction of ammonia and sulphur dioxide, and the hygroscopic growth of sulphuric acid droplets in humid atmospheres. The precision of the data-analyzing procedure is such that it yields modal particle sizes and distribution spread parameters accurate to within 4 and 10 % respectively, even with about 5 % random fluctuations in the measurements of the angular distribution of scattered intensity.

The size distribution of particles or droplets in an aerosol suspension can be deduced from the variation of intensity of scattered light with either the angle of scattering, the polarisation, or the wavelength. The method of sizing has the advantage that the particles need not be disturbed by, e.g., deposition before electron microscopic examination, or by electrification prior to sizing.[1] Minimal interference with the aerosol is essential if it is required to observe the changes of particle-size distribution with time which can often be important in practical cases, both in manufacturing of particulate products, and in atmospheric pollution.[2] Instantaneous measurement of light intensity is a further feature which makes the technique particularly suitable for monitoring rate processes, provided that the input parameters, such as scattering angle or wavelength, can be varied quickly enough.

This paper describes a light-scattering instrument designed for kinetic measurements of size distribution in an aerosol with a time resolution, in its present initial stage of development, which is adequate for the study of aerosols which are developing growth and by coagulation of particles. Our particular interest is in systems in which a vapour from the suspending medium is being transferred to the condensed phase, e.g., a suspension of hygroscopic acid droplets which are growing in a humid atmosphere, or a suspension of solid particles being formed by interaction of gases such as ammonia and hydrogen chloride or ammonia and sulphur dioxide.

The size distribution of the aerosol thus formed, and its variation with time, depend on such processes as condensation, coagulation, diffusion, and sedimentation. In the range of conditions which are relevant to atmospheric pollution, significant size change by condensation growth occurs in general on a time scale of tens of seconds.[3, 4] Coagulation in a given aerosol causes time variation in both the number and the size of the particles. The number concentration varies predominantly according to second-order kinetics, and at a moderately high atmospheric concentration of, say, 10^{13} m^{-3} the half-life would be of the order 100 s.

The times involved in changes in size due to Brownian coagulation are illustrated in fig. 1, in which the successive distributions have been computed for intervals of 110 s.

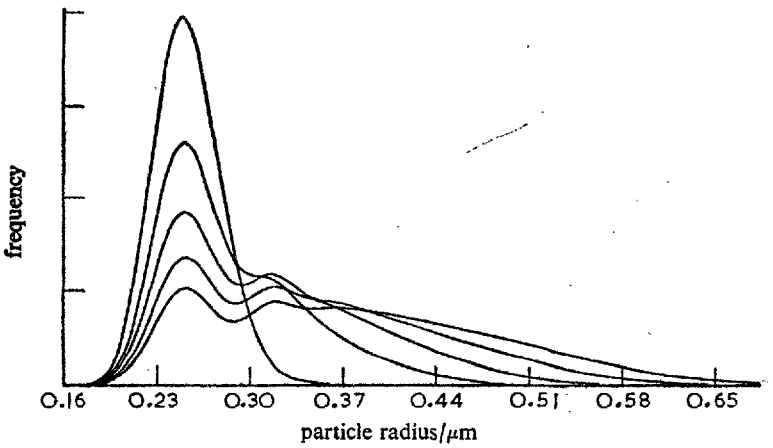

FIG. 1.—The particle size distribution at time intervals of 110 s resulting from the Brownian coagulation of a dispersion initially having a modal radius 0.25 μm and a zeroth-order logarithmic breadth parameter $\sigma_0 = 0.10$.

In the aerosol referred to above which is produced by interaction of ammonia and sulphur dioxide, it has been shown by sampling on filters (with consequent uncertainties), followed by electron microscopy that the particles undergo growth typically from 0.03 μm to 0.2 μm in about 10^3 s, and then to about 0.5 μm in further 5×10^3 s. The aggregates in the 0.2-0.5 μm range are formed of primary particles predominantly of size less than 0.1 μm. The proportion of small particles is augmented when traces of moisture or oxygen are added to the carrier gas.

CRITERIA FOR THE CHOICE OF METHOD

A time interval of about 1-10 s is considered short enough for meaningful size distribution measurements in the systems referred to above, and if angular distribution of intensity is the chosen method, a scan of the angles must be achieved within this time.

To obtain sufficient intensity of scattered light from a dilute suspension of submicrometre particles, a high-intensity light-source such as a continuous laser is required. Besides the high intensity, it has the advantages for light scattering of monochromaticity and linear polarisation—and Harris *et al.*[5] have shown experimentally that there is no difference in scattering behaviour between conventional incoherent light sources and coherent laser sources.

The scanning-speed requirement rules out the use of several techniques, reviewed, e.g., by Kerker [6] which have been developed to study essentially time-invariant dispersions using conventional light sources. Thus the "polarisation ratio" method [7] would require rotating the plane of polarisation of the beam through 90° at each observation angle; while the methods using "scattering ratio" or "turbidity spectra" [8, 9] at different wavelengths would necessitate repeated retuning of the laser.

Hence the only technique compatible with the required scanning speed and the laser source is one using the angular variation of intensity. Angular scanning introduces its own problems which must be carefully considered in the design. The

optically-effective volume is defined by the geometry of the light-receiver system and the incident beam, and contains all the scattering particles which contribute to the measured intensity for a particular angle of scattering θ. Ideally, if the detector receives only parallel light, the optically effective volume varies simply in direct proportion to $\sin\theta$, if the cell containing the aerosol is cylindrical and free from flaws. However, in practice, a finite solid angle also means that data are recorded for an angular range $\theta \pm \Delta\theta$, rather than for the unique angle for which theoretical data are normally computed. Tabibian and Heller [10] have shown that in the absence of steep maxima or minima in the intensity against angle curves, a solid angle not in excess of 10^{-3} steradian is permissible.

Problems common to all light-scattering methods include multiple scattering, and extinction of the beam. These interfere if the concentration of particles is above a certain limit, whose value depends at a given wavelength in a given medium, on the refractive index and the size of the scatterers. These two complications are respectively avoided by working at sufficiently low dilutions, and by using relative intensities of light scattered at the various angles (see eqn (2) later). The more practical difficulties of inadvertent reflections of the incident and scattered beams are specific to individual scattering cells. The devices used to minimize them in this apparatus are described below.

The essence of achieving precision in the size-distribution measurement is to record light intensity for a large number of scattering angles. Before considering the present design, we examine the possible arrangements which are compatible with rapid scanning, a laser source, and a photo-multiplier detector. These alternatives are: (*a*) to use a stationary light source and a single detector which is moved rapidly through a series of angular positions; (*b*) to use a stationary source and a separate photomultiplier stationed at each angle; and (*c*) to hold both source and detector static and to deflect the incident beam itself through the series of angles.

Alternative (*a*) has been previously adopted [11] but mechanical movement of the detector must be relatively slow in a low-cost instrument. Alternative (*b*) is also unsuitable as it demands a number of photomultipliers of known relative sensitivities together with a complex and costly multichannel data-acquisition system.

THE INSTRUMENT

The present instrument, based on alternative (*c*), achieves the measurement economically with one source, one detector, and several inexpensive mirrors. The arrangement is shown schematically in fig. 2. The plane mirror at position R, rotated by a stepper motor about an axis perpendicular to the scattering plane (the plane of the diagram), reflects the source beam sequentially on to a series of static plane mirrors M, at the positions marked. From each of the latter mirrors the beam is directed back to the centre of the scattering system at A, and the photomultiplier detects the light scattered by the optically effective volume of aerosol. There is a slight divergence of the beam over the optical path (less than 1 mradian) and to keep it constant for all the beams, the stationary mirrors are positioned on an ellipse with the principal foci at A and R. The laser beam and the line PM-A define the horizontal scattering plane of the instrument. The scattering angles which range from 8 to 172° have a precision of $\pm 0.33°$, determined by the stepper motor.

A helium–neon laser with a 15 mW output at 632.8 nm is used as the light source. The photomultiplier has a " modified S-20 " spectral response yielding a high quantum efficiency at this wavelength compared with other photocathodes. Plane-front-surface mirrors are used throughout, and precise adjustment of the stationary ones is

effected by three-point spring mountings. A special light trap has been constructed from black, glass-fibre-reinforced resin, to minimize back reflections from the transmitted light beams. Based on the conventional Rayleigh horn, but having a wide curving aperture, it traps any light entering within an angular range of 174°. In this apparatus it is attached directly to the gas-tight scattering cell, opposite to a thin semi-circular glass window which admits the incident beams with negligible distortion.

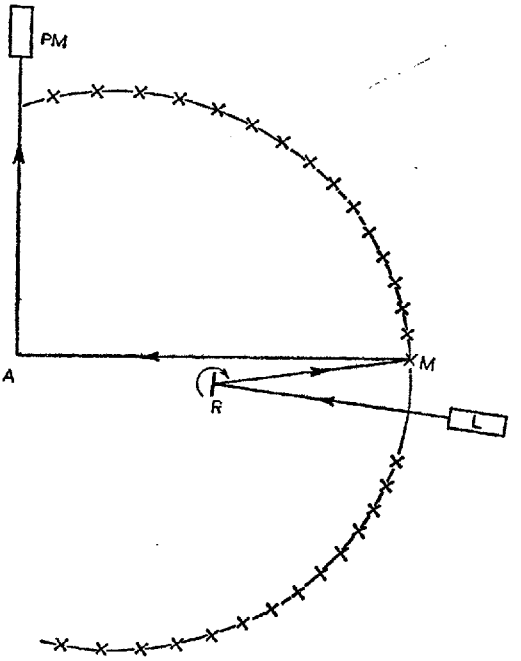

FIG. 2.—Schematic plan view of the optical system. The positions × are locations of stationary mirrors M; R is the rotating mirror; A is the scattering centre; L and PM are the laser source and photomultiplier detector.

ANGULAR SCANNING CONTROL AND DATA ACQUISITION

Initial adjustment of the rotating mirror is made to a start position defined by an infra-red position detector situated under the main baseplate of the instrument. Thereafter, the rotating mirror scans through the predetermined stepping pattern. A count of the number of steps taken determines the end of each scan, whereupon the mirror is rapidly brought around to the start position and the sequence repeated. The mirror can be advanced in single steps to enable alignment of each stationary mirror, and determination of the corresponding scattering angle.

A block diagram of the control circuitry which governs the stepper motor is shown in fig. 3. The motor moves through 3.75°. at each step. When a full scan is required to have readings at eight angular stations, four steps are necessary between each, and for sixteen positions, two steps. Provision is made for half scans and for the peripheral mirrors to be used in " odd " as well as " even " numbered positions.

The control logic is performed by standard integrated circuit techniques, the stepping rate and timing being derived throughout from the mains frequency with basic clock pulses at 100 Hz. The " start " command releases the clock inhibiting gate to enable the motor to step at this rate until the infra-red detector halts it at the

start position. A delay of 300 ms follows before the first reading, and thereafter after each change of position, giving time for internal resets.

The time interval between readings of intensity is 200 ms, derived, like the delay, by division of the clock rate. The motor is stepped to a new position each time the required number of readings is satisfied, and this can be up to eight at each position.

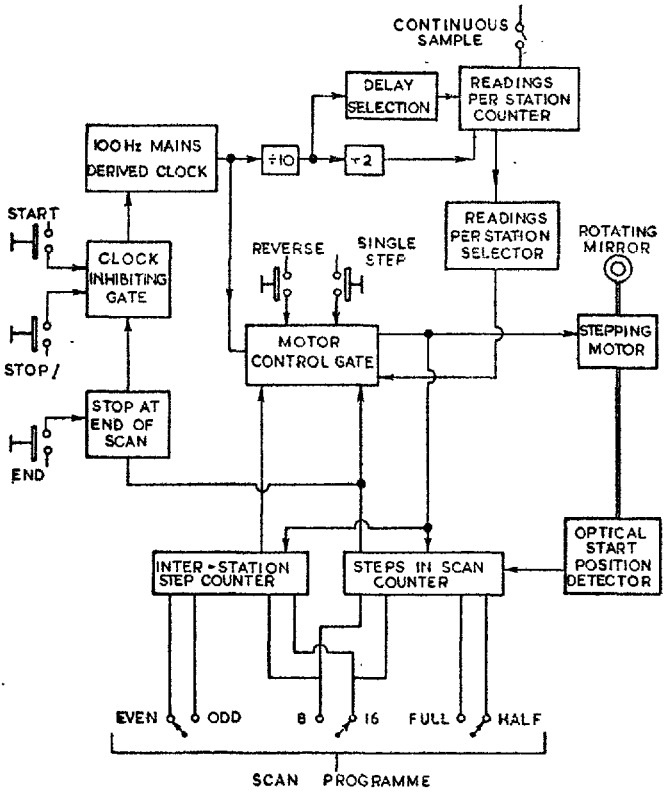

FIG. 3.—Schematic diagram of the electronic system controlling the angular scanning. " Even-Odd " selects which set of mirrors is to be scanned, " 8-16 " selects the number of mirrors to be scanned, " Full-Half " selects full (*ca.* 180 deg.) scan or half (*ca.* 90 deg.) scan.

Selection of " End " inhibits the clock when the current scan is complete. The number of completed scans and angular position are visually displayed on serial counters, and the intensity readings are recorded on paper tape for subsequent analysis.

ANALYSIS OF DATA

The theory of Mie [12] is used to compute the angular intensity functions (i_1 and i_2 for perpendicular- and parallel-polarised incident light respectively) for spherical particles of known size and refractive index. For a system of heterodisperse particles the scattered intensity at a particular angle is given, for the perpendicular polarised case, by

$$I_1(\theta) = \int i_1(\alpha, \theta) p(\alpha)\, d\alpha, \qquad (1)$$

where $p(\alpha)$ is the normalised size-distribution function. The experimentally-determined scattering signals are related to $I_1(\theta)$ as follows

$$I_1(\theta) = c \sin\theta[s_\theta/s_0 - s'_\theta/s'_0], \quad (2)$$

where the symbols are: c, a constant proportional to the number concentration; $\sin\theta$ factor for the change in observed volume at different angles; s_θ photomultiplier signal from aerosol at angle θ; s'_θ correction term for background light e.g. stray light, scattering from edges of stops etc.; s_0, s'_0 incident beam intensities at time of measuring s_θ, s'_θ.

For convenience the two-parameter zeroth order logarithmic distribution (ZOLD) of Espenscheid *et al.*[13] has been adopted in this work, after experimental checks that such a distribution does describe the aerosols under study.[14]

Typical theoretical curves of intensity against the scattering angle are shown in fig. 4, for spherical particles of refractive index 1.52. Readings at suitably chosen angles discriminate well between the different distributions of sizes in this sub-micrometre range. The method is inapplicable if the greater part of the distribution is in the Rayleigh scattering regime, i.e., with diameter $<0.06\ \mu$m. A computer programme has been devised to solve the complex problem of inverting the light scattering data to give the corresponding size distributions. First, the theoretical intensities are computed for an assumed distribution (using eqn (1) and producing curves such as those in fig. 4), and the percentage differences for all angles found between these values and the recorded experimental data. The parameters of this "first-guess" distribution are then adjusted in successive steps to minimize the sum of squares of these differences according to the method developed by Powell,[15] until a final estimate for the aerosol is reached.

In order to evaluate the accuracy of the light-scattering inversion programme, theoretical intensity values for a set of eight angles were computed for several chosen

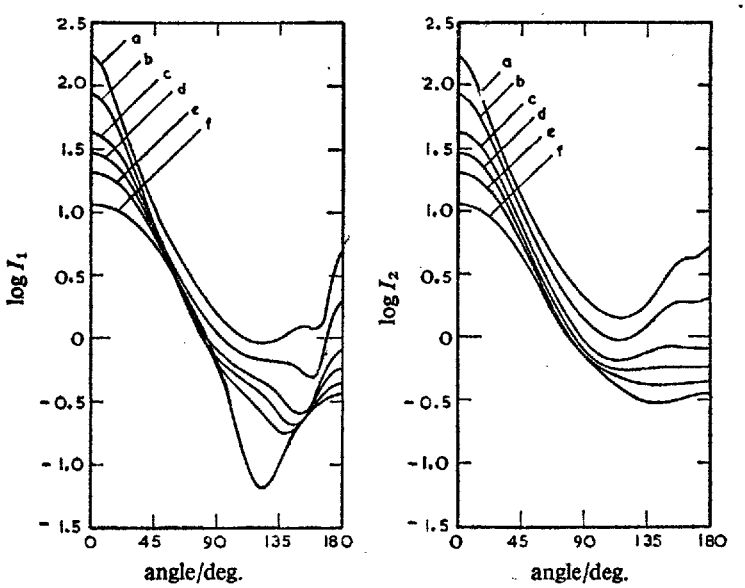

FIG. 4.—Theoretical intensity against scattering angle for light plane-polarised perpendicular (I_1) and parallel (I_2) to the scattering plane. Curves (*a-f*) are for distributions having a modal diameter 0.40 μm and the following ZOLD spread parameters (*a*) $\sigma_0 = 0.50$; (*b*) $\sigma_0 = 0.40$; (*c*) $\sigma_0 = 0.30$; (*d*) $\sigma_0 = 0.25$; (*e*) $\sigma_0 = 0.20$; (*f*) $\sigma_0 = 0.10$.

distributions. These were then used as experimental input data on which to perform the routine search analysis. The resulting " best fit " distributions were within 4 % of the modal diameter and 10 % of σ_0, even when the input intensity data were subjected to 4 % random fluctuations.

The authors acknowledge generous provision by Courtauld's Educational Trust Fund of equipment and a maintenance bursary, and assistance from L. Tyley and T. Hunt in the design of the electronic control system.

[1] B.Y. H. Liu and A. C. Verma, *Analyt. Chem.*, 1968, **40**, 843; B. Y. H. Liu, V. A. Marple and H. Yazdani, *Environmental Sci. Tech.*, 1969, **3**, 381.
[2] M. D. Carabine, *Chem. Soc. Rev.*, 1972, **1**, 411.
[3] B. J. Mason, *Discuss. Faraday Soc.*, 1960, **30**, 20.
[4] L. Coutarel, E. Matijevic, M. Kerker and Chao-Ming Huang, *J. Colloid Interface Sci.*, 1967, **24**, 338.
[5] F. Harris, G. Sherman and F. Morse, *I.E.E.E. Trans. Antenna Propagation* AP-15, 1967, p. 141.
[6] M. Kerker, *The Scattering of Light and Other Electromagnetic Radiation* (Academic Press, N.Y. and London, 1969).
[7] M. Kerker, E. Matijevic, W. Espenscheid, W. Farone and S. Kitani, *J. Colloid Interface Sci.*, 1964, **19**, 213.
[8] W. Heller and M. Wallach, *J. Phys. Chem.*, 1963, **67**, 2577.
[9] W. Heller and M. Wallach, *J. Phys. Chem.*, 1964, **68**, 931.
[10] R. Tabibian and W. Heller, *J. Colloid Interface Sci.*, 1958, **13**, 6.
[11] J. E. L. Maddock, *M.Sc. Thesis* (Univ. London, 1970).
[12] G. Mie, *Ann. Phys.*, 1908, **25**, 377.
[13] W. Espenscheid, M. Kerker and E. Matijevic, *J. Phys. Chem.*, 1964, **68**, 3093.
[14] M. D. Carabine, J. E. L. Maddock and A. P. Moore, *Nature, Phys. Sci.*, 1971, **231**, 18.
[15] M. Powell, *Computer J.*, 1965, **7**, 303.